OBSERVATIONS AND ANALYSIS OF U CEPHEI

By

NORMAN LEE MARKWORTH

A DISSERTATION PRESENTED TO THE GRADUATE COUNCIL OF
THE UNIVERSITY OF FLORIDA
IN PARTIAL FULFILLMENT OF THE REQUIREMENTS FOR THE
DEGREE OF DOCTOR OF PHILOSOPHY

UNIVERSITY OF FLORIDA

1977

ACKNOWLEDGEMENTS

I wish to express my appreciation to Dr. F.B. Wood for suggesting the topic of this dissertation and for his expert advice and guidance throughout the course of the work.

My sincere thanks goes to Dr. J.E. Merrill for many helpful and encouraging conversations, which kept me on the straight and narrow in the "black art" of eclipsing binary solutions. His constant attention to detail is an example that I will carry with me throughout my career.

I wish to thank Dr. R.E. Wilson for his advice on the use of the Wilson-Devinney solution method. Our many fruitful conversations broadened my understanding of the process of solution and helped me avoid the many pitfalls in this difficult numerical problem.

Drs. K-Y. Chen, H.L. Cohen, and E.J. Devinney also deserve thanks for their help in formulating ideas and arranging the manuscript.

Much of the computer time necessary for the completion of this study was provided by the Central Florida Regional Data Center in Tampa. Without their support, as well as the supplemental support of the Northeast Regional Data Center in Gainesville, much of the detailed analysis presented here could not have been accomplished.

Finally, I owe many words of thanks to my family, especially my wife, Mary, whose patience and encouragement provided the necessary impetus to complete this work.

TABLE OF CONTENTS

Abstract of Dissertation Presented to the Graduate Council of the University of Florida in Partial Fulfillment of the Requirements for the Degree of Doctor of Philosophy

OBSERVATIONS AND ANALYSIS OF U CEPHEI

By

Norman Lee Markworth

August, 1977

Chairman: Frank Bradshaw Wood
Cochairman: Kwan-Yu Chen
Major Department: Astronomy

Photoelectric observations of the well-known eclipsing binary system U Cephei commenced following the report of a major outburst on the system in the summer of 1974. Approximately 3200 measurements in the standard Johnson-Morgan UBV system were obtained from October, 1974, through May, 1976. The reported outburst was observed as well as another outburst of approximately the same intensity in the fall of 1975. The conventional Fourier analysis of the outside eclipse variations failed to produce coefficients of the sine and cosine terms in accordance with theory. A trial-and-error approach produced the coefficients used in the rectification procedure. A Russell-Merrill solution was obtained which seemed to confirm the results of Hall and Walter. The light curve synthesis approach of Wilson and Devinney yielded a very similar solution, in which the observed asynchronism of the primary component was used as an additional input

parameter. The computer solution technique of D.B. Wood was also attempted, but it failed because provision is not made for the asynchronous rotation of the components. Residuals of the observations in primary eclipse from the Russell-Merrill solution revealed excess light during the outbursts. This excess was modeled as hot source regions near the poles of the primary star and rotating with that star. Shock heating of the surface by infalling material is suggested as the cause of the excess light. Excess temperatures range from 7000-17000°K, yielding mean velocities of the infalling material in the range 12-21 km/s. A magnetic field on the primary star is suggested as the steering mechanism for the infalling material and conclusions based on the model are discussed.

CHAPTER I

INTRODUCTION

History of the Observations of U Cephei

The variability of U Cephei (BD+81°25, HD 5679, ADS 830) was discovered by Ceraski (1880) on 23 June 1880. It was the seventh eclipsing variable discovered and displayed the deepest primary eclipse known at the time. Because of its circumpolar position at most northern hemisphere sites (declination +82°) and its relative brightness ($m_V = 6^m.8 - 9^m.0$), it has been frequently and faithfully observed. The depth of primary eclipse lends itself to rather accurate visual determination of the time of minimum. This rather substantial bulk of data represents a detailed account of period changes extending for almost a century. Two prediscovery observations may extend the time scale to 150 years. Schwerd observed U Cephei on 12 May 1828, to be two magnitudes fainter than normal. Carrington estimated the variable one magnitude fainter than normal on 30 December 1855. The earlier observation seems the more reliable. Lalande observed U Cephei at normal brightness on 30 March 1790.

Early photometric observers concentrated on the primary minimum. Schmidt, Knott, Wilsing, Chandler, Yendell, Pickering, Searle, Wendell, Lehnert, and Bemporad helped to

confirm that the ingress branch is less steep than the egress branch. Dugan (1920) did the first complete photometric study and found that the shoulder of the eclipse near first contact was depressed, causing ingress to be less steep. He invoked a tidal bulge on the primary star lagging the conjunction by 24°. Although Cowling (1941) later showed that this explanation could not be responsible for the observed asymmetry, Dugan did show that some effects were present in U Cephei that simple theory could not explain.

The next great step in understanding U Cephei came from spectroscopy. The first orbital elements by Carpenter (1930) found $e = 0.47$, $\omega = 25°$. This considerable eccentricity was in complete disagreement with the work of Dugan (1920), who found secondary eclipse at 0.5P. Other spectroscopic studies followed but all found a rather large eccentricity. Struve (1944) was the first to suggest that a conventional approach could not be used to obtain the orbital elements from the radial velocity curve. He postulated a gaseous stream flowing from the cooler toward the hotter star. At times the spectrum of this stream would be seen projected onto the primary (hotter) star, giving aberrant radial velocity measures. Such gaseous streams could also account for the depression of the light curve around first contact.

Batten (1974) observed the system spectroscopically and found rare instances of emission in the hydrogen lines. These lines were red-displaced at second contact and violet-displaced at third contact. The same sort of emission is

more obvious in RW Tauri and Joy (1947) suggested a ring or disk has been formed around the hotter star. The transitory nature of the emission lines in U Cephei suggests that such a ring is not a stable part of the system.

Another observational fact from the spectroscopic work must be considered in any working model of U Cephei. The radial velocity curve clearly indicates that the primary star is rotating at five times the synchronous rate. This will change the brightness distribution of the primary and cause some change in the light curve.

Another step toward the understanding of U Cephei came with the resolution of the so-called "Algol paradox." U Cephei is an example of an Algol type system, in which the deeper eclipse is an occultation. This requires the smaller star to be the hotter, contrary to known stellar relationships on the main sequence. Plavec (1973) has written a summary of the most widely accepted explanation of this strange paradox. Kopal (1959) reconstructs the development of the Roche equipotential surfaces, which give a limit to the size of each star in the system. If the stars are sufficiently close, evolution of the initially more massive star will cause it to fill its critical lobe. Further expansion is impossible, but it can lose its mass through the inner Lagrangian point to the less massive star. Calculations indicate that such mass flow is initially self-sustaining and can, in most cases, reverse the mass ratio. Several stages have been identified for the mass loss, but the net result is to produce a system

in which a cool, large star filling its critical lobe is slowly losing mass to a rather hot, small, main sequence star. This sort of evolutionary history can explain the observations of U Cephei. The system contains a B7V primary with a G8III (spectral types by Batten, 1974) filling its critical lobe. The secondary star is more evolved and is losing mass to the primary. We now have qualitative agreement between the observations and the model. The model also accounts qualitatively for the changes in period which have been noted since the earliest observations.

The mass loss responsible for the gaseous stream in U Cephei must be highly sporadic. Each episode of increased mass flow should be accompanied by a sudden change in period. Hall and Walter (1974) show several suspected period changes separated by nine to eleven years. Walter (1975) has shown that a precessional period of twelve years for the primary star is consistent with changes in the slant of the total phase of primary eclipse.

Several photoelectric studies have recently been done aimed at determining the rates of mass loss and period change. The once inconceivably large values of (2-5) x 10^{-7} $M_{\odot}$/yr. are now accepted as the minimum values of mass loss for U Cephei. Properties of the gaseous stream have been discussed in some detail by Batten (1974).

Attempts at solution of the light curve have always been hampered by contamination of the light from the gaseous stream. Hall and Walter (1974) have solved three sets of

independent data from Tschudovitchev (1950), Khozov and Minaev (1969), and Catalano and Rodono (1974) in order to compare the geometrical parameters of the solutions. Their results are probably influenced by some special assumptions, but their work probably represents the first major attempt to retrieve the true geometry from the confusing effects of the gas flow using current theory.

Current Research

The present study was initiated by the report (Batten et al., 1974) of a major outburst in the U Cephei system in the summer and fall of 1974. During the course of the observations another major outburst occurred in the fall of 1975. These outbursts presented an unique opportunity to obtain information on the dynamical behavior of the gaseous stream and its affect on the hotter star.

This dissertation attempts to bring about the next step in understanding the physical nature of U Cephei. The modeling of the dynamic surface brightness distribution of the primary star should unite the previous work concerning the shape of the components and the properties of the gaseous stream.

Consistent values of the geometrical parameters of the system are essential before convincing theoretical arguments can be made. Since variations in the light curve outside the scope of the solution models were felt to be primarily intrinsic, considerable effort went into the accurate reduction

and standardization of the data. These efforts occupy Chapters II and III. The application of the Russell-Merrill solution method depends on being able to correct the observations to the equivalent spherical model, i.e., remove the variation outside of eclipse. The intrinsic variation in U Cephei causes uncertainty in this "rectification" procedure. Chapter IV outlines the rectification procedure and results. Chapter V deals with the solution techniques and results. Chapter VI presents a new period study, employing all known observations. With a new solution yielding consistent geometrical parameters, a model can now be presented for nights of high photometric activity. Chapter VII discusses this model for the primary star. Chapter VIII concludes the work with the model for the U Cephei system and predictions based on the model.

CHAPTER II

INSTRUMENTATION

Observations were carried out on two telescopes so as to cover the light curve in as short a time as possible within the constraints of scheduling. The descriptions of both photometric systems follows.

The Eighteen-Inch (46 cm.) f/10.5 Ritchey-Chrétien System

The photometer was the same employed by K-Y. Chen and D.A. Rekenthaler (Chen and Rekenthaler, 1966). It uses an uncooled 1P21 photomultiplier operated at 900 volts. Two diaphragms were used (see Chapter III) yielding diameters of 86.2 and 42.5 arc seconds. The filters were ultraviolet (Corning 9863), blue (Corning 5030 and Schott GC15), and yellow (Corning 3389), corresponding to the Johnson-Morgan standard UBV system. Unfortunately, the telescope tailpiece has a diagonal prism before the mount for the photometer. This makes viewing through the photometer much easier, but presents severe transmission problems in the ultraviolet. In fact, it appears that the red leak component alone remains in the "ultraviolet" band. An adapter was built of the proper dimensions, so that good focus could still be achieved without the diagonal prism. It was found, however, that the

new arrangement would not permit the telescope to reach the declination of the variable. Yellow and blue observations should be unaffected by the diagonal prism and, therefore, were the only filter bands used for this system.

The signal is sent from the photometer to a newly designed fast electrometer amplifier (Oliver, 1976). The fine-gain range is such that the same coarse-gain step (5.0) could be used for all observations. Tables 1 and 2 show the calibrations of the PA/10 amplifier for the nights of observation. On two nights (10/31/74 and 11/10/74) no calibration of coarse-gain steps was done since no procedure was available at that time. The mean of the 5.0 magnitude gain step was used on these nights. Although rather large night to night variation in the coarse-gain calibrations is obvious, calibrations at the beginning and end of each night show very little variation (typically $\leq 0^{m}.001$). The trend of the calibrations suggest aging effects. A Heath strip-chart recorder monitored the observations at ½ inch/minute.

The Thirty-Inch (76 cm.) f/16 Cassegrain System

The photometer used was the dual channel photometer of the Astro-Mechanics Company, Inc. Only channel I was used which incorporates an EMI 6256B (S11) photocathode refrigerated with dry ice. The light was initially passed through a dichroic filter which reflects 95% of the light between 3500 Å and 6000 Å into the light path of channel I and passes 80% of the light above 6500 Å into the light path of channel

Table 1

Fine-Gain Calibrations for the PA/10 Amplifier

Gain / Date	2.5	2.0	1.5	1.0	0.5	0.0	-0.5	T (°F)	H (%)
10/31/74	2.5280	1.9870	1.5030	0.9990	0.5100	0.0	-0.5320	55	80
11/10/74	2.5290	1.9860	1.5050	1.0000	0.5120	0.0	-0.5340	45	80
11/15/74	2.5270	1.9850	1.5020	0.9970	0.5090	0.0	-0.5300	45	70
03/25/75	2.5266	1.9856	1.5031	1.0013	0.5123	0.0	-0.5338	68	46
04/04/75	2.5307	1.9890	1.5070	1.0029	0.5127	0.0	-0.5351	48	65
04/06/75	2.5352	1.9923	1.5100	1.0061	0.5131	0.0	-0.5353	57	55
09/18/75	2.5119	1.9760	1.4969	0.9992	0.5093	0.0	-0.5276	72	95
09/25/75	2.4807	1.9649	1.4889	0.9922	0.5009	0.0	-0.5324	58	75
10/12/75	2.4952	1.9692	1.4910	0.9923	0.5042	0.0	-0.5305	65	80
10/21/75	2.5070	1.9722	1.4946	0.9958	0.5074	0.0	-0.5276	64	--

Table 2

Coarse-Gain Calibrations for the PA/10 Amplifier

Gain / Date	12.5	10.0	7.5	5.0	2.5	0.0
10/31/74		No Calibration		4.8624		
11/10/74		No Calibration		4.8624		
11/15/74	--	--	7.3745	4.8521	2.4837	-0.0010
03/25/75	12.4224	9.8202	7.4999	4.8695	2.4899	-0.0010
04/04/75	12.3816	9.7902	7.4747	4.8534	2.4816	-0.0010
04/06/75	12.4455	9.8535	7.4777	4.8559	2.4850	-0.0010
09/18/75	12.3134	9.7407	7.4708	4.8625	2.4873	-0.0010
09/25/75	12.3893	9.7889	7.4877	4.8624	2.4863	-0.0010
10/12/75	12.3724	9.7727	7.4788	4.8659	2.4888	-0.0010
10/21/75	12.3909	9.7960	7.4938	4.8692	2.4883	-0.0010

II. The dichroic filter is typically used for simultaneous photometry in the red and one of the UBV colors. It was thought, however, that its insertion for this one channel work would eliminate the problem of red leak which plagues the broad band ultraviolet filter. A diaphragm of 15.2 arc seconds was inserted in front of the photocathode. The filters used for the ultraviolet (Corning 9863), blue (Corning 5030 and Schott GC13), and yellow (Corning 3389) approximate the Johnson-Morgan standard UBV system.

The amplifier was the PA-1/C, the latest version of the PA-1, designed at the UCLA Astronomy Department and constructed at the University of Florida. Even though the range of the fine-gain steps is 5.0 magnitudes, not all observations could be taken on the same coarse-gain step. The difference between the largest (variable-blue) and the smallest (comparison-ultraviolet) deflections was typically 6.0 magnitudes outside of the eclipse on photometric nights. The variable-blue readings are the only observations taken on a different coarse-gain step. Calibrations were carefully done twice a night for both the ½- and 2½-magnitude gain steps and are presented in Tables 3 and 4. The amplifier was quite stable even in the 2½-magnitude gain steps and variations during the night were negligible.

Observations were monitored on a Honeywell strip-chart recorder, which was replaced in January 1976, by a Texas Instrument strip-chart recorder. Observations were also recorded on digital tape, the tape drive of which was replaced

Table 3

Fine Gain Calibrations for the PA-1/C

Gain / Date	2.5	2.0	1.5	1.0	0.5	0.0	-0.5	-1.0	-1.5	-2.0	-2.5
03/19/75	2.5042	2.0016	1.5014	1.0012	0.5011	0.0	-0.5023	-1.0059	-1.5119	-1.9953	-2.4950
03/21/75	2.5035	2.0006	1.5000	1.0003	0.5010	0.0	-0.5018	-1.0056	-1.5116	-1.9955	-2.4953
04/15/75	2.5131	2.0073	1.5051	1.0051	0.5034	0.0	-0.5036	-1.0090	-1.5174	-2.0047	-2.5075
04/21/75	2.5045	2.0014	1.5009	1.0009	0.5009	0.0	-0.5016	-1.0049	-1.5104	-1.9945	-2.4936
04/22/75	2.5032	2.0004	1.5001	1.0007	0.5004	0.0	-0.5017	-1.0047	-1.5098	-1.9936	-2.4930
08/17/75	2.5045	2.0009	1.5011	1.0017	0.5011	0.0	-0.5027	-1.0063	-1.5117	-1.9947	-2.4939
08/21/75	2.5014	2.0005	1.4997	1.0013	0.5009	0.0	-0.5013	-1.0049	-1.5107	-1.9938	-2.4934
08/25/75	2.5092	2.0048	1.5032	1.0030	0.5018	0.0	-0.5033	-1.0073	-1.5137	-1.9967	-2.4961
10/15/75	2.5289	2.0190	1.5137	1.0096	0.5036	0.0	-0.5034	-1.0075	-1.5143	-1.9991	-2.5005
10/23/75	2.5047	2.0021	1.5019	1.0018	0.5010	0.0	-0.5015	-1.0044	-1.5101	-1.9944	-2.4948
02/03/76	2.5046	2.0017	1.5011	1.0013	0.5009	0.0	-0.5017	-1.0046	-1.5096	-1.9957	-2.4955
02/08/76	2.5041	2.0013	1.5010	1.0010	0.5103	0.0	-0.5016	-1.0044	-1.5091	-1.9956	-2.4952
02/15/76	2.5049	2.0020	1.5015	1.0015	0.5010	0.0	-0.5019	-1.0051	-1.5107	-1.9957	-2.4954
03/02/76	2.5045	2.0016	1.5010	1.0011	0.5009	0.0	-0.5019	-1.0054	-1.5111	-1.9952	-2.4948
03/18/76	2.5038	2.0009	1.5003	1.0004	0.5006	0.0	-0.5014	-1.0034	-1.5069	-1.9964	-2.4960
04/04/76	2.5047	2.0019	1.5013	1.0014	0.5011	0.0	-0.5022	-1.0057	-1.5116	-1.9952	-2.4951
04/18/76	2.5046	2.0018	1.5012	1.0013	0.5012	0.0	-0.5018	-1.0053	-1.5108	-1.9950	-2.4945
04/26/76	2.5019	2.0019	1.5012	1.0013	0.5011	0.0	-0.5017	-1.0047	-1.5097	-1.9965	-2.4963
05/04/76	2.5048	2.0019	1.5014	1.0014	0.5011	0.0	-0.5019	-1.0055	-1.5115	-1.9949	-2.4947
05/19/76	2.5048	2.0018	1.5012	1.0014	0.5012	0.0	-0.5021	-1.0055	-1.5112	-1.9957	-2.4954

Table 4

Coarse Gain Calibrations for the PA-1/C

Gain / Date	12.5	10.0	7.5	5.0	2.5	0.0	T (°F)	H (%)
03/19/75	12.4727	10.0006	7.4993	4.9878	2.4953	-0.0190	60	65
03/21/75	12.5021	10.0253	7.5187	5.0023	2.5050	-0.0145	60	85
04/15/75	12.5052	10.0311	7.5245	5.0071	2.5079	-0.0114	48	90
04/21/75	12.5095	10.0317	7.5227	5.0049	2.5066	-0.0126	56	94
04/22/75	12.5056	10.0292	7.5219	5.0044	2.5064	-0.0132	60	95
08/17/75	12.4925	10.0169	7.5160	5.0012	2.5048	-0.0176	80	95
08/21/75	12.4969	10.0211	7.5189	5.0025	2.5056	-0.0161	73	90
08/25/75	12.4902	10.0159	7.5158	5.0005	2.5048	-0.0170	75	90
10/15/75	12.4984	10.0227	7.5202	5.0016	2.5053	-0.0147	70	85
10/23/75	12.4997	10.0233	7.5185	5.0020	2.5050	-0.0152	64	94
02/03/76	12.5089	10.0319	7.5215	5.0043	2.5063	-0.0120	54	90
02/08/76	12.5181	10.0391	7.5251	5.0064	2.5075	-0.0095	40	70
02/15/76	12.4995	10.0238	7.5191	5.0028	2.5048	-0.0157	68	70
03/02/76	12.4960	10.0208	7.5174	5.0017	2.5049	-0.0162	70	80
03/18/76	12.5156	10.0376	7.5230	5.0048	2.5063	-0.0096	55	80
04/04/76	12.5034	10.0272	7.5205	5.0035	2.5060	-0.0141	60	85
04/18/76	12.5117	10.0339	7.5238	5.0062	2.5081	-0.0118	65	85
04/26/76	12.5119	10.0348	7.5231	5.0051	2.5068	-0.0109	58	80
05/04/76	12.5009	10.0238	7.5192	5.0025	2.5054	-0.0154	55	80
05/19/76	12.4977	10.0220	7.5177	5.0018	2.5049	-0.0156	55	80

in January 1976. By inspecting the ½-magnitude calibrations, it appears as if the system was noisier prior to the installation of the new tape drive unit.

CHAPTER III

THE OBSERVATIONS

Introduction

Thirty nights of observation (ten and twenty on the eighteen-inch and thirty-inch telescopes, respectively) have yielded approximately 3200 measurements of intensity and time for U Cephei. Table 5 lists the dates of observation for each telescope.

The Close Companions of U Cephei

Observations of U Cephei are plagued by the presence of two close companions. The following table (Table 6) lists properties of the stars of the system.

Observations of the two companions were made in 1881 and 1899. Aside from these observations, there is scant information on these stars. The original observations by Knott (Jeffers et al., 1963) gave A0 as the spectral type for both, whereas later photoelectric work gave color differences more consistent with G6-7 for B. The magnitude differences between these companions and U Cephei in conjunction with their estimated spectral type indicate that C is probably a background object, while B is probably at the distance of U Cephei.

Table 5

Date at the Beginning of Each Night of Observation

Eighteen-inch	Thirty-inch
31 Oct. 1974	19 Mar. 1975
10 Nov. 1974	21 Mar. 1975
15 Nov. 1974	15 Apr. 1975
25 Mar. 1975	21 Apr. 1975
4 Apr. 1975	22 Apr. 1975
6 Apr. 1975	17 Aug. 1975
18 Sep. 1975	21 Aug. 1975
25 Sep. 1975	25 Aug. 1975
12 Oct. 1975	15 Oct. 1975
21 Oct. 1975	23 Oct. 1975
	3 Feb. 1976
	8 Feb. 1976
	15 Feb. 1976
	2 Mar. 1976
	18 Mar. 1976
	4 Apr. 1976
	18 Apr. 1976
	26 Apr. 1976
	4 May 1976
	19 May 1976

Table 6

Properties of the Stars In and Near the U Cephei System

Star	V	B-V	U-B	Sp.	PA	D
U Cephei						
Combined	$6^m.83$	$-0^m.05$	$-0^m.40$			
Primary	6.95	-0.11	-0.43	B7V		
Secondary	9.11	+0.88	+0.40	G8III[a]		
B	11.83	+0.73	+0.29	(G6-7)	62°	13".8
C	12.9			A0(?)	321°	21".2

[a]From Batten (1974).

Figure 1 shows the positions of the companions superimposed on the smallest diaphragm of the eighteen-inch telescope system. This diaphragm was used until 6 April 1975. An observing note on 10 November 1974, noted the two companions with no diaphragm in place. Calculations show that C is below the sky limit on all but moonless nights with little haze. These conditions were obtained only on 10 November 1974, and 6 April 1975, when the smallest diaphragm was still in use. Even under ideal conditions C is only about $0^m.2$ above the typical sky through the eighteen-inch telescope system. Tests of the Fabry lens of the eighteen-inch telescope indicate that edge effects may reduce the intensity of C by half at its position. The maximum error introduced by not correcting for C is $0^m.036$ in the visual

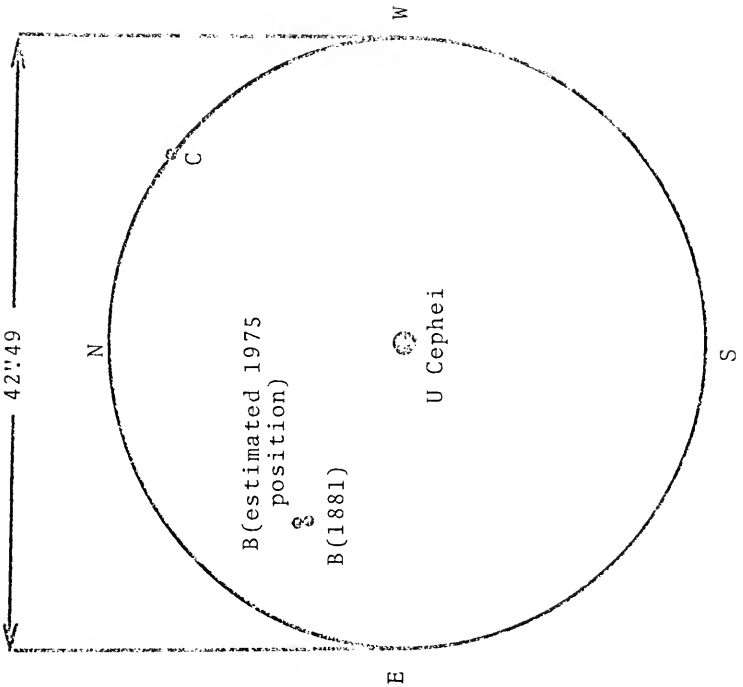

Figure 1. U Cephei and its companions.

and $0^m.041$ in the blue. The variable must be about 70% into eclipse before the relative intensity of C compared to the variable could introduce as much magnitude variation in the light curve as the typical error of the observations ($0^m.01$).

For all these reasons C was assumed negligible and corrections were made only for B on nights before 6 April 1975. After that time the next larger diaphragm was used and both companions were used for correction. Observations in eclipse (i.e., 10/31/74, 11/10/74, 11/15/74, 04/06/75) were checked for abnormal fluctuations after corrections and none were found.

No such problems were encountered on the thirty-inch telescope, since the chosen diaphragms were small enough to consistently exclude both companions. On moonless nights of superior photometric quality, deflections were taken on these companions. Table 7 shows the magnitude differences with respect to BD+81°29 of both companions in the three colors as well as the ratio of intensities. The weights reflect the quality of the other observations around the time of the deflections.

Reduction of the Observations

Observations were taken in the sequence comparison VBU, variable UBV, comparison, VBU. The typical time between consecutive variable star measurements was four to five minutes. Sky readings at all gains used were taken every

Table 7

Differential Magnitudes of the Close Companions
With Respect to BD+81°29

	Companion B				Companion C			
Date	ΔV	ΔB	ΔU	Wt.	ΔV	ΔB	ΔU	Wt.
04/15/75	$3^m.38$	$2^m.94$	$2^m.71$	1	$4^m.38$	$4^m.38$	$5^m.61$	½
					4.58	4.71	4.60	1
08/17/75	3.33	3.21	3.00	1	4.24	4.35	4.54	1
02/03/76	3.22	3.17	2.94	2	4.34	4.54	4.96	2
Means	3.29 ± 5	3.12 ± 8	2.90 ± 8		4.38 ± 7	4.54 ± 7	4.86 ± 19	
Ratio of Intensities								
	0.0484 ± 3	0.0563 ± 6	0.0695 ± 6		0.0177 ± 2	0.0153 ± 2	0.0114 ± 4	

½-hour on moonless nights, more frequently on nights with a moon, and after every comparison star observation if the moon was rising or setting. All sky readings were taken just north of the comparison star in a field clear of stars. Check star observations were taken two to three times per night.

My initial reduction routine removed the effect of the sky, found differential magnitudes (m_{var}-m_{comp}) and color differences by linear interpolation. All data were then rechecked on the strip-chart records to insure that all usable data were free of keypunch errors.

The Reduction to the Standard UBV System

Stars in the Hyades cluster were used as standards. Two observing runs were done on the thirty-inch telescope (one run each on the eastern and western halves of the sky) and one run of excellent quality was done on the eighteen-inch telescope. Since the declination of U Cephei is almost +82°, good atmospheric extinction information cannot be obtained from the comparison stars. Extinction information from the standard stars was used to transform the variable star observations to the standard UBV system. The symbols and equations that follow in this section are those of R.H. Hardie (Hardie, 1962). Table 8 lists the data for the standard stars. The stars were observed sequentially as given in the table and this sequence was repeated four to seven times as the stars progressed through approximately 1½ air masses.

Table 8

Data on Stars in the Hyades Cluster

Star	BD#	V	B - V	U - B	RA (1950.0)	Dec
72	15°632	$3^m.41$	$0^m.179$	$0^m.132$	$4^h25^m48^s$	15°45'42"
71	15°631	3.85	.955	.741	4 25 43	15 51 10
75	15°633	6.59	.531	.060	4 26 08	16 03 00
82	15°647	4.78	.173	.126	4 27 42	16 05 12
85	15°640	6.51	.426	.009	4 27 55	16 02 30
83	15°639	5.48	.259	.097	4 27 48	15 35 05
80	15°636	5.58	.319	.009	4 27 17	15 31 49

From Johnson and Knuckles (1955).

The second order coefficients were calculated first by least squares solutions of Hardie's equations 25,

$$\Delta(b - v) = k''_{bv}\Delta(b - v)X + \Delta(b - v)_0 \quad ,$$

$$\Delta(u - b) = k''_{ub}\Delta(u - b)X + \Delta(u - b)_0 \quad ,$$

where small case letters refer to observed quantities, X is the air mass, and the second order coefficients are k''_{bv} and k''_{ub}. The Δ quantities in the equations refer to differential measures between the standards. The procedure followed was to take each standard star in sequence as the base star and calculate the second order coefficients, using all the other stars in combination with the base star. This yielded forty-two determinations of each coefficient. Useful information, however, can only be obtained between stars having sufficiently different color indices. Table 9 shows the combinations of stars used for each color index. Weighted means

Table 9

Star Combinations Used to Calculate Second Order Extinction Coefficients

Nomenclature is that of Table 8.

B-V	U-B
72-71	71-75
71-72	71-85
71-82	75-71
82-71	85-71
	80-71

were taken of the coefficients resulting from the above combinations with the weights being the normalized ratio of the coefficient and its standard error. The results of the two runs on the thirty-inch telescope were averaged to give the values used.

Having established values for the second order coefficients, Hardie's equations 26 were used to determine the first order coefficients, namely,

$$(b - v)J_X = k'_{bv}X + (b - v)_o \quad ,$$

$$(u - b)G_X = k'_{ub}X + (u - b)_o \quad ,$$

where $J_X = 1 - k''_{bv}X$ and $G_X = 1 - k''_{ub}X$. The first order coefficients were calculated for each star and straight means taken to give the results of Table 10. The primary coefficient k_v is given by Hardie's equation 22,

$$v_o = v - k_vX \quad .$$

The coefficient k_v was also calculated for each star and means taken. The large differences in the standard errors quoted for the two telescopes are misleading in that the error shown for the thirty-inch telescope results from two nights and that from the eighteen-inch telescope from only one. The latter error is more typical of the single night error for the primary coefficient, whereas the former error is useful for showing, but not strictly indicative of, the range of k_v for photometric nights.

Table 10

Extinction Coefficients and Auxiliary Quantities

	Telescope	
	18 inch	30 inch
k_v	0.26 ± 2	0.32 ± 9
k'_{bv}	0.15 ± 1	0.18 ± 3
k''_{bv}	-0.050 ± 9	-0.035 ± 8
k'_{ub}		0.36 ± 5
k''_{ub}		0.001 ± 12
μ	1.039 ± 11	1.185 ± 16
ε	0.019 ± 10	-0.144 ± 11
ψ		0.986 ± 20

Three auxiliary quantities are needed before the transformation to the standard system can be done. These quantities, μ, ε, ψ, are found by linear regressions of $(V - v_o)$ with $(B - V)$ for ε, $(B - V) - (b - v)_o$ with $(B - V)$ for μ, and $(U - B) - (u - b)_o$ with $(U - B)$ for ψ. Upper case letters here stand for magnitudes in Table 8.

The differential magnitudes for the variable were then transformed to the standard system via Hardie's equations 28,

$$\Delta V = \Delta v - k_v \Delta X + \varepsilon \Delta (B - V) \quad ,$$

$$\Delta (B - V) = \mu \Delta (b - v) - \mu k'_{bv} \Delta X - \mu k''_{bv} \Delta (b - v) \overline{X} \quad ,$$

$$\Delta (U - B) = \psi \Delta (u - b) - \psi k'_{ub} \Delta X - \psi k''_{ub} \Delta (u - b) \overline{X} \quad .$$

Here Δ stands for differential quantities and $\overline{X}$ is the mean air mass for the variable and comparison. The differential air mass, ΔX, is given by,

$$\Delta X = (P \sin \overline{h} + Q \cos \overline{h} + R) \overline{X}^2 \quad ,$$

where $\overline{h}$ is the mean hour angle between the variable and comparison (positive east) and,

$$P = \Delta\alpha \cos\phi \cos\overline{\delta} \quad ,$$

$$Q = \Delta\delta \cos\phi \sin\overline{\delta} \quad ,$$

$$R = -\Delta\delta \sin\phi \cos\overline{\delta} \quad .$$

Here $\Delta\alpha$ and $\Delta\delta$ are the differences in right ascension and declination in radians, respectively, and ϕ is the observer's latitude. P, Q, R are constant for a pair of stars and at Rosemary Hill Observatory have the values,

P = 0.00248		R = -0.00169	
Q = 0.00046	BD+81°29,	Q = 0.00130	BD+81°30.
R = -0.00004		R = 0.00011	

The Comparison Stars

My original choice of a comparison star was BD+81°30. This star has colors strikingly close to the variable and its

proximity was also alluring. An early paper on U Cephei (Dugan, 1920), however, indicates that this star may be variable. It is interesting to note that most observers of U Cephei still use BD+81°30 as a comparison despite the warning. This may be due to the difficulty in finding a nearby star of substantially the same colors or finding any color information on the nearby stars. All data until 15 April 1975, used BD+81°27 as a check. On 15 April 1975, and for all subsequent data, BD+81°29 was used as a comparison and BD+81°30 as a check. This change required that data taken earlier be transformed to the new comparison star. Table 11 gives the pertinent information for all stars used.

Table 11

Data for the Comparison Stars

Star	RA (1975.0)	Dec	V	B - V	U - B
BD+81°30	$1^h03^m06^s$	81°49'43"	$7^m.89$	$0^m.019$	$-0^m.080$
BD+81°27	1 01 30	81 58 12	8.41	∿0.6	∿0.1
BD+81°29	1 02 17	82 06 58	8.58	0.49	∿0.0

Figure 2 shows the differential magnitude (BD+81°30 - BD+81°29) versus time for the three colors used. This figure indicates no trends or unusual fluctuations. Nights on which BD+81°30 was used as a comparison required the addition to the data of the magnitude difference between BD+81°30 and

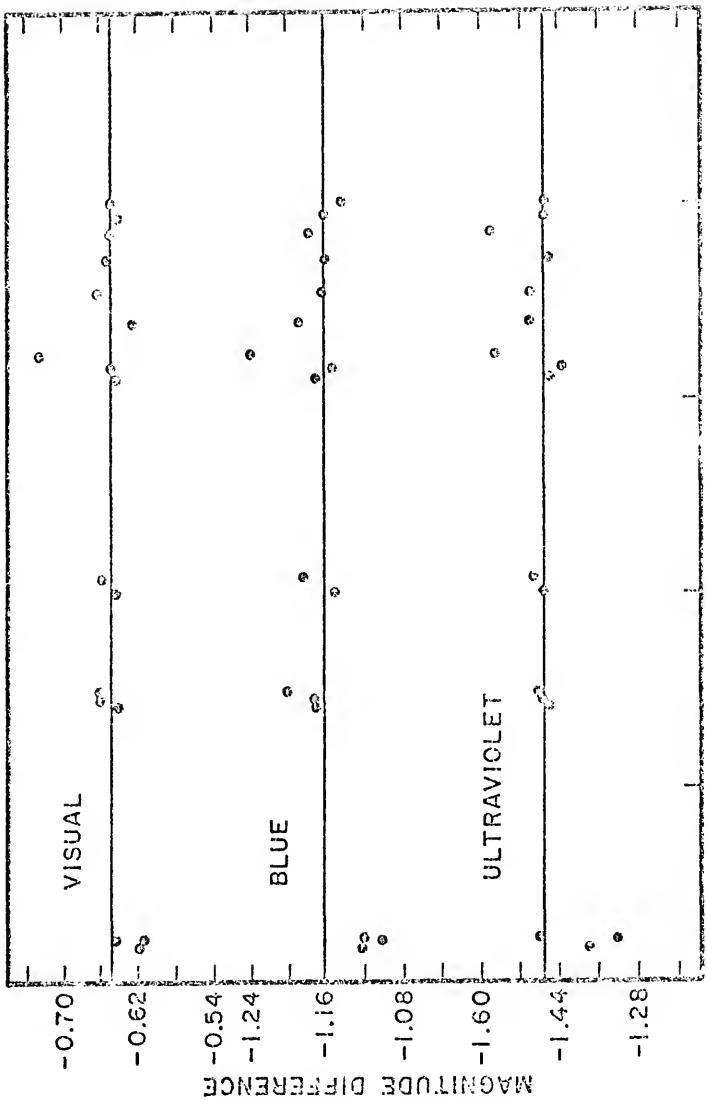

Figure 2. Magnitude difference (BD+81°30 - BD+81°29) versus time.

BD+81 29 to transform them to differential measures with respect to BD+81 29. These magnitude differences on the natural photometric system are listed below.

	Telescope	
	eighteen-inch	thirty-inch
v	-0.55	-0.65
b	-1.13	-1.17
u		-1.47

After all corrections were made, an inspection of the light curve reveals no systematic deviations between nights on the eighteen-inch and thirty-inch telescopes with either comparison star. Thus all transformations are compatible.

The data reduced to the standard system were thoroughly scanned and compared to the chart records to eliminate data suspected of being affected by weather. These scanned data are presented tabularly in Table 12 and as the light curves of Figure 3. The phase has been claculated using the ephemeris Min JD = 2442352.6999 + $2^{d}.4930709 \cdot E$ (see Chapter VI). Two major outbursts were noted, one in August 1974, and one in September/October 1975. Data around these dates were eliminated from the initial analysis in an attempt to obtain less perturbed light curves for solution. Specifically, the nights of 31 October; 10 and 15 November 1974; 18 and 25

TABLE 12
STANDARD DIFFERENTIAL MAGNITUDES
U CEPHEI

VISUAL

HEL JD (2440000+)	DMAG.	HEL JD (2440000+)	DMAG.	HEL JD (2440000+)	DMAG.
2352.54285	-1.343	2362.59536	-0.372	2362.73115	-0.054
2352.54980	-1.309	2362.59860	-0.288	2362.73464	-0.133
2352.55484	-1.266	2362.59952	-0.264	2362.73502	-0.152
2352.55935	-1.223	2362.60057	-0.224	2362.73991	-0.236
2352.56369	-1.174	2362.60363	-0.166	2362.74424	-0.329
2352.56853	-1.137	2362.60451	-0.144	2362.74564	-0.364
2352.57443	-1.076	2362.60565	-0.106	2362.74955	-0.442
2352.59655	-0.773	2362.60859	-0.051	2362.74995	-0.451
2352.60151	-0.700	2362.60919	-0.043	2362.75053	-0.462
2352.61180	-0.507	2362.61007	-0.012	2362.75401	-0.511
2352.61911	-0.352	2362.61401	0.079	2362.75589	-0.531
2352.62444	-0.223	2362.61403	0.089	2362.75945	-0.564
2352.63015	-0.077	2362.61538	0.132	2362.75962	-0.570
2352.63549	0.061	2362.61914	0.225	2362.76504	-0.648
2352.64242	0.250	2362.62211	0.299	2362.76912	-0.747
2352.64823	0.391	2362.62570	0.393	2362.77265	-0.830
2352.65498	0.565	2362.62657	0.421	2362.77349	-0.847
2352.66436	0.686	2362.62759	0.443	2362.78201	-0.947
2352.67201	0.884	2362.63113	0.516	2362.78592	-1.014
2362.50837	-1.395	2362.63213	0.566	2362.79000	-1.044
2362.51319	-1.362	2362.63275	0.596	2362.80215	-1.155
2362.51822	-1.328	2362.63629	0.638	2362.81076	-1.214
2362.52401	-1.296	2362.63744	0.655	2362.81654	-1.255
2362.52707	-1.253	2362.63871	0.645	2362.82354	-1.304
2362.53036	-1.222	2362.64068	0.698	2362.82602	-1.351
2362.53517	-1.197	2362.64809	0.697	2367.50342	-1.303
2362.53911	-1.154	2362.64873	0.726	2367.50743	-1.325
2362.54253	-1.132	2362.64966	0.760	2367.50843	-1.310
2362.54594	-1.101	2362.66631	0.746	2367.51329	-1.276
2362.54936	-1.063	2362.66741	0.751	2367.51451	-1.265
2362.54963	-1.063	2362.67952	0.746	2367.51775	-1.219
2362.55081	-0.960	2362.68037	0.744	2367.51867	-1.210
2362.56001	-0.930	2362.68035	0.737	2367.52214	-1.172
2362.56325	-0.886	2362.68773	0.732	2367.52335	-1.165
2362.56439	-0.865	2362.69206	0.687	2367.52653	-1.141
2362.56753	-0.840	2362.69316	0.670	2367.52705	-1.131
2362.56828	-0.828	2362.69675	0.644	2367.53029	-1.098
2362.57065	-0.785	2362.69982	0.582	2367.53134	-1.087
2362.57130	-0.759	2362.70069	0.593	2367.53475	-1.029
2362.57394	-0.737	2362.70762	0.471	2367.53603	-1.014
2362.57499	-0.735	2362.70872	0.452	2367.53874	-0.980
2362.57928	-0.676	2362.71258	0.380	2367.53949	-0.966
2362.58025	-0.655	2362.71380	0.355	2367.54203	-0.932
2362.58426	-0.598	2362.71839	0.241	2367.54373	-0.911
2362.58471	-0.576	2362.71931	0.221	2367.54632	-0.876
2362.58541	-0.549	2362.71994	0.208	2367.54714	-0.871
2362.58843	-0.512	2362.72487	0.090	2367.54969	-0.852
2362.58922	-0.504	2362.72555	0.070	2367.55091	-0.822
2362.59015	-0.481	2362.72931	-0.007	2367.55385	-0.783
2362.59426	-0.403	2362.73036	-0.034	2367.55460	-0.771

TABLE 12(CONT'D)

VISUAL

HEL JD (2440000+)	DMAG.	HEL JD (2440000+)	DMAG.	HEL JD (2440000+)	DMAG.
2367.55791	-0.757	2367.68514	0.718	2491.57121	-1.643
2367.55871	-0.716	2367.68429	0.719	2491.58095	-1.622
2367.56278	-0.691	2367.68950	0.655	2491.58345	-1.638
2367.56347	-0.680	2367.69020	0.653	2491.59265	-1.627
2367.56736	-0.615	2367.69361	0.618	2491.59717	-1.635
2367.56821	-0.598	2367.69443	0.603	2491.59915	-1.629
2367.57110	-0.559	2367.69857	0.551	2491.60360	-1.604
2367.57198	-0.531	2367.69905	0.545	2491.60564	-1.616
2367.57544	-0.479	2367.70254	0.502	2491.61155	-1.627
2367.57659	-0.465	2367.70359	0.501	2491.61397	-1.629
2367.57938	-0.385	2367.70688	0.418	2491.61744	-1.625
2367.58013	-0.372	2367.70780	0.417	2491.61933	-1.621
2367.58307	-0.327	2367.71034	0.336	2491.62302	-1.621
2367.58359	-0.307	2367.71301	0.293	2491.62524	-1.545
2367.58429	-0.266	2367.71363	0.270	2491.63937	-1.623
2367.58713	-0.199	2367.71512	0.161	2491.64202	-1.623
2367.58778	-0.173	2367.71695	0.140	2491.64371	-1.617
2367.58828	-0.146	2367.71747	0.140	2491.65058	-1.586
2367.58880	-0.127	2367.71971	0.094	2491.65553	-1.611
2367.59177	-0.097	2367.72041	0.080	2491.65745	-1.594
2367.59262	-0.089	2367.72362	-0.046	2491.66451	-1.610
2367.59367	-0.055	2367.72832	-0.058	2491.66535	-1.591
2367.59388	0.119	2367.72926	-0.120	2491.66939	-1.595
2367.59992	0.166	2367.72990	-0.142	2491.67276	-1.583
2367.60132	0.202	2367.73280	-0.198	2491.67727	-1.613
2367.60790	0.486	2367.73360	-0.225	2491.67804	-1.599
2367.60895	0.488	2367.73604	-0.287	2491.68372	-1.603
2367.61757	0.599	2367.73674	-0.289	2491.68564	-1.595
2367.61924	0.657	2367.73946	-0.358	2493.54203	-1.495
2367.62336	0.623	2367.74003	-0.368	2493.54523	-1.519
2367.62458	0.652	2367.74280	-0.430	2493.55125	-1.597
2367.62922	0.727	2367.74343	-0.448	2493.55376	-1.617
2367.63068	0.736	2367.74652	-0.509	2493.55589	-1.635
2367.63637	0.721	2367.74714	-0.514	2493.55994	-1.623
2367.63789	0.721	2367.75322	-0.643	2493.56729	-1.644
2367.64176	0.758	2367.75375	-0.659	2493.59781	-1.586
2367.64268	0.735	2367.75669	-0.679	2493.59845	-1.583
2367.64749	0.735	2367.75773	-0.696	2493.60007	-1.589
2367.64854	0.727	2367.76023	-0.745	2493.60495	-1.586
2367.65235	0.713	2367.76088	-0.754	2493.60561	-1.579
2367.65300	0.754	2367.76452	-0.826	2493.61371	-1.598
2367.65392	0.746	2367.76466	-0.817	2493.61453	-1.571
2367.66033	0.721	2367.76574	-0.822	2493.61882	-1.586
2367.66115	0.720	2367.76885	-0.870	2493.63453	-1.590
2367.66641	0.775	2367.76973	-0.878	2493.63543	-1.572
2367.66729	0.781	2367.79017	-1.149	2493.64390	-1.585
2367.67389	0.745	2367.79520	-1.171	2493.65175	-1.583
2367.67464	0.745	2367.80221	-1.239	2493.65235	-1.630
2367.67840	0.719	2491.55832	-1.646	2493.67053	-1.638
2367.67933	0.723	2491.57034	-1.668	2497.57757	-1.559

TABLE 12(CONT'D)

VISUAL

HEL JD (2440000+)	DMAG.	HEL JD (2440000+)	DMAG.	HEL JD (2440000+)	DMAG.
2497.57889	-1.654	2497.73920	-1.681	2497.90748	-1.645
2497.58400	-1.662	2497.73989	-1.679	2497.90845	-1.638
2497.58764	-1.653	2497.74057	-1.677	2497.91015	-1.643
2497.58896	-1.646	2497.74127	-1.675	2497.91715	-1.636
2497.59303	-1.654	2497.74196	-1.673	2507.57985	-1.635
2497.59407	-1.654	2497.74266	-1.672	2507.58688	-1.643
2497.59754	-1.650	2497.74336	-1.670	2507.59745	-1.612
2497.59876	-1.642	2497.74959	-1.659	2507.60577	-1.634
2497.60253	-1.618	2497.75629	-1.649	2507.60867	-1.600
2497.60355	-1.633	2497.75699	-1.659	2507.60941	-1.598
2497.60534	-1.593	2497.75777	-1.651	2507.61205	-1.587
2497.60901	-1.649	2497.75767	-1.657	2507.61275	-1.590
2497.61038	-1.647	2497.76654	-1.651	2507.61629	-1.592
2497.61404	-1.668	2497.77305	-1.647	2507.61915	-1.605
2497.61549	-1.651	2497.77390	-1.637	2507.61975	-1.591
2497.62451	-1.654	2497.77389	-1.633	2507.62455	-1.597
2497.62584	-1.656	2497.77998	-1.638	2507.62512	-1.615
2497.63140	-1.631	2497.78357	-1.631	2507.62571	-1.605
2497.63279	-1.659	2497.78484	-1.647	2507.62652	-1.594
2497.63671	-1.617	2497.78661	-1.663	2507.63015	-1.611
2497.63809	-1.651	2497.78971	-1.637	2507.63709	-1.630
2497.64109	-1.634	2497.79387	-1.625	2507.64011	-1.626
2497.64291	-1.651	2497.79514	-1.635	2507.64389	-1.651
2497.64720	-1.639	2497.79950	-1.637	2507.64597	-1.611
2497.64992	-1.650	2497.80065	-1.620	2507.64484	-1.594
2497.65189	-1.676	2497.80394	-1.617	2507.64781	-1.660
2497.65370	-1.639	2497.80564	-1.625	2507.64893	-1.594
2497.65702	-1.641	2497.80888	-1.628	2507.65181	-1.595
2497.66074	-1.650	2497.80997	-1.614	2507.65306	-1.598
2497.66144	-1.647	2497.81471	-1.627	2507.65147	-1.607
2497.66214	-1.647	2497.81593	-1.637	2507.66309	-1.585
2497.66842	-1.573	2497.82364	-1.637	2507.66139	-1.582
2497.66974	-1.584	2497.82478	-1.638	2507.69311	-1.611
2497.67373	-1.599	2497.82900	-1.632	2507.69642	-1.587
2497.67512	-1.652	2497.83548	-1.644	2507.69712	-1.597
2497.67981	-1.646	2497.84266	-1.642	2507.70123	-1.634
2497.68108	-1.647	2497.84371	-1.644	2507.70274	-1.605
2497.68542	-1.655	2497.84769	-1.651	2507.77894	-1.566
2497.68659	-1.657	2497.84874	-1.645	2507.75602	-1.598
2497.69160	-1.665	2497.85250	-1.655	2507.78677	-1.598
2497.69282	-1.672	2497.85378	-1.666	2509.55281	-1.568
2497.69654	-1.650	2497.85829	-1.656	2509.55301	-1.535
2497.69769	-1.649	2497.85969	-1.659	2509.55974	-1.541
2497.70180	-1.645	2497.87564	-1.662	2509.56219	-1.512
2497.70307	-1.624	2497.87666	-1.664	2509.56305	-1.568
2497.70893	-1.613	2497.87774	-1.659	2509.56565	-1.525
2497.71524	-1.641	2497.88277	-1.654	2509.56635	-1.531
2497.71651	-1.652	2497.88399	-1.641	2509.56894	-1.522
2497.72154	-1.668	2497.89977	-1.631	2509.56964	-1.521
2497.72292	-1.691	2497.90082	-1.635	2509.57191	-1.594

TABLE 12(CONT'D)

VISUAL

HEL JD (2440000+)	DMAG.	HEL JD (2440000+)	DMAG.	HEL JD (2440000+)	DMAG.
2509.57261	-1.516	2509.65819	-0.801	2518.69324	-1.505
2509.57537	-1.503	2509.66134	-0.745	2518.71567	-1.548
2509.57607	-1.506	2509.66261	-0.753	2518.72033	-1.570
2509.57632	-1.492	2509.66515	-0.706	2518.74565	-1.567
2509.57901	-1.495	2509.66565	-0.697	2518.75057	-1.614
2509.58128	-1.474	2509.66792	-0.647	2518.76565	-1.604
2509.58198	-1.471	2509.66861	-0.642	2518.77122	-1.569
2509.58422	-1.467	2509.67171	-0.602	2518.77595	-1.541
2509.58492	-1.467	2509.67240	-0.510	2518.78049	-1.597
2509.58839	-1.449	2509.67450	-0.509	2518.78495	-1.566
2509.58909	-1.455	2509.67526	-0.542	2518.78909	-1.568
2509.59135	-1.454	2509.67779	-0.478	2518.79565	-1.612
2509.59223	-1.457	2509.67849	-0.463	2518.80105	-1.618
2509.59465	-1.419	2509.68145	-0.413	2518.82677	-1.559
2509.59534	-1.411	2509.68213	-0.397	2518.82804	-1.625
2509.59779	-1.407	2509.69255	-0.113	2518.83801	-1.591
2509.59846	-1.407	2509.69525	-0.080	2518.85555	-1.612
2509.60055	-1.395	2509.69604	0.075	2518.86104	-1.574
2509.60125	-1.379	2509.70140	0.142	2518.86949	-1.592
2509.60419	-1.356	2509.70210	0.160	2518.87521	-1.590
2509.60489	-1.360	2509.70279	0.178	2524.55495	-1.591
2509.60734	-1.341	2509.70559	0.262	2524.59565	-1.[illegible]
2509.60801	-1.355	2509.71013	0.361	2524.60295	-0.[illegible]
2509.61063	-1.323	2509.71045	0.361	2524.60779	-0.[illegible]
2509.61132	-1.322	2509.71553	0.475	2524.61565	-0.715
2509.61444	-1.299	2509.71912	0.579	2524.61901	-0.681
2509.61514	-1.293	2509.72224	0.643	2524.62265	-0.[illegible]
2509.61723	-1.290	2509.72563	0.614	2524.62567	-0.[illegible]
2509.61791	-1.272	2509.72653	0.633	2524.63185	-0.637
2509.62127	-1.252	2509.73174	0.707	2524.63514	-0.[illegible]
2509.62192	-1.226	2509.73528	0.785	2524.64394	-0.104
2509.62451	-1.199	2509.73909	0.754	2524.64795	0.[illegible]
2509.62521	-1.204	2509.74273	0.765	2524.65239	0.155
2509.62763	-1.196	2509.74760	0.776	2524.65821	0.297
2509.62833	-1.207	2509.75315	0.730	2524.66162	0.386
2509.63199	-1.111	2509.75924	0.635	2524.66850	0.412
2509.63268	-1.162	2509.77208	0.767	2524.67331	0.535
2509.63857	-1.128	2518.61009	-1.515	2524.67817	0.741
2509.63927	-1.089	2518.61550	-1.569	2524.68244	0.732
2509.64171	-1.122	2518.62208	-1.546	2524.71565	0.881
2509.64239	-1.056	2518.62592	-1.539	2524.71941	0.810
2509.64553	-0.970	2518.63095	-1.537	2524.72432	0.788
2509.64623	-0.954	2518.63926	-1.560	2524.73155	0.805
2509.64847	-0.921	2518.64374	-1.558	2524.73589	0.795
2509.64917	-0.915	2518.65005	-1.567	2524.73993	0.785
2509.65161	-0.887	2518.65499	-1.638	2524.74414	0.775
2509.65229	-0.874	2518.66010	-1.591	2524.74865	0.756
2509.65455	-0.855	2518.66551	-1.625	2524.75369	0.838
2509.65525	-0.848	2518.67065	-1.581	2525.55089	-1.566
2509.65750	-0.813	2518.67528	-1.540	2525.56795	-1.571

TABLE 12(CONT'D)

VISUAL

HEL JD (2440000+)	DMAG.	HEL JD (2440000+)	DMAG.	HEL JD (2440000+)	DMAG.
2525.57154	-1.590	2642.65833	-1.584	2646.79649	-0.000
2525.58119	-1.641	2642.66048	-1.628	2646.80015	-0.265
2525.58653	-1.567	2642.66700	-1.575	2646.80377	-0.164
2525.59265	-1.596	2642.67165	-1.591	2646.80758	-0.085
2525.59572	-1.587	2642.67804	-1.604	2646.81175	0.034
2525.60011	-1.571	2642.68387	-1.603	2646.81635	0.202
2525.60305	-1.569	2642.69000	-1.590	2646.82042	0.322
2525.60699	-1.580	2642.70155	-1.617	2646.82429	0.435
2525.61275	-1.621	2642.70643	-1.610	2646.82915	0.545
2525.63162	-1.587	2642.71042	-1.600	2646.83519	0.614
2525.63616	-1.605	2642.71458	-1.587	2646.83814	0.684
2525.63988	-1.606	2642.71812	-1.596	2646.84456	0.682
2525.64354	-1.595	2642.72456	-1.613	2646.85211	0.701
2525.65167	-1.582	2642.72679	-1.581	2646.85627	0.656
2525.65675	-1.597	2642.73219	-1.607	2646.86166	0.735
2525.66216	-1.575	2642.74373	-1.618	2646.86497	0.736
2525.66538	-1.570	2642.74961	-1.629	2646.86965	0.651
2525.66879	-1.564	2642.75518	-1.622	2646.87457	0.664
2525.67435	-1.601	2642.75951	-1.621	2646.87859	0.701
2525.67765	-1.578	2642.76362	-1.621	2646.88754	0.712
2525.68779	-1.584	2642.76652	-1.632	2650.68239	-1.581
2525.69141	-1.616	2642.77300	-1.628	2650.68584	-1.606
2525.69532	-1.631	2642.77716	-1.603	2650.69109	-1.597
2525.70736	-1.569	2642.78073	-1.590	2650.69512	-1.602
2525.71178	-1.582	2642.78407	-1.630	2650.70178	-1.605
2525.71601	-1.605	2642.78758	-1.611	2650.70555	-1.601
2525.72319	-1.566	2642.79082	-1.645	2650.71115	-1.582
2525.72634	-1.552	2642.79618	-1.576	2650.71555	-1.603
2525.72980	-1.585	2642.80294	-1.582	2650.71956	-1.599
2525.73474	-1.597	2642.80982	-1.591	2650.72454	-1.592
2525.73952	-1.586	2642.81954	-1.582	2650.73076	-1.573
2525.74299	-1.611	2642.82553	-1.595	2650.73435	-1.614
2525.79587	-1.622	2642.83206	-1.569	2650.73771	-1.617
2525.80155	-1.595	2642.84978	-1.600	2650.74128	-1.603
2525.81030	-1.584	2642.86024	-1.581	2650.74651	-1.597
2525.81741	-1.605	2642.87177	-1.585	2650.75023	-1.584
2525.82115	-1.591	2646.69946	-1.442	2650.75444	-1.589
2525.82566	-1.584	2646.70609	-1.599	2650.75825	-1.619
2525.83237	-1.601	2646.71025	-1.590	2650.76545	-1.615
2525.83610	-1.602	2646.71457	-1.541	2650.76887	-1.615
2525.84049	-1.575	2646.72070	-1.547	2650.81075	-1.593
2525.84466	-1.569	2646.75005	-0.999	2650.81394	-1.581
2525.85214	-1.575	2646.76171	-0.921	2650.81901	-1.621
2525.85712	-1.570	2646.76630	-0.850	2650.82257	-1.614
2525.86542	-1.576	2646.77140	-0.796	2650.82592	-1.599
2525.87098	-1.591	2646.77744	-0.686	2650.82875	-1.592
2642.63104	-1.604	2646.78123	-0.604	2650.83239	-1.613
2642.63964	-1.592	2646.78516	-0.572	2650.83641	-1.617
2642.64518	-1.570	2646.78969	-0.573	2650.83965	-1.616
2642.65089	-1.569	2646.79011	-0.492	2650.84249	-1.626

TABLE 12(CONT'D)

VISUAL

HEL JD (2440000+)	DMAG.	HEL JD (2440000+)	DMAG.	HEL JD (2440000+)	DMAG.
2650.84955	-1.635	2698.59029	-1.477	2701.60356	-1.628
2674.71674	-1.620	2698.59517	-1.451	2701.61022	-1.643
2674.72230	-1.580	2698.60036	-1.476	2701.61536	-1.599
2674.72614	-1.601	2698.60554	-1.477	2701.61861	-1.644
2674.73175	-1.599	2698.61075	-1.491	2707.61618	-1.635
2674.73584	-1.580	2698.61631	-1.478	2707.63251	-1.643
2674.73973	-1.570	2698.62083	-1.475	2707.63804	-1.650
2674.74626	-1.556	2698.62604	-1.475	2707.64226	-1.646
2674.75321	-1.591	2698.63100	-1.468	2707.64639	-1.637
2674.76119	-1.578	2698.63681	-1.504	2707.65262	-1.635
2674.76570	-1.566	2698.64307	-1.460	2707.65681	-1.620
2674.77161	-1.587	2698.64758	-1.523	2707.66167	-1.627
2674.77784	-1.553	2698.65174	-1.517	2707.66584	-1.625
2674.78490	-1.555	2698.65590	-1.561	2707.67312	-1.629
2674.79033	-1.550	2698.66063	-1.561	2707.67835	-1.628
2674.79520	-1.551	2698.66979	-1.526	2707.68319	-1.648
2674.80233	-1.567	2698.67550	-1.512	2707.68735	-1.653
2674.80781	-1.575	2698.69028	-1.533	2707.69361	-1.[illegible]
2674.81188	-1.554	2698.69564	-1.519	2707.69777	-1.647
2674.81604	-1.559	2698.70277	-1.520	2707.7.194	-1.642
2674.82090	-1.559	2698.70694	-1.522	2707.71629	-1.[illegible]
2674.82576	-1.525	2698.71250	-1.535	2707.71446	-1.671
2674.82992	-1.542	2698.71666	-1.504	2707.71931	-1.654
2681.68430	-0.812	2698.72292	-1.548	2707.72452	-1.[illegible]
2681.69178	-0.751	2698.73022	-1.536	2707.73255	-1.654
2681.69519	-0.673	2698.73506	-1.544	2707.73667	-1.[illegible]
2681.69918	-0.589	2698.73925	-1.560	2707.74153	-1.655
2681.70225	-0.555	2698.74723	-1.527	2707.74589	-1.622
2681.70537	-0.512	2698.75209	-1.525	2707.75195	-1.632
2681.70960	-0.465	2698.75781	-1.537	2707.75611	-1.623
2681.71357	-0.420	2698.76737	-1.540	2707.76167	-1.597
2681.71392	-0.428	2698.77467	-1.549	2707.76586	-1.632
2681.72035	-0.245	2698.77954	-1.557	2707.77279	-1.594
2681.82516	0.523	2698.78402	-1.562	2707.77735	-1.610
2681.83072	0.439	2698.78956	-1.573	2707.78251	-1.638
2681.83466	0.358	2698.79419	-1.573	2707.78737	-1.610
2698.51804	-1.422	2698.79861	-1.560	2707.79154	-1.635
2698.52430	-1.414	2698.80414	-1.544	2707.79640	-1.607
2698.52846	-1.465	2698.80796	-1.550	2707.80745	-1.564
2698.53332	-1.443	2701.53914	-1.593	2707.81235	-1.593
2698.53818	-1.454	2701.54575	-1.574	2707.81801	-1.560
2698.54304	-1.441	2701.55048	-1.568	2707.82354	-1.572
2698.54790	-1.454	2701.55420	-1.556	2707.83320	-1.577
2698.55207	-1.398	2701.55986	-1.500	2707.83835	-1.565
2698.56007	-1.441	2701.56402	-1.488	2707.84432	-1.607
2698.56458	-1.439	2701.56853	-1.452	2707.85192	-1.578
2698.57396	-1.455	2701.58474	-1.356	2707.85815	-1.575
2698.57812	-1.450	2701.58925	-1.336	2707.86444	-1.559
2698.58228	-1.459	2701.59337	-1.271	2707.86930	-1.545
2698.58610	-1.470	2701.59760	-1.195	2707.87435	-1.571

TABLE 12(CONT'D)

VISUAL

HEL JD (2440000+)	DMAG.	HEL JD (2440000+)	DMAG.	HEL JD (2440000+)	DMAG.
2707.87902	-1.580	2812.56975	-1.578	2817.65746	-1.555
2707.88458	-1.558	2812.57404	-1.588	2817.64125	-1.567
2707.89037	-1.537	2812.58059	-1.572	2817.64795	-1.590
2707.90123	-1.542	2812.58516	-1.582	2817.65222	-1.558
2707.91026	-1.558	2812.58977	-1.575	2817.65956	-1.543
2707.91442	-1.535	2812.59366	-1.579	2817.66032	-1.544
2709.61375	-1.569	2812.59770	-1.574	2817.66866	-1.537
2709.61873	-1.594	2812.61141	-1.574	2817.67252	-1.554
2709.62280	-1.587	2812.62397	-1.559	2817.67766	-1.557
2709.62706	-1.569	2812.62790	-1.551	2817.68349	-1.510
2709.63344	-1.590	2812.63168	-1.551	2817.68786	-1.515
2709.63706	-1.597	2812.63554	-1.554	2817.69286	-1.549
2709.64272	-1.583	2812.64217	-1.569	2817.71215	-1.534
2709.64743	-1.561	2812.64564	-1.555	2817.72236	-1.547
2709.65152	-1.615	2812.64958	-1.538	2817.72759	-1.531
2709.65693	-1.551	2812.65329	-1.570	2817.73356	-1.561
2709.66124	-1.569	2812.65721	-1.568	2817.73436	-1.538
2709.66516	-1.559	2812.66399	-1.559	2817.74024	-1.572
2709.67032	-1.554	2812.66743	-1.553	2817.74456	-1.568
2709.68056	-1.566	2812.67211	-1.545	2817.74895	-1.557
2709.68408	-1.574	2812.67578	-1.535	2817.77099	-1.558
2709.68899	-1.568	2812.68598	-1.553	2817.78421	-1.553
2709.69477	-1.594	2817.51033	-1.597	2817.78855	-1.579
2709.69826	-1.556	2817.52206	-1.600	2817.79287	-1.627
2709.70956	-1.547	2817.52552	-1.615	2817.80021	-1.610
2709.71404	-1.568	2817.52951	-1.606	2817.80437	-1.615
2709.71861	-1.609	2817.53318	-1.598	2817.80911	-1.659
2709.72247	-1.606	2817.53984	-1.592	2817.81931	-1.656
2709.72649	-1.579	2817.54360	-1.586	2817.82347	-1.577
2709.73107	-1.570	2817.54729	-1.585	2817.83372	-1.605
2709.74152	-1.580	2817.55235	-1.580	2824.51555	-1.593
2709.74556	-1.617	2817.55597	-1.587	2824.52153	-1.615
2709.74967	-1.550	2817.55996	-1.567	2824.52512	-1.610
2709.75346	-1.601	2817.56374	-1.583	2824.52995	-1.626
2709.75790	-1.585	2817.56791	-1.584	2824.53327	-1.625
2709.76368	-1.623	2817.57172	-1.570	2824.53661	-1.630
2709.76772	-1.606	2817.57638	-1.570	2824.54037	-1.641
2709.78796	-1.597	2817.58219	-1.569	2824.54674	-1.605
2709.79288	-1.567	2817.58583	-1.570	2824.55132	-1.627
2709.80063	-1.549	2817.58960	-1.577	2824.55431	-1.629
2812.52253	-1.605	2817.59078	-1.581	2824.55822	-1.630
2812.52719	-1.599	2817.60089	-1.559	2824.56275	-1.624
2812.53111	-1.600	2817.60488	-1.550	2824.55591	-1.653
2812.53829	-1.590	2817.60857	-1.550	2824.56922	-1.631
2812.54160	-1.606	2817.61218	-1.547	2824.57231	-1.629
2812.54594	-1.590	2817.61577	-1.572	2824.57870	-1.624
2812.55005	-1.595	2817.62039	-1.573	2824.58235	-1.615
2812.55541	-1.599	2817.62410	-1.570	2824.58655	-1.615
2812.56247	-1.579	2817.62782	-1.570	2824.59054	-1.614
2812.56586	-1.582	2817.63290	-1.562	2824.59426	-1.603

TABLE 12(CONT'D)

VISUAL

HEL JD (2440000+)	DMAG.	HEL JD (2440000+)	DMAG.	HEL JD (2440000+)	DMAG.
2824.60375	-1.618	2840.69046	-1.537	2856.80097	-1.621
2824.60739	-1.625	2840.69350	-1.552	2856.87207	-1.612
2824.61076	-1.621	2856.60351	-1.567	2856.87628	-1.613
2824.61415	-1.628	2856.60591	-1.591	2856.88174	-1.596
2824.62051	-1.638	2856.61254	-1.533	2856.88528	-1.635
2824.62407	-1.626	2856.61663	-1.556	2856.88872	-1.618
2824.62831	-1.591	2856.62261	-1.586	2856.89431	-1.625
2824.63210	-1.641	2856.63525	-1.562	2856.89736	-1.597
2824.63551	-1.619	2856.64135	-1.565	2856.90124	-1.613
2824.65204	-1.620	2856.64874	-1.563	2856.90666	-1.614
2824.65703	-1.648	2856.65210	-1.601	2856.91345	-1.615
2824.66092	-1.629	2856.65587	-1.602	2856.91677	-1.621
2824.66548	-1.636	2856.66136	-1.605	2856.92231	-1.615
2824.66905	-1.618	2856.66509	-1.586	2856.92345	-1.610
2824.67336	-1.625	2856.66853	-1.566	2873.57406	-1.533
2824.67757	-1.593	2856.67472	-1.584	2873.57855	-1.538
2840.55584	-1.611	2856.67536	-1.570	2873.58196	-1.533
2840.55998	-1.620	2856.68202	-1.538	2873.58542	-1.588
2840.56354	-1.634	2856.68574	-1.593	2873.59207	-1.610
2840.56718	-1.627	2856.69768	-1.566	2873.59548	-1.135
2840.57407	-1.594	2856.70159	-1.599	2873.59886	-1.152
2840.66985	-1.554	2856.70523	-1.609	2873.60244	-1.143
2840.67484	-1.610	2856.70902	-1.663	2873.60815	-1.598
2840.67895	-1.607	2856.72520	-1.556	2873.61254	-1.670
2840.68271	-1.592	2856.73041	-1.566	2873.61565	-1.552
2840.75920	-1.575	2856.73457	-1.581	2873.62545	-0.670
2840.76409	-1.610	2856.73891	-1.565	2873.63251	-0.797
2840.76830	-1.613	2856.74203	-1.665	2873.63617	-0.711
2840.77231	-1.566	2856.74654	-1.625	2873.64019	-0.655
2840.77610	-1.576	2856.75160	-1.618	2873.64677	-0.592
2840.77982	-1.563	2856.76554	-1.604	2873.65355	-0.527
2840.78635	-1.553	2856.76868	-1.543	2873.65486	-0.595
2840.78942	-1.572	2856.77195	-1.621	2873.65972	-0.258
2840.79261	-1.592	2856.77551	-1.585	2873.76824	0.796
2840.79617	-1.542	2856.76952	-1.603	2873.79443	0.553
2840.82419	-1.571	2856.79341	-1.622	2873.79723	0.563
2840.82856	-1.528	2856.79912	-1.629	2873.83333	0.450
2840.83205	-1.609	2856.80912	-1.621	2873.83666	0.230
2840.83654	-1.549	2856.81235	-1.586	2873.81029	0.105
2840.83973	-1.574	2856.81667	-1.583	2873.81469	0.001
2840.84294	-1.500	2856.81934	-1.615	2873.81934	-0.172
2840.84606	-1.550	2856.82375	-1.576	2873.82355	-0.163
2840.85083	-1.529	2856.82961	-1.590	2873.82627	-0.152
2840.86005	-1.519	2856.83290	-1.596	2873.83118	-0.451
2840.86316	-1.555	2856.83679	-1.613	2873.83841	-0.611
2840.86728	-1.591	2856.84093	-1.612	2873.84366	-0.700
2840.87156	-1.547	2856.84694	-1.634	2873.84666	-0.783
2840.87470	-1.554	2856.85048	-1.622	2887.77566	-1.586
2840.87780	-1.540	2856.85394	-1.603	2887.77909	-1.591
2840.88712	-1.557	2856.85746	-1.605	2887.78560	-1.619

TABLE 12(CONT'D)

VISUAL

HEL JD (2440000+)	DMAG.	HEL JD (2440000+)	DMAG.	HEL JD (2440000+)	DMAG.
2887.78929	-1.609	2895.81560	-1.534	2903.76865	-0.695
2887.79260	-1.613	2895.81862	-1.557	2903.77159	-0.753
2887.79627	-1.636	2895.82752	-1.591	2903.77475	-0.782
2887.80068	-1.666	2895.83081	-1.572	2903.77819	-0.881
2887.80492	-1.615	2895.83562	-1.587	2903.78067	-1.082
2887.80833	-1.662	2895.84293	-1.563	2903.83492	-1.442
2887.82304	-1.619	2895.84622	-1.558	2918.65104	0.596
2887.83489	-1.609	2895.84964	-1.535	2918.65556	0.703
2887.84237	-1.611	2895.85278	-1.549	2918.65932	0.820
2887.84905	-1.618	2895.85584	-1.567	2918.66455	0.794
2887.85291	-1.654	2895.85843	-1.548	2918.66656	0.025
2887.85660	-1.648	2895.85477	-1.515	2918.70137	-0.144
2887.85999	-1.626	2895.86846	-1.524	2918.70671	-0.241
2887.86715	-1.615	2895.87034	-1.558	2918.71224	-0.393
2887.87056	-1.575	2895.87970	-1.543	2918.71585	-0.455
2887.87393	-1.613	2903.56474	-0.778	2918.71942	-0.529
2887.88283	-1.605	2903.56816	-0.715	2918.72319	-0.515
2887.89390	-1.657	2903.57136	-0.667	2918.73555	-0.871
2887.89780	-1.674	2903.57439	-0.611	2918.73714	-0.879
2895.74408	-1.543	2903.58110	-0.478	2918.74989	-1.051
2895.74904	-1.557	2903.58451	-0.433	2918.75336	-1.098
2895.75241	-1.568	2903.58763	-0.387	2918.75654	-1.110
2895.75659	-1.571	2903.59065	-0.294	2918.76025	-1.110
2895.76056	-1.584	2903.59374	-0.225	2918.76415	-1.172
2895.76382	-1.573	2903.59822	-0.095	2918.77406	-1.330
2895.76749	-1.573	2903.60154	0.078	2918.77835	-1.324
2895.77048	-1.572	2903.60403	0.186	2918.78417	-1.311
2895.76015	-1.599	2903.60892	0.253	2918.78785	-1.424
2895.78571	-1.570	2903.72909	0.348	2918.79137	-1.397
2895.78690	-1.578	2903.73327	0.248	2918.79554	-1.440
2895.79222	-1.540	2903.73597	0.160	2918.80545	-1.476
2895.79630	-1.554	2903.74165	-0.029	2918.80872	-1.482
2895.79902	-1.565	2903.74402	-0.070	2918.81192	-1.504
2895.80301	-1.559	2903.74776	-0.159	2918.81515	-1.510
2895.80638	-1.579	2903.75761	-0.428	2918.82229	-1.528
2895.80957	-1.572	2903.75992	-0.506	2918.82635	-1.532

TABLE 12(CONT'D)

BLUE

HEL JD (2440000+)	DMAG.	HEL JD (2440000+)	DMAG.	HEL JD (2440000+)	DMAG.
2352.53417	-2.012	2362.59015	-0.882	2362.72931	-0.255
2352.53798	-2.026	2362.59426	-0.765	2362.73035	-0.283
2352.54285	-1.961	2362.59536	-0.753	2362.73118	-0.364
2352.54980	-1.915	2362.59660	-0.616	2362.73484	-0.423
2352.55484	-1.869	2362.59952	-0.589	2362.73582	-0.459
2352.55935	-1.828	2362.60057	-0.509	2362.73991	-0.594
2352.56369	-1.747	2362.60363	-0.443	2362.74424	-0.717
2352.56853	-1.703	2362.60451	-0.417	2362.74504	-0.739
2352.57443	-1.635	2362.60565	-0.358	2362.74953	-0.845
2352.59655	-1.293	2362.60850	-0.268	2362.74990	-0.851
2352.60151	-1.191	2362.60919	-0.244	2362.75065	-0.878
2352.61180	-0.941	2362.61007	-0.220	2362.75401	-0.954
2352.61911	-0.755	2362.61401	-0.116	2362.75585	-0.977
2352.62444	-0.570	2362.61403	-0.080	2362.75945	-1.050
2352.63015	-0.345	2362.61538	-0.041	2362.75952	-1.077
2352.63549	-0.132	2362.61914	0.120	2362.76064	-1.182
2352.64242	0.155	2362.62211	0.228	2362.75912	-1.256
2352.64823	0.385	2362.62570	0.361	2362.77265	-1.321
2352.65498	0.714	2362.62657	0.421	2362.77549	-1.338
2352.66436	0.956	2362.62759	0.475	2362.77601	-1.454
2352.67201	0.918	2362.63118	0.636	2362.78042	-1.571
2362.50837	-1.958	2362.63210	0.677	2362.79056	-1.853
2362.51319	-1.951	2362.63279	0.703	2362.80215	-1.715
2362.51822	-1.914	2362.63629	0.827	2362.81075	-1.811
2362.52401	-1.858	2362.63744	0.845	2362.81664	-1.848
2362.52707	-1.827	2362.63871	0.854	2362.82534	-1.917
2362.53036	-1.806	2362.64060	0.869	2362.82602	-1.917
2362.53517	-1.757	2362.64809	0.916	2367.50542	-1.973
2362.53911	-1.715	2362.64878	0.944	2367.50745	-1.925
2362.54253	-1.688	2362.64966	0.977	2367.50845	-1.921
2362.54594	-1.655	2362.66651	0.957	2367.51569	-1.872
2362.54936	-1.618	2362.66741	0.956	2367.51451	-1.856
2362.54963	-1.615	2362.67952	0.982	2367.51775	-1.811
2362.55081	-1.487	2362.68037	0.981	2367.51867	-1.795
2362.56001	-1.440	2362.68835	0.963	2367.52214	-1.755
2362.56325	-1.395	2362.68773	0.945	2367.52536	-1.736
2362.56439	-1.379	2362.69206	0.869	2367.52603	-1.706
2362.56753	-1.330	2362.69315	0.841	2367.52705	-1.691
2362.56828	-1.322	2362.69675	0.788	2367.53029	-1.655
2362.57065	-1.279	2362.69982	0.722	2367.53154	-1.643
2362.57130	-1.269	2362.70069	0.704	2367.53475	-1.586
2362.57394	-1.234	2362.70762	0.562	2367.53603	-1.556
2362.57499	-1.223	2362.70872	0.478	2367.53874	-1.525
2362.57928	-1.159	2362.71258	0.350	2367.53949	-1.519
2362.58025	-1.119	2362.71380	0.303	2367.54263	-1.478
2362.58426	-1.024	2362.71839	0.130	2367.54375	-1.454
2362.58471	-1.012	2362.71931	0.098	2367.54632	-1.407
2362.58541	-0.997	2362.71994	0.072	2367.54714	-1.398
2362.58843	-0.928	2362.72467	-0.116	2367.54965	-1.371
2362.58922	-0.903	2362.72555	-0.141	2367.55091	-1.359

TABLE 12(CONT'D)

BLUE

HEL JD (2440000+)	DMAG.	HEL JD (2440000+)	DMAG.	HEL JD (2440000+)	DMAG.
2367.55385	-1.294	2367.67840	0.937	2491.55832	-2.219
2367.55460	-1.266	2367.67955	0.955	2491.57034	-2.237
2367.55791	-1.255	2367.68314	0.965	2491.57121	-2.227
2367.55871	-1.217	2367.68429	0.960	2491.58090	-2.251
2367.56278	-1.182	2367.68950	0.813	2491.58203	-2.251
2367.56347	-1.174	2367.69020	0.806	2491.58345	-2.245
2367.56756	-1.084	2367.69361	0.754	2491.59202	-2.254
2367.56821	-1.074	2367.69443	0.737	2491.59717	-2.240
2367.57110	-1.003	2367.69837	0.643	2491.59915	-2.243
2367.57198	-0.985	2367.69905	0.623	2491.60307	-2.220
2367.57544	-0.911	2367.70254	0.548	2491.60564	-2.242
2367.57659	-0.881	2367.70339	0.526	2491.61153	-2.249
2367.57938	-0.776	2367.70688	0.432	2491.61397	-2.257
2367.58018	-0.757	2367.70786	0.394	2491.61744	-2.244
2367.58307	-0.675	2367.71034	0.279	2491.61955	-2.253
2367.58359	-0.652	2367.71161	0.185	2491.62302	-2.244
2367.58429	-0.631	2367.71363	0.163	2491.62524	-2.229
2367.58713	-0.556	2367.71512	0.044	2491.63937	-2.252
2367.58776	-0.508	2367.71695	0.018	2491.64202	-2.245
2367.58828	-0.473	2367.71747	-0.011	2491.64371	-2.221
2367.58880	-0.445	2367.71971	-0.087	2491.65056	-2.149
2367.59177	-0.376	2367.72041	-0.108	2491.65255	-2.118
2367.59262	-0.349	2367.72362	-0.319	2491.65745	-2.242
2367.59367	-0.312	2367.72632	-0.341	2491.66456	-2.251
2367.59688	-0.031	2367.72925	-0.435	2491.66552	-2.260
2367.59992	0.010	2367.72990	-0.456	2491.66939	-2.253
2367.60132	0.057	2367.73260	-0.550	2491.67270	-2.222
2367.60790	0.430	2367.73363	-0.580	2491.67727	-2.207
2367.60895	0.474	2367.73604	-0.664	2491.67854	-2.209
2367.61757	0.729	2367.73674	-0.683	2491.68572	-2.231
2367.61924	0.790	2367.73940	-0.763	2491.68864	-2.240
2367.62336	0.828	2367.74003	-0.784	2493.54525	-2.155
2367.62458	0.840	2367.74280	-0.864	2493.58729	-2.200
2367.62922	0.920	2367.74343	-0.882	2493.59781	-2.217
2367.63060	0.952	2367.74652	-0.955	2493.59840	-2.213
2367.63637	0.957	2367.74714	-0.969	2493.60307	-2.208
2367.63789	0.932	2367.75322	-1.119	2493.60496	-2.222
2367.64176	0.970	2367.75375	-1.124	2493.60561	-2.223
2367.64268	0.977	2367.75669	-1.175	2493.61371	-2.235
2367.64749	0.953	2367.75773	-1.197	2493.61458	-2.240
2367.64854	0.951	2367.76023	-1.258	2493.61832	-2.242
2367.65235	0.977	2367.76088	-1.272	2493.63453	-2.145
2367.65300	0.976	2367.76452	-1.354	2493.64395	-2.196
2367.65392	0.978	2367.76480	-1.365	2493.66175	-2.292
2367.66033	0.944	2367.76574	-1.378	2493.66253	-2.304
2367.66115	0.949	2367.76885	-1.427	2493.67055	-2.242
2367.66641	1.000	2367.76973	-1.442	2497.58396	-2.325
2367.66729	0.995	2367.79017	-1.731	2497.59306	-2.293
2367.67389	0.948	2367.79526	-1.769	2497.59407	-2.296
2367.67464	0.942	2367.80221	-1.850	2497.59754	-2.298

TABLE 12(CONT'D)

BLUE

HEL JD (2440000+)	DMAG.	HEL JD (2440000+)	DMAG.	HEL JD (2440000+)	DMAG.
2497.59876	-2.297	2497.74959	-2.290	2507.60867	-2.218
2497.60253	-2.285	2497.75029	-2.290	2507.60941	-2.216
2497.60355	-2.285	2497.75099	-2.289	2507.61203	-2.214
2497.60534	-2.291	2497.75777	-2.271	2507.61275	-2.231
2497.60901	-2.277	2497.76767	-2.271	2507.61829	-2.222
2497.61038	-2.281	2497.76854	-2.266	2507.61916	-2.222
2497.61404	-2.291	2497.77305	-2.282	2507.61975	-2.223
2497.61549	-2.288	2497.77390	-2.268	2507.62439	-2.231
2497.62451	-2.302	2497.77889	-2.279	2507.62512	-2.232
2497.62584	-2.290	2497.77998	-2.276	2507.62671	-2.233
2497.63140	-2.299	2497.78357	-2.270	2507.63256	-2.240
2497.63279	-2.289	2497.78484	-2.278	2507.63316	-2.239
2497.63671	-2.290	2497.78861	-2.244	2507.63709	-2.240
2497.63800	-2.286	2497.78971	-2.243	2507.63810	-2.239
2497.64169	-2.282	2497.79387	-2.254	2507.64069	-2.212
2497.64291	-2.281	2497.79514	-2.255	2507.64397	-2.239
2497.64720	-2.292	2497.79950	-2.267	2507.64464	-2.233
2497.64992	-2.305	2497.80065	-2.268	2507.64781	-2.219
2497.65189	-2.301	2497.80594	-2.271	2507.64869	-2.219
2497.65570	-2.289	2497.80604	-2.271	2507.65182	-2.232
2497.65702	-2.285	2497.80988	-2.259	2507.65302	-2.234
2497.66074	-2.303	2497.80997	-2.263	2507.65817	-2.231
2497.66144	-2.306	2497.81471	-2.263	2507.66039	-2.214
2497.66214	-2.313	2497.81593	-2.261	2507.66109	-2.217
2497.66842	-2.292	2497.82364	-2.264	2507.66511	-2.251
2497.66974	-2.298	2497.82476	-2.264	2507.66942	-2.251
2497.67373	-2.291	2497.82900	-2.270	2507.67712	-2.246
2497.67512	-2.284	2497.83548	-2.281	2507.70125	-2.221
2497.67981	-2.284	2497.84266	-2.275	2507.70274	-2.212
2497.68108	-2.277	2497.84371	-2.267	2507.77394	-2.231
2497.68542	-2.298	2497.84769	-2.272	2507.78042	-2.217
2497.68659	-2.296	2497.84874	-2.274	2507.78077	-2.216
2497.69160	-2.306	2497.85256	-2.290	2509.55281	-2.165
2497.69282	-2.305	2497.85578	-2.282	2509.55361	-2.176
2497.69654	-2.318	2497.85829	-2.278	2509.55974	-2.151
2497.69769	-2.313	2497.85969	-2.271	2509.56219	-2.122
2497.70180	-2.293	2497.87564	-2.293	2509.56305	-2.113
2497.70307	-2.281	2497.87665	-2.291	2509.56365	-2.125
2497.70893	-2.291	2497.87774	-2.288	2509.56665	-2.128
2497.71524	-2.277	2497.88277	-2.272	2509.56894	-2.131
2497.71651	-2.302	2497.88399	-2.278	2509.56964	-2.123
2497.72154	-2.346	2497.89977	-2.245	2509.57191	-2.134
2497.72292	-2.352	2497.90082	-2.249	2509.57201	-2.129
2497.73920	-2.291	2497.90748	-2.271	2509.57537	-2.134
2497.73989	-2.289	2497.90843	-2.272	2509.57607	-2.132
2497.74057	-2.286	2497.91610	-2.277	2509.57832	-2.128
2497.74127	-2.284	2497.91715	-2.279	2509.57901	-2.126
2497.74196	-2.281	2507.57985	-2.246	2509.58128	-2.099
2497.74266	-2.279	2507.58588	-2.230	2509.58198	-2.095
2497.74336	-2.277	2507.60577	-2.215	2509.58422	-2.081

TABLE 12(CONT'D)

BLUE

HEL JD (2440000+)	DMAG.	HEL JD (2440000+)	DMAG.	HEL JD (2440000+)	DMAG.
2509.58492	-2.074	2509.67240	-1.057	2518.75049	-2.159
2509.58839	-2.062	2509.67450	-0.997	2518.75495	-2.174
2509.58909	-2.065	2509.67520	-0.980	2518.75909	-2.193
2509.59135	-2.057	2509.67779	-0.884	2518.76062	-2.205
2509.59223	-2.049	2509.67849	-0.858	2518.80109	-2.213
2509.59465	-2.020	2509.68143	-0.796	2518.80697	-2.231
2509.59534	-2.020	2509.68213	-0.773	2518.81340	-2.249
2509.59779	-2.017	2509.69255	-0.593	2518.81781	-2.234
2509.59846	-2.008	2509.69325	-0.593	2518.82277	-2.205
2509.60055	-2.000	2509.69604	-0.079	2518.82504	-2.196
2509.60125	-1.995	2509.70140	-0.053	2518.83067	-2.217
2509.60419	-1.957	2509.70210	-0.008	2518.83538	-2.205
2509.60489	-1.955	2509.70279	0.036	2518.83914	-2.243
2509.60734	-1.952	2509.70559	0.127	2518.84949	-2.258
2509.60801	-1.942	2509.71010	0.218	2518.87525	-2.292
2509.61063	-1.918	2509.71045	0.535	2518.88305	-2.277
2509.61132	-1.910	2509.71553	0.592	2518.88837	-2.276
2509.61444	-1.898	2509.71912	0.709	2524.58463	-1.977
2509.61514	-1.892	2509.72224	0.866	2524.59305	-1.983
2509.61723	-1.872	2509.72586	1.078	2524.60595	-1.947
2509.61791	-1.863	2509.72658	1.120	2524.60779	-1.958
2509.62127	-1.865	2509.73174	1.008	2524.61555	-1.931
2509.62192	-1.792	2509.73528	1.061	2524.61861	-1.956
2509.62451	-1.777	2509.73909	1.059	2524.62205	-1.918
2509.62521	-1.768	2509.74273	1.075	2524.62867	-1.909
2509.62763	-1.756	2509.74760	1.072	2524.63195	-1.894
2509.62833	-1.754	2509.75315	1.058	2524.63614	-1.870
2509.63199	-1.687	2509.75924	1.012	2524.64294	-1.850
2509.63268	-1.675	2509.77200	1.127	2524.64795	-1.844
2509.63857	-1.553	2518.58508	-2.159	2524.65289	-1.874
2509.63927	-1.550	2518.61009	-2.130	2524.65842	-1.852
2509.64171	-1.504	2518.61550	-2.175	2524.65182	-1.835
2509.64239	-1.553	2518.62208	-2.182	2524.65855	-1.892
2509.64553	-1.504	2518.62592	-2.180	2524.67331	-1.781
2509.64623	-1.485	2518.63096	-2.179	2524.67817	-1.895
2509.64847	-1.470	2518.63926	-2.183	2524.68244	-1.867
2509.64917	-1.457	2518.64374	-2.159	2524.71085	-1.853
2509.65161	-1.418	2518.65005	-2.203	2524.71941	-1.821
2509.65229	-1.406	2518.65499	-2.197	2524.72431	-1.884
2509.65455	-1.389	2518.66010	-2.179	2524.73153	-1.827
2509.65525	-1.375	2518.66551	-2.152	2524.73589	-1.811
2509.65750	-1.329	2518.67528	-2.203	2524.73995	-1.795
2509.65819	-1.323	2518.71500	-2.177	2524.74414	-1.791
2509.66154	-1.262	2518.72083	-2.168	2524.74803	-1.813
2509.66201	-1.246	2518.74803	-2.174	2524.75389	-1.850
2509.66515	-1.183	2518.75585	-2.165	2525.56089	-2.194
2509.66585	-1.170	2518.76067	-2.219	2525.56796	-2.170
2509.66792	-1.117	2518.76506	-2.199	2525.57154	-2.207
2509.66861	-1.112	2518.77122	-2.200	2525.55119	-2.200
2509.67171	-1.053	2518.77595	-2.222	2525.58056	-2.219

TABLE 12(CONT'D)

BLUE

HEL JD (2440000+)	DMAG.	HEL JD (2440000+)	DMAG.	HEL JD (2440000+)	DMAG.
2525.59263	-2.171	2642.70643	-2.231	2646.82915	0.000
2525.59572	-2.113	2642.71042	-2.252	2646.83319	0.780
2525.60011	-2.111	2642.71456	-2.229	2646.83812	0.871
2525.60305	-2.154	2642.71812	-2.226	2646.84456	0.880
2525.60699	-2.172	2642.72456	-2.216	2646.85211	0.914
2525.61275	-2.127	2642.72870	-2.223	2646.85627	0.890
2525.63162	-2.179	2642.73219	-2.208	2646.86165	0.922
2525.63615	-2.173	2642.74373	-2.190	2646.86497	0.908
2525.63988	-2.169	2642.74961	-2.150	2646.86955	0.915
2525.64334	-2.155	2642.75318	-2.140	2646.87457	0.915
2525.64708	-2.218	2642.75951	-2.129	2646.87855	0.910
2525.65107	-2.179	2642.76302	-2.135	2646.88754	0.897
2525.65675	-2.173	2642.76652	-2.141	2650.66239	-2.243
2525.66215	-2.148	2642.77300	-2.140	2650.66583	-2.245
2525.66538	-2.178	2642.77716	-2.138	2650.69169	-2.250
2525.66879	-2.151	2642.78070	-2.119	2650.69516	-2.234
2525.67435	-2.167	2642.78407	-2.112	2650.70195	-2.257
2525.67705	-2.184	2642.78753	-2.122	2650.70558	-2.247
2525.68779	-2.190	2642.79082	-2.124	2650.71115	-2.267
2525.69141	-2.232	2642.79815	-2.255	2650.71555	-2.253
2525.69532	-2.223	2642.80294	-2.242	2650.71956	-2.261
2525.70735	-2.186	2642.80962	-2.270	2650.72432	-2.237
2525.71178	-2.186	2642.81954	-2.249	2650.73076	-2.248
2525.71601	-2.141	2642.82553	-2.255	2650.73400	-2.279
2525.72319	-2.174	2642.83205	-2.252	2650.73771	-2.247
2525.72634	-2.197	2642.84975	-2.253	2650.74123	-2.245
2525.72980	-2.207	2642.85624	-2.251	2650.74481	-2.254
2525.73474	-2.166	2642.87177	-2.201	2650.75025	-2.281
2525.74299	-2.172	2646.69946	-2.079	2650.75444	-2.246
2525.79587	-2.269	2646.70609	-2.057	2650.75825	-2.244
2525.80158	-2.194	2646.71025	-2.045	2650.76454	-2.252
2525.81030	-2.197	2646.71457	-2.064	2650.76867	-2.234
2525.81741	-2.207	2646.72070	-1.972	2650.81075	-2.226
2525.82115	-2.217	2646.75603	-1.597	2650.81594	-2.212
2525.82566	-2.220	2646.76171	-1.565	2650.81961	-2.256
2525.83237	-2.229	2646.76656	-1.456	2650.82257	-2.257
2525.83610	-2.225	2646.77146	-1.309	2650.82592	-2.248
2525.84049	-2.194	2646.77744	-1.234	2650.82878	-2.250
2642.63104	-2.242	2646.78123	-1.198	2650.83233	-2.239
2642.63964	-2.227	2646.78510	-1.115	2650.83641	-2.248
2642.64518	-2.205	2646.78569	-1.101	2650.83965	-2.218
2642.65089	-2.251	2646.79011	-0.999	2650.84249	-2.232
2642.65630	-2.237	2646.79549	-0.813	2650.84955	-2.229
2642.66040	-2.246	2646.80315	-0.708	2674.71074	-2.199
2642.66768	-2.207	2646.80577	-0.572	2674.72230	-2.165
2642.67185	-2.214	2646.80758	-0.407	2674.72614	-2.191
2642.67804	-2.223	2646.81175	-0.217	2674.73175	-2.162
2642.68387	-2.251	2646.81636	-0.005	2674.73584	-2.158
2642.69606	-2.228	2646.82042	0.214	2674.73975	-2.151
2642.70155	-2.235	2646.82429	0.405	2674.74625	-2.147

TABLE 12(CONT'D)

BLUE

HEL JD (2440000+)	DMAG.	HEL JD (2440000+)	DMAG.	HEL JD (2440000+)	DMAG.
2674.75321	-2.166	2698.65160	-2.020	2707.64639	-2.198
2674.76119	-2.146	2698.65681	-2.040	2707.65252	-2.172
2674.76570	-2.145	2698.64307	-2.041	2707.65681	-2.180
2674.77161	-2.173	2698.64758	-2.050	2707.66167	-2.206
2674.77784	-2.141	2698.65174	-2.069	2707.66584	-2.177
2674.78490	-2.112	2698.65590	-2.060	2707.67316	-2.205
2674.79033	-2.111	2698.66063	-2.078	2707.67933	-2.217
2674.79520	-2.122	2698.65979	-2.086	2707.68515	-2.223
2674.80233	-2.122	2698.67535	-2.065	2707.68755	-2.227
2674.80781	-2.121	2698.69028	-2.059	2707.69381	-2.223
2674.81188	-2.102	2698.69584	-2.070	2707.69777	-2.231
2674.81604	-2.115	2698.70277	-2.112	2707.70194	-2.245
2674.82090	-2.104	2698.70694	-2.066	2707.71023	-2.272
2674.82576	-2.117	2698.71250	-2.098	2707.71445	-2.237
2674.82992	-2.111	2698.71666	-2.079	2707.71951	-2.228
2681.68430	-1.268	2698.72292	-2.100	2707.72482	-2.229
2681.69178	-1.161	2698.73022	-2.087	2707.73256	-2.226
2681.69519	-1.083	2698.73506	-2.127	2707.73667	-2.212
2681.69918	-1.062	2698.73925	-2.134	2707.74155	-2.215
2681.70225	-0.952	2698.74723	-2.122	2707.74564	-2.239
2681.70537	-0.882	2698.75209	-2.107	2707.75196	-2.220
2681.70900	-0.769	2698.75681	-2.120	2707.75611	-2.214
2681.71357	-0.664	2698.76737	-2.121	2707.76167	-2.193
2681.71392	-0.653	2698.77467	-2.147	2707.76584	-2.210
2681.72035	-0.529	2698.77954	-2.128	2707.77479	-2.192
2681.82516	0.038	2698.78402	-2.144	2707.77896	-2.190
2681.83072	0.038	2698.78950	-2.127	2707.78231	-2.214
2681.83466	0.096	2698.79410	-2.135	2707.78727	-2.211
2698.51604	-1.952	2698.79801	-2.132	2707.79154	-2.256
2698.52430	-1.941	2698.80414	-2.116	2707.79540	-2.187
2698.52846	-1.937	2698.80793	-2.110	2707.80749	-2.166
2698.53332	-1.973	2701.53914	-2.185	2707.81235	-2.204
2698.53818	-1.987	2701.54573	-2.174	2707.81861	-2.195
2698.54304	-1.980	2701.55048	-2.176	2707.82234	-2.171
2698.54790	-1.989	2701.55420	-2.142	2707.83320	-2.187
2698.55207	-1.966	2701.55986	-2.100	2707.83802	-2.139
2698.56007	-1.998	2701.56402	-2.089	2707.84434	-2.191
2698.56458	-2.013	2701.56853	-2.053	2707.85192	-2.203
2698.57396	-2.045	2701.56474	-1.935	2707.85815	-2.206
2698.57812	-2.040	2701.56925	-1.900	2707.85444	-2.165
2698.58228	-2.040	2701.59337	-1.646	2707.86933	-2.141
2698.58610	-2.054	2701.59760	-1.784	2707.87485	-2.181
2698.59029	-2.027	2701.60356	-1.723	2707.87902	-2.209
2698.59617	-1.964	2701.61022	-1.606	2707.88495	-2.217
2698.60086	-2.024	2701.61530	-1.538	2707.89537	-2.197
2698.60554	-2.045	2701.61860	-1.484	2707.90123	-2.211
2698.61075	-2.070	2707.61618	-2.246	2707.91020	-2.172
2698.61631	-2.056	2707.63251	-2.226	2707.91442	-2.176
2698.62083	-2.059	2707.63564	-2.243	2709.61575	-2.222
2698.62604	-2.045	2707.64223	-2.244	2709.61875	-2.205

TABLE 12(CONT'D)

BLUE

HEL JD (2440000+)	DMAG.	HEL JD (2440000+)	DMAG.	HEL JD (2440000+)	DMAG.
2709.62280	-2.197	2812.62597	-2.235	2817.67765	-2.201
2709.62706	-2.213	2812.62796	-2.228	2817.68349	-2.210
2709.63344	-2.205	2812.63168	-2.230	2817.68750	-2.220
2709.63766	-2.205	2812.63554	-2.234	2817.69286	-2.207
2709.64272	-2.222	2812.64217	-2.227	2817.70175	-2.175
2709.64743	-2.212	2812.64584	-2.220	2817.70215	-2.174
2709.65152	-2.221	2812.64936	-2.217	2817.71215	-2.215
2709.65693	-2.218	2812.65329	-2.225	2817.72255	-2.195
2709.66124	-2.198	2812.65721	-2.229	2817.72759	-2.233
2709.66516	-2.204	2812.66099	-2.223	2817.73255	-2.217
2709.67632	-2.195	2812.66743	-2.217	2817.75499	-2.188
2709.68056	-2.175	2812.67211	-2.221	2817.76026	-2.224
2709.68408	-2.172	2812.67578	-2.221	2817.76456	-2.217
2709.68899	-2.203	2812.68598	-2.220	2817.76695	-2.214
2709.69477	-2.199	2817.51033	-2.247	2817.77095	-2.198
2709.69826	-2.177	2817.52260	-2.236	2817.78221	-2.156
2709.70950	-2.173	2817.52552	-2.241	2817.78636	-2.223
2709.71464	-2.179	2817.52951	-2.243	2817.79387	-2.193
2709.71661	-2.186	2817.53313	-2.250	2817.80524	-2.221
2709.72247	-2.172	2817.53984	-2.253	2817.80957	-2.227
2709.72649	-2.177	2817.54360	-2.239	2817.81911	-2.178
2709.73167	-2.195	2817.54729	-2.247	2817.82951	-2.195
2709.74152	-2.194	2817.55253	-2.252	2817.83372	-2.264
2709.74556	-2.199	2817.55597	-2.257	2824.51555	-2.258
2709.74967	-2.188	2817.55990	-2.271	2824.52155	-2.257
2709.75346	-2.196	2817.56374	-2.261	2824.52512	-2.255
2709.75790	-2.193	2817.56791	-2.250	2824.52945	-2.255
2709.76368	-2.185	2817.57172	-2.245	2824.53527	-2.255
2709.76772	-2.185	2817.57853	-2.240	2824.53961	-2.265
2709.78796	-2.154	2817.58219	-2.253	2824.54337	-2.251
2709.79288	-2.165	2817.58583	-2.247	2824.54674	-2.254
2709.80063	-2.176	2817.58960	-2.239	2824.55102	-2.257
2812.52253	-2.207	2817.59573	-2.242	2824.55431	-2.256
2812.52719	-2.203	2817.60089	-2.240	2824.55826	-2.254
2812.53111	-2.202	2817.60488	-2.251	2824.56279	-2.227
2812.53829	-2.264	2817.60857	-2.243	2824.56591	-2.242
2812.54160	-2.201	2817.61218	-2.243	2824.56922	-2.244
2812.54594	-2.203	2817.61577	-2.240	2824.57231	-2.240
2812.55005	-2.209	2817.62039	-2.232	2824.57870	-2.241
2812.55541	-2.255	2817.62410	-2.242	2824.58256	-2.242
2812.56247	-2.256	2817.62782	-2.236	2824.58605	-2.241
2812.56586	-2.258	2817.63290	-2.224	2824.59034	-2.220
2812.56975	-2.253	2817.63746	-2.210	2824.59426	-2.240
2812.57404	-2.248	2817.64123	-2.223	2824.60375	-2.216
2812.58059	-2.243	2817.64793	-2.228	2824.60739	-2.232
2812.58518	-2.255	2817.65222	-2.219	2824.61076	-2.238
2812.58977	-2.232	2817.65953	-2.219	2824.61415	-2.230
2812.59366	-2.231	2817.66392	-2.225	2824.62051	-2.221
2812.59770	-2.255	2817.66860	-2.233	2824.62407	-2.225
2812.61141	-2.239	2817.67252	-2.207	2824.62831	-2.243

TABLE 12(CONT'D)

BLUE

HEL JD (2440000+)	DMAG.	HEL JD (2440000+)	DMAG.	HEL JD (2440000+)	DMAG.
2824.63210	-2.262	2856.65210	-2.194	2856.91345	-2.219
2824.63551	-2.218	2856.65687	-2.184	2856.91677	-2.220
2824.65204	-2.229	2856.66138	-2.243	2856.92001	-2.221
2824.65703	-2.222	2856.66509	-2.219	2856.92345	-2.218
2824.66092	-2.258	2856.66853	-2.193	2873.57406	-1.947
2824.66548	-2.235	2856.67472	-2.183	2873.57855	-1.936
2824.66905	-2.262	2856.67858	-2.186	2873.58196	-1.917
2824.67336	-2.205	2856.68202	-2.158	2873.58542	-1.885
2824.67737	-2.187	2856.68574	-2.205	2873.59207	-1.810
2840.55584	-2.249	2856.69768	-2.164	2873.59545	-1.784
2840.55968	-2.256	2856.70159	-2.190	2873.59886	-1.748
2840.56354	-2.255	2856.70523	-2.191	2873.60244	-1.724
2840.56713	-2.243	2856.70902	-2.194	2873.60815	-1.664
2840.57407	-2.201	2856.72520	-2.147	2873.61204	-1.612
2840.57484	-2.192	2856.73041	-2.164	2873.61568	-1.545
2840.67895	-2.242	2856.73457	-2.182	2873.62045	-1.590
2840.68271	-2.192	2856.73891	-2.192	2873.63251	-1.343
2840.70800	-2.179	2856.74263	-2.230	2873.63617	-1.254
2840.77231	-2.183	2856.74654	-2.257	2873.64319	-1.184
2840.77610	-2.157	2856.75160	-2.228	2873.64677	-1.083
2840.77982	-2.166	2856.76554	-2.140	2873.65056	-0.899
2840.78635	-2.159	2856.76688	-2.198	2873.65466	-0.736
2840.78942	-2.116	2856.77195	-2.144	2873.65975	-0.590
2840.79281	-2.107	2856.77531	-2.162	2873.76825	0.912
2840.79617	-2.165	2856.78952	-2.221	2873.79443	0.845
2840.82419	-2.152	2856.79341	-2.151	2873.79725	0.815
2840.82856	-2.190	2856.79912	-2.240	2873.80355	0.225
2840.83265	-2.196	2856.80912	-2.253	2873.80660	0.041
2840.83654	-2.115	2856.81253	-2.184	2873.81029	-0.147
2840.83973	-2.156	2856.81607	-2.190	2873.81456	-0.332
2840.84294	-2.090	2856.81954	-2.218	2873.81734	-0.559
2840.84660	-2.107	2856.82375	-2.175	2873.82305	-0.682
2840.85083	-2.158	2856.82901	-2.191	2873.82627	-0.761
2840.85005	-2.133	2856.83290	-2.184	2873.83115	-0.936
2840.85316	-2.155	2856.83679	-2.211	2873.83541	-1.106
2840.86728	-2.152	2856.84093	-2.182	2873.84300	-1.207
2840.87150	-2.121	2856.84694	-2.214	2873.84655	-1.316
2840.87470	-2.142	2856.85048	-2.223	2887.77154	-2.146
2840.87780	-2.141	2856.85394	-2.196	2887.77560	-2.139
2840.88712	-2.156	2856.85746	-2.221	2887.77909	-2.160
2840.89046	-2.120	2856.86097	-2.222	2887.78560	-2.190
2840.89350	-2.136	2856.87207	-2.218	2887.78929	-2.172
2856.60551	-2.174	2856.87828	-2.213	2887.79265	-2.193
2856.60591	-2.173	2856.88174	-2.215	2887.79627	-2.217
2856.61254	-2.143	2856.88526	-2.214	2887.80000	-2.173
2856.61663	-2.204	2856.88872	-2.217	2887.80492	-2.156
2856.62281	-2.203	2856.89431	-2.228	2887.80833	-2.201
2856.63520	-2.186	2856.89780	-2.209	2887.82364	-2.240
2856.64133	-2.207	2856.90124	-2.190	2887.83489	-2.212
2856.64874	-2.196	2856.90660	-2.213	2887.84905	-2.179

TABLE 12(CONT'D)

BLUE

HEL JD (2440000+)	DMAG.	HEL JD (2440000+)	DMAG.	HEL JD (2440000+)	DMAG.
2887.85291	-2.213	2895.84964	-2.150	2903.83432	-2.050
2887.85660	-2.216	2895.85278	-2.183	2918.65104	0.960
2887.85999	-2.214	2895.85584	-2.180	2918.65535	0.955
2887.86715	-2.215	2895.86143	-2.190	2918.65932	0.954
2887.87056	-2.215	2895.86477	-2.195	2918.66456	0.971
2887.87393	-2.217	2895.86848	-2.198	2918.66956	-0.265
2887.88283	-2.235	2895.87634	-2.172	2918.71107	-0.427
2887.89390	-2.248	2895.87970	-2.172	2918.71471	-0.555
2887.89786	-2.247	2903.56474	-1.267	2918.71224	-0.823
2895.74071	-2.167	2903.56815	-1.210	2918.71585	-0.952
2895.74408	-2.169	2903.57130	-1.157	2918.71942	-0.996
2895.74904	-2.187	2903.57439	-1.157	2918.72519	-1.038
2895.75241	-2.187	2903.58110	-0.959	2918.73553	-1.345
2895.75659	-2.188	2903.58451	-0.823	2918.73914	-1.417
2895.76056	-2.169	2903.58763	-0.755	2918.74989	-1.591
2895.76382	-2.209	2903.59065	-0.674	2918.75353	-1.619
2895.76749	-2.175	2903.59374	-0.585	2918.75684	-1.682
2895.77048	-2.188	2903.59822	-0.381	2918.76025	-1.682
2895.78015	-2.203	2903.60154	-0.254	2918.76410	-1.735
2895.78571	-2.211	2903.60463	-0.107	2918.77402	-1.909
2895.78890	-2.197	2903.60692	0.073	2918.77815	-1.897
2895.79222	-2.204	2903.72909	0.260	2918.78417	-1.925
2895.79656	-2.223	2903.73527	0.625	2918.78785	-1.969
2895.79962	-2.218	2903.73597	-0.097	2918.79197	-2.033
2895.80301	-2.210	2903.74165	-0.358	2918.79564	-2.042
2895.80638	-2.202	2903.74462	-0.481	2918.80345	-2.094
2895.80957	-2.197	2903.74778	-0.588	2918.80672	-2.136
2895.81560	-2.204	2903.75701	-0.893	2918.81192	-2.137
2895.81882	-2.195	2903.75992	-0.957	2918.81515	-2.153
2895.82752	-2.198	2903.75568	-1.166	2918.82229	-2.115
2895.83081	-2.212	2903.77159	-1.203	2918.82525	-2.118
2895.83562	-2.191	2903.77476	-1.263	2918.82881	-2.115
2895.84293	-2.193	2903.78109	-1.365	2918.82665	-2.136
2895.84622	-2.186	2903.79067	-1.569	2918.83067	-2.193

TABLE 12(CONT'D)

UV

HEL JD (2440000+)	DMAG.	HEL JD (2440000+)	DMAG.	HEL JD (2440000+)	DMAG.
2491.55773	-2.869	2493.66130	-2.831	2524.65659	-1.340
2491.56949	-2.844	2493.66295	-2.770	2524.64357	-1.173
2491.57176	-2.855	2493.66996	-2.715	2524.64745	-0.973
2491.58149	-2.819	2493.67090	-2.750	2524.65274	-0.836
2491.58298	-2.818	2518.58528	-2.869	2524.65297	-0.556
2491.59223	-2.863	2518.59443	-2.712	2524.65866	-0.656
2491.59523	-2.852	2518.60971	-2.702	2524.66257	0.207
2491.59772	-2.864	2518.61592	-2.724	2524.66813	0.259
2491.59874	-2.863	2518.62248	-2.736	2524.67289	0.985
2491.60402	-2.863	2518.62644	-2.704	2524.67855	0.444
2491.60519	-2.856	2518.63188	-2.801	2524.68284	0.576
2491.61195	-2.842	2518.64968	-2.883	2524.73651	1.198
2491.61297	-2.875	2518.65461	-2.855	2524.74046	1.230
2491.61360	-2.843	2518.65908	-2.821	2524.74926	1.141
2491.61788	-2.868	2518.66459	-2.701	2524.75431	1.243
2491.61891	-2.848	2518.66962	-2.825	2525.58755	-2.811
2491.62339	-2.851	2518.67581	-2.774	2525.57144	-2.857
2491.62484	-2.845	2518.71290	-2.765	2525.58151	-2.765
2491.64005	-2.852	2518.72033	-2.827	2525.58675	-2.793
2491.64154	-2.845	2518.73041	-2.705	2525.59226	-2.804
2491.64650	-2.822	2518.76042	-2.787	2525.59545	-2.770
2491.64748	-2.850	2518.76465	-2.796	2525.60155	-2.778
2491.64980	-2.809	2518.77077	-2.792	2525.60645	-2.800
2491.65003	-2.835	2518.77548	-2.706	2525.64982	-2.729
2491.65708	-2.841	2518.77999	-2.725	2525.65706	-2.746
2491.66413	-2.855	2518.78446	-2.733	2525.67466	-2.891
2491.66576	-2.867	2518.78662	-2.726	2525.67755	-2.892
2491.66994	-2.839	2518.79724	-2.756	2525.68106	-2.854
2491.67233	-2.851	2518.80155	-2.748	2525.70779	-2.765
2491.67687	-2.852	2518.80719	-2.834	2525.71267	-2.744
2491.67847	-2.828	2518.81395	-2.819	2525.72292	-2.774
2491.68525	-2.862	2518.81853	-2.840	2525.72601	-2.770
2491.68729	-2.859	2518.83815	-2.831	2525.72956	-2.854
2493.54326	-2.764	2518.85468	-2.827	2525.73534	-2.841
2493.54473	-2.782	2518.86024	-2.866	2525.73990	-2.834
2493.55173	-2.823	2518.86869	-2.861	2525.74539	-2.872
2493.55326	-2.802	2518.87403	-2.895	2525.79554	-2.970
2493.55849	-2.828	2518.88415	-2.789	2525.80188	-2.720
2493.56051	-2.815	2518.88691	-2.790	2525.80998	-2.778
2493.59708	-2.840	2524.58518	-2.290	2525.81775	-2.913
2493.59933	-2.842	2524.59025	-2.122	2525.82152	-2.853
2493.60451	-2.821	2524.60351	-2.176	2525.82603	-2.805
2493.60606	-2.809	2524.60742	-2.032	2525.83202	-2.835
2493.61329	-2.805	2524.61248	-1.977	2525.83501	-2.764
2493.61503	-2.796	2524.61300	-2.036	2525.84082	-2.754
2493.61925	-2.796	2524.61899	-1.779	2525.84501	-2.843
2493.62104	-2.829	2524.62306	-1.596	2525.85184	-2.811
2493.63411	-2.722	2524.62709	-1.368	2525.85745	-2.744
2493.63598	-2.810	2524.62726	-1.287	2525.86435	-2.789
2493.64343	-2.735	2524.63230	-1.206	2525.87125	-2.805

TABLE 12(CONT'D)

UV

HEL JD (2440000+)	DMAG.	HEL JD (2440000+)	DMAG.	HEL JD (2440000+)	DMAG.
2642.63164	-2.797	2646.77782	-1.821	2650.82855	-2.805
2642.63929	-2.789	2646.78161	-1.781	2650.83190	-2.830
2642.64475	-2.791	2646.78662	-1.715	2650.83678	-2.817
2642.65144	-2.801	2646.79068	-1.583	2650.83993	-2.815
2642.65667	-2.775	2646.79604	-1.445	2650.84215	-2.811
2642.66086	-2.789	2646.79963	-1.334	2650.84985	-2.828
2642.66732	-2.765	2646.80347	-1.114	2701.53984	-2.755
2642.67148	-2.787	2646.80716	-0.936	2701.54540	-2.758
2642.67764	-2.841	2646.81150	-0.802	2701.55009	-2.780
2642.68452	-2.825	2646.81668	-0.583	2701.55365	-2.736
2642.69576	-2.810	2646.82047	-0.340	2701.55855	-2.695
2642.70115	-2.811	2646.82461	0.079	2701.56455	-2.659
2642.70686	-2.818	2646.82892	0.366	2701.56900	-2.622
2642.71084	-2.817	2646.83356	0.650	2701.57330	-2.597
2642.71496	-2.795	2646.83925	0.960	2701.58429	-2.524
2642.71847	-2.798	2646.84426	1.014	2701.58886	-2.479
2642.72416	-2.833	2646.85270	1.139	2701.59242	-2.438
2642.72832	-2.859	2646.85857	1.159	2701.59705	-2.375
2642.73186	-2.824	2646.86141	1.105	2701.60409	-2.291
2642.74405	-2.810	2646.86467	1.140	2701.60754	-2.241
2642.75021	-2.823	2646.86859	1.133	2701.61406	-2.171
2642.75548	-2.816	2646.87345	1.129	2701.61916	-2.131
2642.75916	-2.795	2646.87804	1.152	2709.61325	-2.776
2642.76268	-2.801	2646.88274	1.141	2709.61915	-2.787
2642.76622	-2.810	2650.68246	-2.848	2709.62525	-2.775
2642.77270	-2.814	2650.68877	-2.844	2709.62781	-2.788
2642.77771	-2.827	2650.69149	-2.849	2709.63309	-2.788
2642.78105	-2.813	2650.69563	-2.858	2709.63716	-2.771
2642.78442	-2.824	2650.70164	-2.874	2709.64219	-2.807
2642.78773	-2.821	2650.70543	-2.884	2709.64675	-2.763
2642.79115	-2.853	2650.71079	-2.869	2709.65107	-2.777
2642.79716	-2.787	2650.71517	-2.868	2709.65743	-2.782
2642.79703	-2.794	2650.71921	-2.873	2709.66159	-2.749
2642.80261	-2.797	2650.72487	-2.862	2709.66553	-2.764
2642.80937	-2.818	2650.73110	-2.845	2709.67293	-2.763
2642.81989	-2.813	2650.73442	-2.819	2709.67977	-2.741
2642.82515	-2.808	2650.73811	-2.849	2709.68370	-2.711
2642.83238	-2.812	2650.74162	-2.853	2709.68939	-2.739
2642.84933	-2.830	2650.74649	-2.871	2709.69515	-2.736
2642.86654	-2.823	2650.74978	-2.859	2709.69869	-2.711
2642.87132	-2.841	2650.75594	-2.829	2709.70915	-2.712
2646.70028	-2.642	2650.75716	-2.921	2709.71504	-2.701
2646.70559	-2.596	2650.75790	-2.847	2709.71895	-2.697
2646.70981	-2.595	2650.76421	-2.844	2709.72295	-2.675
2646.71407	-2.559	2650.76857	-2.808	2709.72691	-2.709
2646.72117	-2.517	2650.81103	-2.764	2709.73207	-2.706
2646.75548	-2.187	2650.81567	-2.775	2709.74114	-2.741
2646.76241	-2.104	2650.81916	-2.795	2709.74515	-2.713
2646.76672	-2.041	2650.82228	-2.803	2709.74925	-2.719
2646.77116	-1.955	2650.82554	-2.821	2709.75299	-2.731

TABLE 12(CONT'D)

UV

HEL JD (2440000+)	DMAG.	HEL JD (2440000+)	DMAG.	HEL JD (2440000+)	DMAG.
2709.75752	-2.713	2817.56831	-2.833	2824.51595	-2.822
2709.76408	-2.714	2817.57225	-2.829	2824.52105	-2.848
2709.76817	-2.707	2817.57750	-2.821	2824.52472	-2.850
2709.78866	-2.664	2817.58179	-2.826	2824.53033	-2.817
2709.79345	-2.643	2817.58543	-2.840	2824.53365	-2.836
2709.80021	-2.679	2817.58915	-2.834	2824.53726	-2.845
2812.52211	-2.840	2817.59638	-2.830	2824.54306	-2.842
2812.52764	-2.834	2817.60054	-2.830	2824.54694	-2.828
2812.53148	-2.833	2817.60426	-2.816	2824.55053	-2.821
2812.53784	-2.824	2817.60790	-2.852	2824.55392	-2.819
2812.54123	-2.816	2817.61176	-2.861	2824.55708	-2.834
2812.54552	-2.814	2817.61535	-2.827	2824.55315	-2.824
2812.54963	-2.837	2817.62086	-2.740	2824.56031	-2.828
2812.55589	-2.837	2817.62450	-2.797	2824.56363	-2.830
2812.56287	-2.822	2817.62826	-2.777	2824.57271	-2.835
2812.56621	-2.819	2817.63330	-2.797	2824.57636	-2.820
2812.57025	-2.822	2817.63769	-2.806	2824.58194	-2.819
2812.57451	-2.844	2817.64158	-2.767	2824.58555	-2.816
2812.58012	-2.820	2817.64761	-2.859	2824.58992	-2.815
2812.58473	-2.814	2817.65177	-2.849	2824.59360	-2.796
2812.58952	-2.854	2817.65965	-2.809	2824.60415	-2.756
2812.59311	-2.801	2817.66317	-2.804	2824.60779	-2.778
2812.59725	-2.815	2817.66808	-2.855	2824.61115	-2.756
2812.61198	-2.852	2817.67192	-2.797	2824.61459	-2.784
2812.62455	-2.790	2817.67605	-2.810	2824.62211	-2.747
2812.62839	-2.794	2817.68401	-2.802	2824.62567	-2.783
2812.63215	-2.797	2817.68875	-2.830	2824.62791	-2.809
2812.63591	-2.795	2817.69333	-2.787	2824.63167	-2.842
2812.64172	-2.807	2817.69953	-2.782	2824.63559	-2.797
2812.64544	-2.814	2817.70263	-2.793	2824.65102	-2.792
2812.64893	-2.809	2817.71178	-2.773	2824.65661	-2.794
2812.65279	-2.805	2817.72290	-2.745	2824.65986	-2.813
2812.65683	-2.851	2817.72586	-2.811	2824.66947	-2.757
2812.66354	-2.856	2817.73407	-2.857	2824.67376	-2.749
2812.66703	-2.856	2817.75367	-2.793	2840.53537	-2.835
2812.67254	-2.822	2817.75384	-2.794	2840.56036	-2.846
2812.67615	-2.814	2817.75419	-2.745	2840.56394	-2.851
2812.68550	-2.783	2817.76062	-2.788	2840.56773	-2.845
2817.51593	-2.911	2817.76496	-2.765	2840.57559	-2.852
2817.52246	-2.811	2817.76947	-2.812	2840.66945	-2.772
2817.52605	-2.801	2817.77640	-2.842	2840.67957	-2.779
2817.52986	-2.847	2817.78266	-2.755	2840.68314	-2.769
2817.53353	-2.836	2817.78662	-2.712	2840.75385	-2.671
2817.53949	-2.839	2817.79518	-2.714	2840.76446	-2.644
2817.54313	-2.839	2817.79969	-2.745	2840.76835	-2.713
2817.54694	-2.858	2817.80385	-2.769	2840.77269	-2.811
2817.55280	-2.840	2817.80871	-2.720	2840.77648	-2.790
2817.55644	-2.874	2817.81583	-2.750	2840.78019	-2.745
2817.56025	-2.832	2817.82295	-2.730	2840.78383	-2.721
2817.56424	-2.828	2817.82990	-2.846	2840.78907	-2.698

TABLE 12(CONT'D)

UV

HEL JD (2440000+)	DMAG.	HEL JD (2440000+)	DMAG.	HEL JD (2440000+)	DMAG.
2840.79241	-2.711	2856.84661	-2.708	2887.77109	-2.834
2840.79582	-2.688	2856.85015	-2.807	2887.77597	-2.865
2840.82382	-2.648	2856.85357	-2.820	2887.77947	-2.811
2840.82883	-2.744	2856.85706	-2.828	2887.78517	-2.810
2840.83300	-2.755	2856.86062	-2.740	2887.78891	-2.833
2840.83686	-2.756	2856.87773	-2.798	2887.79233	-2.847
2840.84005	-2.794	2856.88134	-2.786	2887.79589	-2.872
2840.84337	-2.677	2856.88463	-2.777	2887.80125	-2.834
2840.84638	-2.668	2856.88830	-2.736	2887.80552	-2.864
2840.85048	-2.762	2856.89470	-2.796	2887.80871	-2.862
2840.85970	-2.691	2856.89814	-2.756	2887.84220	-2.767
2840.86281	-2.663	2856.90161	-2.803	2887.84552	-2.857
2840.86762	-2.757	2856.90697	-2.811	2887.84197	-2.867
2840.87121	-2.735	2856.91383	-2.793	2887.84521	-2.922
2840.87433	-2.725	2856.91714	-2.791	2887.84860	-2.872
2840.87745	-2.714	2856.92050	-2.601	2887.85535	-2.858
2840.88744	-2.750	2856.92562	-2.786	2887.85737	-2.767
2840.89083	-2.762	2873.57362	-2.510	2887.86039	-2.851
2840.89388	-2.716	2873.57901	-2.485	2887.86567	-2.951
2856.60661	-2.700	2873.58227	-2.525	2887.87015	-2.931
2856.61187	-2.717	2873.58584	-2.475	2887.87355	-2.863
2856.61615	-2.769	2873.59107	-2.434	2887.87623	-2.851
2856.62226	-2.730	2873.59509	-2.404	2887.89432	-2.809
2856.63480	-2.792	2873.59938	-2.357	2895.74057	-2.758
2856.64178	-2.813	2873.60204	-2.351	2895.74445	-2.791
2856.64831	-2.782	2873.60853	-2.264	2895.74818	-2.799
2856.65170	-2.779	2873.61244	-2.225	2895.74872	-2.851
2856.65729	-2.774	2873.61630	-2.119	2895.75105	-2.832
2856.66185	-2.822	2873.62005	-1.952	2895.75674	-2.796
2856.66547	-2.794	2873.63288	-1.965	2895.75955	-2.782
2856.66891	-2.829	2873.63655	-1.910	2895.76417	-2.818
2856.67437	-2.828	2873.64059	-1.750	2895.75731	-2.744
2856.67796	-2.776	2873.64640	-1.650	2895.77305	-2.748
2856.68160	-2.752	2873.65019	-1.401	2895.77855	-2.843
2856.66534	-2.728	2873.65435	-1.253	2895.78334	-2.851
2856.69810	-2.708	2873.66018	-1.244	2895.75856	-2.859
2856.70197	-2.783	2873.78858	1.170	2895.79136	-2.837
2856.70565	-2.779	2873.79409	0.684	2895.79673	-2.823
2856.70939	-2.711	2873.79763	0.371	2895.80082	-2.822
2856.72562	-2.750	2873.80286	-0.112	2895.80339	-2.849
2856.73081	-2.705	2873.80625	-0.373	2895.80575	-2.820
2856.73495	-2.747	2873.81066	-0.592	2895.80990	-2.794
2856.74303	-2.757	2873.81495	-0.827	2895.81521	-2.806
2856.74694	-2.760	2873.81902	-0.989	2895.81845	-2.770
2856.79944	-2.691	2873.82266	-1.216	2895.82796	-2.858
2856.80879	-2.722	2873.82592	-1.331	2895.83119	-2.786
2856.81198	-2.759	2873.83156	-1.389	2895.83630	-2.730
2856.81577	-2.749	2873.83881	-1.632	2895.84336	-2.785
2856.82410	-2.721	2873.84335	-1.780	2895.84662	-2.804
2856.84130	-2.796	2873.84706	-1.600	2895.85001	-2.793

TABLE 12(CONT'D)

JV

HEL JD (2440000+)	DMAG.	HEL JD (2440000+)	DMAG.	HEL JD (2440000+)	DMAG.
2895.85313	-2.791	2903.73288	-0.461	2918.71907	-1.935
2895.85619	-2.801	2903.73634	-0.416	2918.72284	-1.912
2895.86108	-2.821	2903.74133	-0.791	2918.73595	-1.880
2895.86439	-2.830	2903.74429	-0.981	2918.73956	-1.970
2895.86806	-2.810	2903.74745	-1.159	2918.74945	-2.170
2895.87671	-2.756	2903.75671	-1.400	2918.75366	-2.145
2895.88010	-2.780	2903.75960	-1.435	2918.75784	-2.169
2903.56437	-1.686	2903.76835	-1.751	2918.76056	-2.234
2903.56851	-1.637	2903.77194	-1.726	2918.76455	-2.346
2903.57165	-1.770	2903.77511	-1.835	2918.77552	-2.511
2903.57474	-1.716	2903.78077	-1.847	2918.77845	-2.459
2903.58077	-1.588	2903.79632	-2.201	2918.78374	-2.543
2903.58416	-1.486	2918.63062	1.104	2918.78751	-2.586
2903.58728	-1.576	2918.63585	1.175	2918.79105	-2.589
2903.59030	-1.266	2918.63992	1.088	2918.79514	-2.647
2903.59339	-1.169	2918.64500	1.045	2918.80511	-2.658
2903.59860	-0.942	2918.69051	-0.693	2918.80933	-2.722
2903.60185	-0.742	2918.70145	-0.662	2918.81152	-2.745
2903.60505	-0.639	2918.70708	-1.125	2918.81469	-2.771
2903.60924	-0.393	2918.71189	-1.310	2918.82191	-2.711
2903.72876	0.196	2918.71545	-1.434	2918.82665	-2.745

Figure 3. Three color light curves of U Cephei in magnitudes. The data are that of Table 12.

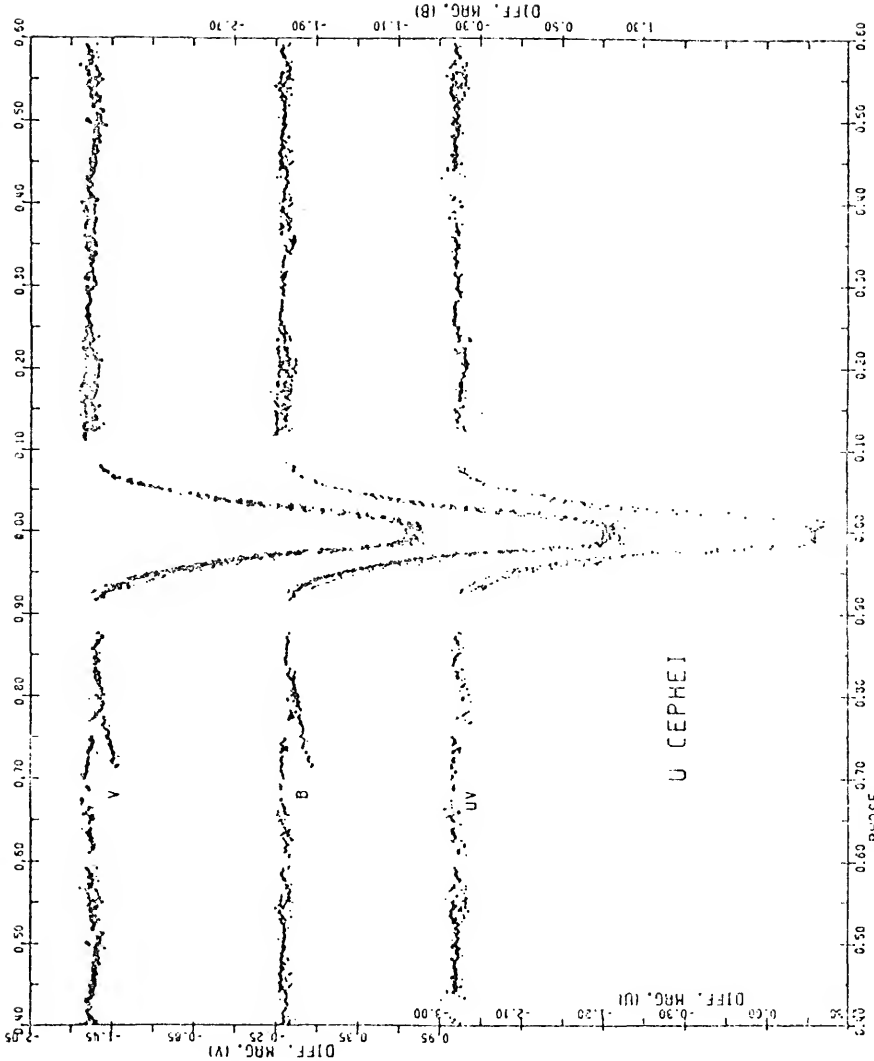
U CEPHEI
V
B
UV
DIFF. MAG. (V)
DIFF. MAG. (B)
DIFF. MAG. (UV)
PHASE

September; 12, 15, 21, and 23 October 1975, were initially eliminated.

Data in the region 0.12-0.25P show two distinct levels, corresponding to observations separated by about one year. Since the transformations discussed above gave consistent results, this separation of about $0^{m}.1$ appears to be real. The question as to which level represents the "less perturbed" state of the system is thoroughly discussed in the next chapter.

Normal points were obtained by taking simple means of the magnitudes in bins 0.005P wide. These normal points, converted to intensity units and normalized, appear in Table 13 and are plotted in Figure 4. The normalization factors were 4.330859 for visual, 7.790122 for blue, and 13.033839 for ultraviolet. For reasons alluded to in the previous paragraph and discussed fully in Chapter IV, the higher level in the region 0.12-0.25P was not used in forming the normals of Table 13. Observations on 25 March, 4 April, and 18 September 1975, form this higher level.

TABLE 15
NORMAL POINT INTENSITIES
U CEPHEI

VISUAL

PHASE	INTEN.	PHASE	INTEN.	PHASE	INTEN.
0.00297	0.1159	0.29770	1.0102	0.56725	1.0319
0.00725	0.1121	0.30272	0.9844	0.57225	0.9967
0.01278	0.1111	0.30707	1.0258	0.57755	1.0065
0.01771	0.1057	0.31245	1.0210	0.58210	1.0027
0.02264	0.1772	0.31880	1.0061	0.58731	1.0264
0.02789	0.2502	0.32190	1.0113	0.59145	0.9927
0.03253	0.3093	0.32745	1.0063	0.60411	0.9778
0.03689	0.3917	0.33314	1.0059	0.60962	1.0214
0.04192	0.4642	0.33712	0.9980	0.61195	0.9954
0.04649	0.5438	0.34258	1.0207	0.61638	0.9957
0.05191	0.6304	0.34780	1.0147	0.62165	1.0077
0.05712	0.7250	0.35273	1.0029	0.62691	1.0104
0.06274	0.8028	0.35771	1.0255	0.63285	1.0154
0.06865	0.8891	0.36291	1.0056	0.63681	1.0358
0.07290	0.9067	0.36786	1.0073	0.64220	1.0128
0.07794	0.9091	0.37207	0.9954	0.64836	1.0077
0.12255	0.9658	0.37721	0.9856	0.65351	1.0088
0.12718	0.9702	0.38269	1.0014	0.65701	1.0465
0.13456	0.9729	0.38852	1.0021	0.66524	1.0087
0.13833	0.9756	0.39394	1.0152	0.66817	1.0765
0.14364	1.0102	0.39709	0.9942	0.67340	1.0765
0.14706	0.9946	0.40299	0.9736	0.68476	1.0153
0.15244	0.9838	0.40800	1.0080	0.68780	1.0329
0.15944	0.9712	0.41199	1.0197	0.69227	1.0020
0.16249	1.0114	0.41800	1.0129	0.69770	1.0512
0.17243	0.9769	0.44220	1.0043	0.70279	1.0365
0.17730	1.0100	0.44741	1.0065	0.70734	1.0363
0.18107	1.0251	0.45223	0.9905	0.71333	1.0363
0.18796	1.0292	0.45751	0.9869	0.71723	1.0228
0.19058	0.9943	0.46211	0.9902	0.72242	1.0223
0.19706	1.0190	0.46750	0.9841	0.73235	1.0141
0.20214	1.0012	0.47146	0.9857	0.73665	1.0072
0.20687	1.0065	0.47691	0.9780	0.74170	0.9973
0.21194	0.9902	0.48214	0.9873	0.74733	1.0097
0.21715	1.0267	0.48722	0.9760	0.75610	1.0087
0.22283	1.0200	0.49270	0.9803	0.77310	0.9849
0.22939	1.0196	0.49744	0.9815	0.77849	0.9825
0.23328	1.0124	0.50177	0.9738	0.78115	0.9857
0.23803	1.0202	0.50689	0.9810	0.79223	0.9819
0.24217	1.0204	0.51219	0.9405	0.79792	0.9898
0.24731	1.0257	0.51725	0.9957	0.80117	0.9453
0.25217	1.0107	0.52308	0.9708	0.80749	0.9569
0.25795	1.0351	0.52703	0.9851	0.81265	0.9500
0.26265	1.0295	0.53202	0.9910	0.81831	0.9595
0.26727	1.0357	0.53791	1.0107	0.82244	0.9866
0.27231	1.0371	0.54296	0.9882	0.82795	0.9861
0.27701	1.0245	0.54816	0.9915	0.83140	0.9826
0.28159	1.0183	0.55252	0.9897	0.83779	0.9910
0.28701	1.0260	0.55745	1.0120	0.84226	0.9713
0.29310	1.0304	0.56250	1.0003	0.84656	0.9803

TABLE 15(CONT'D)

VISUAL

PHASE	INTEN.	PHASE	INTEN.	PHASE	INTEN.
0.85212	0.9717	0.92773	0.6709	0.96704	0.3171
0.85717	0.9689	0.93244	0.6291	0.97217	0.2241
0.86240	0.9643	0.93777	0.7005	0.97685	0.1724
0.86739	0.9552	0.94204	0.7040	0.98204	0.1273
0.87288	0.9545	0.94754	0.8227	0.98777	0.1165
0.87581	0.9504	0.95269	0.5533	0.99211	0.1154
0.91775	0.9516	0.95756	0.4568	0.99707	0.1146

TABLE 13(CONT'D)

BLUE

PHASE	INTEN.	PHASE	INTEN.	PHASE	INTEN.
0.00297	0.0515	0.29510	1.0006	0.56250	0.9594
0.00725	0.0515	0.29770	1.0078	0.56757	0.9627
0.01276	0.0515	0.30272	0.9950	0.57264	0.9616
0.01771	0.0752	0.30767	1.0035	0.57766	0.9965
0.02264	0.1171	0.31245	0.9883	0.58245	1.0134
0.02789	0.1825	0.31506	0.9909	0.58731	1.0035
0.03253	0.2595	0.32198	1.0013	0.59145	0.9856
0.03689	0.3381	0.32745	1.0060	0.60411	0.9508
0.04192	0.4050	0.33314	0.9912	0.60821	0.9665
0.04649	0.4910	0.33712	0.9534	0.61193	0.9759
0.05191	0.5924	0.34256	0.9540	0.61668	0.9722
0.05712	0.6875	0.34788	0.9578	0.62241	0.9587
0.06274	0.7650	0.35273	0.9152	0.62668	0.9625
0.06685	0.8467	0.35761	0.9141	0.63250	0.9821
0.07293	0.9065	0.36382	0.9909	0.63681	0.9556
0.07836	0.9079	0.36766	0.9883	0.64220	0.9994
0.08412	0.9072	0.37165	0.9966	0.64836	1.0151
0.12255	0.9563	0.37721	0.9579	0.65403	1.0129
0.12718	0.9589	0.38269	0.9612	0.65777	1.0010
0.13438	0.9610	0.38852	0.9959	0.66247	1.0010
0.13533	0.9749	0.39094	1.0168	0.66817	1.0056
0.14304	0.9801	0.39709	0.9587	0.67540	1.0175
0.14706	0.9769	0.40299	0.9554	0.68470	1.0193
0.15244	0.9591	0.40796	0.9437	0.68780	1.0189
0.15944	0.9422	0.43199	1.0114	0.69267	1.0500
0.16249	0.9666	0.43866	0.9755	0.69776	0.9967
0.17243	0.9422	0.44220	1.0136	0.70275	1.0029
0.17756	0.9977	0.44741	1.0098	0.70752	1.0168
0.18137	0.9991	0.45238	1.0227	0.71366	1.0175
0.18796	0.9410	0.45765	1.0231	0.71725	1.0134
0.19058	0.9575	0.46254	1.0238	0.72242	1.0138
0.19706	0.9615	0.46750	1.0098	0.73265	0.9965
0.20214	1.0098	0.47140	1.0109	0.73665	0.9895
0.20687	0.9712	0.47691	1.0129	0.74170	1.0094
0.21194	0.9569	0.48214	1.0070	0.74753	0.9941
0.21715	0.9757	0.48722	1.0027	0.76986	0.9549
0.22283	0.9676	0.49263	0.9896	0.77516	0.9386
0.22939	0.9963	0.49734	0.9942	0.77649	0.9110
0.23328	0.9863	0.50222	0.9974	0.78116	0.9429
0.23803	0.9899	0.50659	0.9820	0.79528	0.9392
0.24217	0.9750	0.51219	0.9869	0.79792	0.9191
0.24731	0.9921	0.51741	0.9779	0.80117	0.8940
0.25217	1.0115	0.52306	0.9997	0.80749	0.9209
0.25795	1.0280	0.52703	0.9987	0.81265	0.9168
0.26265	1.0222	0.53225	0.9812	0.81851	0.9197
0.26727	1.0185	0.53808	0.9992	0.82190	0.9464
0.27231	1.0125	0.54290	1.0200	0.82793	0.9030
0.27761	1.0115	0.54816	0.9736	0.83143	0.9476
0.28159	1.0062	0.55252	0.9902	0.83779	0.9772
0.28761	0.9990	0.55745	0.9795	0.84226	0.9875

TABLE 15(CONT'D)

BLUE

PHASE	INTEN.	PHASE	INTEN.	PHASE	INTEN.
0.84638	0.9765	0.92278	0.9125	0.96230	0.3208
0.85212	0.9727	0.92773	0.8677	0.96704	0.2572
0.85717	0.9756	0.93244	0.8111	0.97217	0.1613
0.86240	0.9618	0.93727	0.7351	0.97653	0.1032
0.86739	0.9623	0.94234	0.6663	0.98204	0.0595
0.87288	0.9666	0.94754	0.5883	0.98777	0.0512
0.87831	0.9496	0.95269	0.4936	0.99211	0.0365
0.91775	0.9249	0.95758	0.4076	0.99707	0.0319

TABLE 15(CONT'D)

uV

PHASE	INTEN.	PHASE	INTEN.	PHASE	INTEN.
0.00235	0.0268	0.31625	1.0328	0.58790	1.0131
0.00647	0.0268	0.32184	1.0211	0.59212	1.0375
0.01290	0.0258	0.32759	1.0181	0.60804	0.9815
0.01772	0.0472	0.33299	1.0456	0.61283	0.9974
0.02258	0.0940	0.33725	1.0230	0.61759	0.9405
0.02785	0.1035	0.34245	1.0250	0.62257	0.9554
0.03254	0.2403	0.34779	1.0122	0.62679	1.0244
0.03883	0.3103	0.35267	1.0171	0.63192	1.0514
0.04199	0.4020	0.35766	1.0422	0.63699	1.0024
0.04644	0.4821	0.36287	1.0015	0.64201	1.0102
0.05199	0.5777	0.36721	1.0133	0.64621	1.0369
0.05728	0.7182	0.37161	1.0219	0.65325	1.0921
0.06208	0.7977	0.37537	0.9932	0.65790	1.0263
0.06675	0.8552	0.38235	1.0795	0.66241	1.0919
0.07274	0.9381	0.38903	1.0479	0.66835	1.0394
0.07674	0.9582	0.39118	1.0505	0.67278	1.0782
0.08018	0.9977	0.39849	0.9702	0.68457	1.0441
0.12291	0.9225	0.40287	1.0109	0.68804	1.0499
0.12698	0.9620	0.40621	1.0578	0.69186	1.0419
0.13422	1.0035	0.41198	1.0542	0.69752	1.0781
0.13833	1.0094	0.41806	1.0544	0.70276	1.0557
0.14212	0.9698	0.42425	1.0347	0.70735	1.0296
0.14650	1.0254	0.42739	1.0183	0.71286	1.0593
0.15228	0.9548	0.43225	1.0441	0.71851	1.0343
0.15961	0.9825	0.43756	1.0311	0.72536	1.0576
0.16265	0.9727	0.44221	1.0378	0.73247	1.0224
0.17259	0.9518	0.44757	1.0344	0.73671	1.0253
0.17542	0.9755	0.45128	1.0396	0.74177	1.0422
0.20214	0.9260	0.45683	1.0370	0.74735	1.0546
0.20665	0.9695	0.46215	1.0303	0.75732	0.8575
0.21015	0.9406	0.46727	1.0007	0.77244	0.9791
0.21812	0.9959	0.47275	1.0068	0.77852	0.9306
0.22268	1.0103	0.49734	1.0501	0.78102	0.8956
0.23309	0.9992	0.50147	1.0305	0.79325	0.9193
0.23807	0.9922	0.50653	1.0082	0.79739	0.9732
0.24232	1.0178	0.51306	1.0118	0.80069	0.8990
0.24746	1.0068	0.51753	1.0320	0.80745	0.9424
0.25210	1.0317	0.52365	1.0144	0.81251	0.9455
0.25811	1.0496	0.52737	1.0328	0.81694	0.9838
0.26529	1.0338	0.53197	1.0240	0.82250	1.0035
0.26794	1.0373	0.53810	1.0143	0.82606	1.0095
0.27247	1.0410	0.54274	1.0010	0.83153	0.9621
0.27744	1.0367	0.54684	1.0146	0.83774	1.0538
0.28142	1.0165	0.55217	1.0170	0.84231	1.0372
0.28778	0.9810	0.55703	0.9851	0.84736	1.0276
0.29248	0.9851	0.56324	0.9983	0.85124	0.9855
0.29704	1.0122	0.56757	1.0190	0.85655	1.0033
0.30164	1.0077	0.57257	0.9837	0.86255	1.0357
0.30679	0.9994	0.57760	0.9914	0.86736	1.0213
0.31249	1.0017	0.58232	1.0253	0.87286	0.9953

TABLE 15(CONT'D)

UV

PHASE	INTEN.	PHASE	INTEN.	PHASE	INTEN.
0.87597	0.9928	0.95368	0.5013	0.98256	0.3427
0.92825	0.8279	0.95774	0.4033	0.98695	0.2272
0.93193	0.7808	0.96256	0.3613	0.99305	0.2272
0.93738	0.7578	0.96771	0.2455	0.99746	0.2208

Figure 4. Three color light curves of U Cephei in normalized intensity units. The data are that of Table 13.

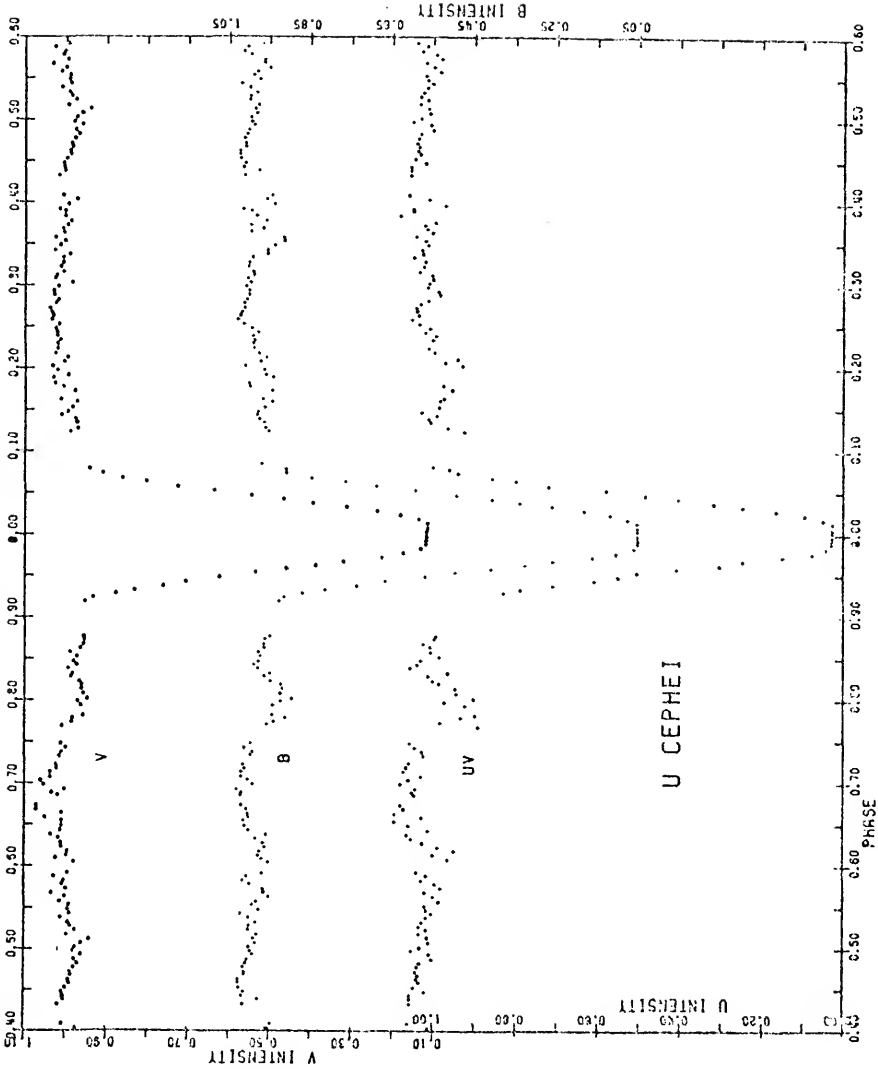
U CEPHEI
V
B
UV
V INTENSITY
B INTENSITY
U INTENSITY
PHASE

CHAPTER IV

RECTIFICATION

Fourier Analyses

The initial Fourier analysis was obtained for normal points taken as described above, including both levels in the region 0.12-0.25P. These coefficients are labelled F_1 in Table 14. Data in the regions 0.90-0.10P and 0.40-0.60P were not used in the analysis in order to avoid the eclipses. The defining relationship is

$$I = A_0 + A_1\cos\phi + A_2\cos 2\phi + A_3\cos 3\phi + A_4\cos 4\phi + B_1\sin\phi + B_2\sin 2\phi + B_3\sin 3\phi + B_4\sin 4\phi \quad .$$

The phase angle inside eclipse was rectified by

$$\sin^2\phi = \frac{\sin^2\phi}{1 - z\cos^2\phi} \quad ,$$

with $z = 0.021$. The result of this Fourier analysis was unsatisfactory since if left secondary eclipse inverted in all three colors and put the bottom of primary negative in the blue and ultraviolet. This was anticipated since the shoulders of primary eclipse do not match for this choice of normal points.

Next a graphical analysis was made following the procedure of J.E. Merrill (Merrill, 1970). These coefficients are labelled F_2 in Table 14. This gave reasonable results for A_2, but positive values for A_1, contrary to theory. The B_1 and B_3 coefficients in the ultraviolet are quite unacceptable. Higher order harmonics may be present in the blue and ultraviolet, which leads to the suspicion that even the data treated here, considered to be less perturbed, are somewhat affected.

At this point a reexamination of the data seemed appropriate. Two regions in particular were felt to be responsible for the peculiar results of the first analyses. The region from 0.75P to primary eclipse has a noticeable downward trend, seemingly indicative of gas streaming effects. This downward trend is a permanent feature of the light curve. Likewise the dual level of light from after primary to 0.25P requires resolution.

Consideration of the Roche model in conjunction with the hydrodynamical gas streaming models (e.g., Prendergast and Taam, 1974) indicate that during periods of increased activity, the light level just after primary should be slightly depressed. Thus it was assumed that the higher level represented the "less perturbed" state of the system. The Fourier analysis of the tops when the higher level is used, however, again yielded aberrant results for A_1. This result can also be anticipated since no equivalent "less perturbed" level exists prior to primary eclipse. A short region analysis of

the same data excluding the points greater than 0.75P did not improve the situation. The cause of this failure, however, seemed to be that the solution was not sufficiently constrained to yield valid results.

Similar Fourier analyses were run to test the results when the lower level after primary is used. These coefficients came closer to matching theory, especially in the ultraviolet. The same short region analysis indicated in the previous paragraph seemed to improve the situation in the visual and blue. The same caution concerning the constraint on the solution should be emphasized here, especially in view of the very unusual values obtained in the ultraviolet. These coefficients are listed as F_3 in Table 14.

A recent solution of the U Cephei system by Hall and Walter (1974) obtained Fourier coefficients closely matching theory by means of a very short region analysis in the region 0.25P to just before secondary eclipse. This is probably the only region of the light curve relatively undisturbed by gas streaming effects. When this approach was applied to my data, completely unrealistic results were obtained. Hall and Walter's analysis is on only five normal points to find A_0, A_1, and A_2. It would seem mathematically fortuitous that such a procedure would yield usable results. In addition, these three coefficients cannot account for the harmonic variation of the tops of the light curve. At this point numerical least squares methods were abandoned since consistent, realistic results seemed impossible to obtain. The

lower level following primary eclipse yielded the most encouraging results and will be used in the next analysis.

The data for the graphical solutions were now reexamined. If only terms up to 2ϕ are important, then linear solutions result from the graphical approach. Data points which deviated significantly from the apparent linear solutions were temporarily ignored, in order to obtain better approximations to the more important terms. This approach appeared to reap better results. Using the linear coefficients thus obtained, a process of trial-and-error was followed to obtain the other terms and better the approximations to the linear terms. During the trial-and-error process, the following guidelines were helpful:

1) Fix the coefficients to approximate theory;
2) Produce flat tops to the light curves tempered with knowledge of known nonconformity from other solutions;
3) Fix the sine terms to reproduce in shape the total portion of the unrectified primary eclipse;
4) Produce secondary eclipse of roughly the same depth as the original data.

The following comments need to be emphasized about the above guidelines:

1) Number one may not be important since U Cephei is known to be highly unstable. It was thus accorded low weight in the trial-and-error process;

2) Number two was adhered to so long as terms up to 4ϕ were still apparent in the residuals;

3) Number three is valid only as long as the sine terms affect both eclipses in a similar way. The secondary eclipse was sufficiently shallow in the blue and ultraviolet to render it useless for this determination. The shape of the rectified curve in the total portion of the primary eclipse is somewhat sensitive to the sine terms, and the complete symmetrization of the eclipse cannot be achieved without doing severe damage to the resulting total portion. Assuming gas streaming to be important in the observed asymmetry, such gas streaming cannot be rectified by any simple combination of sine terms. Guideline three was used as a compromise, realizing that the full asymmetry could not be removed by the sine terms;

4) Number four was very difficult to achieve, especially in light of guideline three. The resulting secondary eclipses were shallower than have been previously reported. A possible explanation for this will be discussed in a later chapter.

The resulting coefficients of the trial-and-error process are labelled F_4 in Table 14. These will be used in the initial solution, with the caution that rerectification may be necessary. A word about the errors of the coefficients listed in Table 14 seems appropriate. The machine solutions do indeed yield errors for the coefficients. These errors,

Table 14

Fourier Coefficients

F_1 is the machine solution for all normal points outside eclipse. F_2 is the graphical approach. F_3 is the machine short region solution using the lower level after primary eclipse. F_4 is the trial-and-error approach. σ is the standard error of the coefficient above it and r^2 is the statistical coefficient of determination.

	A_0	A_1	A_2	A_3	A_4	B_1	B_2	B_3	B_4
Visual									
F_{1_σ}	1.002	0.023	-0.017	0.025	-0.003	0.014	0.0134	0.002	-0.014
	± 8	± 9	± 12	± 5	± 6	± 2	± 28	± 3	± 3
$F_{2_{r^2}}$	0.990	-0.0033	-0.0382	0.012	-0.0101	-0.0945	0.0122	-0.018	-0.0159
	0.62	0.48	0.62	0.48	0.62	0.27	0.76	0.27	0.76
F_{3_σ}	0.960	-0.06	-0.04	0.019	0.009	0.035	0.04	0.02	-0.005
	± 37	± 7	± 3	± 12	± 7	± 29	± 4	± 3	± 12
F_4	0.994	-0.023	-0.016	0 0	0.0	0.0065	0.0122	0.0	-0.012
Blue									
F_{1_σ}	1.004	0.073	0.024	0.045	0.014	0.015	0.012	-0.005	-0.020
	± 11	± 13	± 17	± 8	± 9	± 3	± 4	± 4	± 4
$F_{2_{r^2}}$	0.933	0.084	-0.084	0.046	-0.044	0.048	0.0051	0.0	-0.024
	0.92	0.84	0.92	0.84	0.92	0.52	0.87		0.87
F_{3_σ}	0.977	-0.002	0.03	0.051	0.049	0.03	0.05	0.02	-0.005
	± 53	± 98	± 5	± 18	± 11	± 4	± 6	± 4	± 17
F_4	0.976	-0.020	-0.006	0.0	0.0	0.023	0.005	0.0	-0.010
Ultraviolet									
F_{1_σ}	1.028	0.062	0.033	0.061	0.021	-0.013	-0.016	-0.013	-0.032
	± 27	± 32	± 43	± 19	± 21	± 6	± 10	± 9	± 10
$F_{2_{r^2}}$	0.941	0.095	-0.076	0.070	-0.066	-0.63	-0.070	-0.11	-0.066
	0.96	0.76	0.96	0.76	0.96	0.90	0.89	0.90	0.89
F_{3_σ}	1.19	0.35	0.17	0.11	0.004	-0.13	-0.18	-0.12	-0.083
	± 7	± 12	± 6	± 2	± 13	± 5	± 7	± 5	± 21
F_4	1.004	-0.018	-0.003	0.0	0.0	0.020	0.005	0.0	-0.008

however, are mathematical in nature, dependent upon the number of coefficients to be solved for in the solution. They are important as an indication of the mathematical significance of a given coefficient, but beyond that their use is illusory at best. The errors involved in the graphical approach and especially in the trial-and-error approach would be difficult to evaluate and have not been given. The coefficient of determination, r^2, is given to indicate the "goodness of fit" for the graphical solution.

Listed in Table 15 are the theoretical reradiation coefficients, C_0, C_1, C_2, obtained from the theory of Russell and Merrill (1952). Using their equations 107 we have

$$\begin{aligned} C_1 &= -A_1 = 0.40(G_c - G_h)\sin i \quad , \\ C_0 &= -(0.75 - 0.25\cos^2 i)\frac{G_c + G_h}{G_c - G_h} A_1 \csc i \quad , \\ C_2 &= -0.25 \frac{G_c + G_h}{G_c - G_h} A_1 \sin i \quad , \end{aligned} \tag{4-1}$$

where i is the angle of inclination. In order to obtain $G_c + G_h$ and $G_c - G_h$, use Russell and Merrill's equation 104,

$$G_c/G_h = J_h/E_h^2 \Big/ J_c/E_c^2 \quad , \tag{4-2}$$

where J's are apparent surface brightnesses and E's are luminous efficiencies. If we assume that the J's can be given by Planck's law, then the E's are given by,

$$E_{\lambda,T} = J_{\lambda,T}/\sigma T^4 \quad ,$$

Table 15

Reradiation Coefficients

Russell-Merrill Theory

	C_0	C_1	C_2	λ_{eff} (Å)
Visual	0.040	0.051	0.013	5500
Blue	0.020	0.024	0.007	4300
Ultraviolet	0.010	0.011	0.003	3500

where σ is the Stefan-Boltzmann constant. We can write $J_{\lambda,T}$ as,

$$J_{\lambda,T} = \frac{c_1 \lambda^{-5}}{e^{c_2/\lambda T} - 1} \quad ,$$

where $c_1 = 3.74 \times 10^{-5}$ erg cm^2 sec^{-1},

$c_2 = 1.439$ cm deg,

λ is wavelength in cm,

T is temperature in degrees Kelvin.

Letting,

$$\beta = c_2/T \quad ,$$

and expanding $(e^{\beta} - 1)$ by the binomial theorem, the maximum value of β can be obtained by differentiating $E_{\lambda,T}$ with respect to β and setting the result equal to zero. This results for a specific wavelength in,

$$\beta_{max} = 4 \quad ,$$

Letting,

$$E = E_{\lambda,T}/E_{max} \quad ,$$

and

$$J = J_{\lambda,T}/J_{max} \quad ,$$

it can easily be shown that,

$$\log(J/E^2) = 3.0946 - 8\log\beta + \log(e^{\beta} - 1) \quad . \qquad (4\text{-}3)$$

Using approximate values derived from my Wilson-Devinney computer solution (Wilson and Devinney, 1971) of U Cephei,

equation (4-3) is solved for both stars. Then equation (4-2) is solved and the results are inserted into equations 108 of Russell and Merrill in the form

$$G_c + G_h = \left[\left(\frac{G_c}{G_h}\right)^{\frac{1}{2}} + \left(\frac{G_h}{G_c}\right)^{\frac{1}{2}}\right](I_c I_h)^{\frac{1}{2}}\, r_c r_h \quad ,$$

$$G_c - G_h = \left[\left(\frac{G_c}{G_h}\right)^{\frac{1}{2}} - \left(\frac{G_h}{G_c}\right)^{\frac{1}{2}}\right](I_c I_h)^{\frac{1}{2}}\, r_c r_h \quad ,$$

where the I's are the specific intensities of the stars and the r's are the fractional radii of the stars. Equations (4-1) then yield C_0, C_1, and C_2. In the absence of effects other than reradiation, C_1 equals $-A_1$.

Rectification Formulas

The following formulas were used to rectify the intensities with the coefficients F_4 of Table 14. The formulas follow from the Russell-Merrill theory.

Visual

$$I' = I - 0.040 + 0.023\cos\phi + 0.013\cos 2\phi - 0.0065\sin\phi - 0.0122\sin 2\phi + 0.012\sin 4\phi \quad ,$$

$$I'' = I'/(1.034 - 0.003\cos 2\phi) \quad ,$$

Blue

$$I' = I + 0.030 + 0.020\cos\phi + 0.010\cos 2\phi - 0.023\sin\phi - 0.005\sin 2\phi + 0.010\sin 4\phi \quad ,$$

$$I'' = I'/(1.006 + 0.004\cos 2\phi) \quad ,$$

Ultraviolet

$$I' = I + 0.010 + 0.018\cos\phi + 0.003\cos 2\phi - 0.020\sin\phi - 0.005\sin 2\phi + 0.008\sin 4\phi \quad ,$$

$$I'' = I'/(1.014 + 0.0007\cos 2\phi) \quad ,$$

where ϕ is the phase angle and I the observed intensity. Notice that in the blue, the constant term on the right hand side of the first equation is not C_0. Some adjustment was necessary to obtain a better fit. The coefficient of $\cos 2\phi$ in the same equation was also adjusted from the model value C_2.

Table 16 shows the mean intensities after the above rectification taken over quarter phase intervals. No obvious residual periodicity remains that can be accounted for by sine or cosine terms up to 4ϕ.

In light of the guidelines stated earlier for the trial-and-error analysis, it would be instructive to examine the relative success of each before proceeding with the solution. By carefully examining Table 14 it is clear the size and sign of several of the coefficients (notably A_1 and A_2) are critically dependent upon the particular set of data used in the Fourier analysis. This seems to support the observation made earlier that some residual perturbations remain of which proper account cannot be taken by the standard analysis. Indeed, these perturbations should be expected since the observations were taken during a period of increased activity. It appears doubtful, in fact, after examining light curves of U Cephei from past epochs, whether anyone has observed

this system in a state when problems with the formal rectification do not arise. It would seem advisable, therefore, to find a set of coefficients which closely resemble what one would expect from the Russell-Merrill theory. Table 16 shows that some nonconformity exists of which gas streaming models can, hopefully, take account. Overall, however, no severe damage is done to the light curve by achieving the first guideline. Table 16 also shows that the second guideline was reasonably successful, expecially in light of the preceding discussion.

Table 16

Mean Intensities Outside of Eclipse After Rectification

	Interval				
Color	0.0-0.25	0.25-0.5	0.5-0.75	0.75-1.0	0.0-1.0
Visual	0.9885	1.0093	1.0004	1.0005	0.9997
Blue	0.9709	1.0047	1.0198	1.0075	1.0007
Ultraviolet	0.9591	1.0003	1.0367	1.0037	1.0000

The eclipses are rather insensitive to any sine term adjustment since the functions are smallest here. It was noticed, however, that changes of 20% in the coefficients of the sine terms had a perceptible effect on the slant of the total eclipse. The maximum effect of the sine terms occurs at quadrature points. Close examination of the residuals

near the quadratures show a much better fit of the rectified curves to unity than even Table 16 (which has already been noted as being passably good) reveals. It appears, then, that requiring the sine terms to preserve the shape of the observed total portion of the light curves favorably affects the rectification outside of the primary eclipse.

The agreement in the depths of the secondary eclipses between the rectified and original data was the most difficult of the guidelines to achieve. Any adjustment of the cosine terms to achieve a reasonable fit in the secondary eclipse resulted in a deterioration of the fit outside eclipse. Examination of Figure 3 shows that only in the visual is the secondary well defined. The blue data show only a hint of the eclipse and it is invisible in the ultraviolet. Notice also that the scatter (presumably intrinsic to the system) is much greater in all colors just after 0.5P. The visibility of the eclipse makes it difficult to work with in all but visual light and even there the scatter during egress causes additional problems. Less weight was placed, therefore, upon achieving the final guideline.

The difficulties presented here in achieving a workable rectification of U Cephei seems to have been minimized in previous attempts at solution. These difficulties are primarily responsible for the noticeable lack of all but preliminary solutions of the system. We have in U Cephei, however, an outstanding opportunity to gather information about the geometry of the system. The total primary eclipse

is the ideal case for eclipsing binary systems. A patient approach to the solution should reap rich rewards, not only in the geometry of the system, but also in further understanding of the dynamics of these unstable close binary systems. Three solution procedures were followed in order to compare the geometrical properties of U Cephei. The Russell-Merrill solution is presented first. Following this solution are the computer approaches of Wilson and Devinney and David B. Wood.

CHAPTER V

THE SOLUTIONS

The Russell-Merrill Solutions

Nomographic Solutions

Figure 5 shows the normal points inside of primary eclipse from Table 13. It is obvious that some asymmetry exists and that this asymmetry is not simply a result of an inaccurate ephemeris, since the asymmetry increases with decreasing wavelength. This asymmetry has long been known for U Cephei. For solution purposes symmetric eclipses are required. Assuming that gas streaming effects are responsible for the lower level of light on the ingress branch, only egress was used for the Russell-Merrill solutions. Egress is presumably less affected by these perturbations and the resulting solution should be much closer to the true geometrical parameters.

The previously noted difficulty with the secondary eclipses made it very difficult to get a reliable nomographic solution. From the estimated depth of secondary eclipse in the visual (0.9595), a nomographic solution was done. Solutions only exist for limb darkening coefficients greater than 0.4. This solution fit the primary eclipse rather poorly. It was discovered that a good fit to the primary eclipse

could not be obtained using the observed depth line. In fact, acceptable solutions for primary eclipse could only be obtained for a secondary eclipse considerably deeper than that observed. Due to the observational scatter after 0.5P and the poorly determined eclipse in the blue and ultraviolet, less weight should, perhaps, be given to the secondary eclipse. Little information will come from the secondary eclipses and progress beyond a preliminary solution will be difficult by the Russell-Merrill approach.

Some further attempt was made to restrict the area of the nomographs in which solutions lie. Since the depth line, given by,

$$(1 - l_o^{tr})/l_o^{oc} \quad ,$$

has a very well determined denomiantor due to the deep total primary eclipse, any range in solutions can be ascribed to variations in the numerator. Values of l_o^{tr} consistent with the observed depth of secondary eclipse give depth lines 50% less than values of l_o^{tr} giving good fits of primary eclipse. Values for the depth line vary from 0.2 to 0.4. There is insufficient constraint here to make the nomographic solution meaningful.

Perturbations in secondary eclipse are probably responsible for the unusually shallow depths. The assumption was made, therefore, that the observations do not show the expected variations due to the transit eclipse and the secondary eclipses were not used for solution purposes. An

important constraint on the problem is thus removed and great care must now be taken to insure physically reasonable results.

The ψ Solution

The ψ function is given by,

$$\psi = \frac{\sin^2\phi - \sin^2\phi_{(\alpha = 0.6)}}{\sin^2\phi_{(\alpha = 0.6)} - \sin^2\phi_{(\alpha = 0.9)}} \qquad (5\text{-}1)$$

where subscripts refer to the value of the phase angle, ϕ, at the specified value of α, which, for an occultation eclipse, is simply the fractional light loss. Values of ϕ for $\alpha = 0.6$ and $\alpha = 0.9$ can be read directly from the light curve and thus ψ can be calculated for any other value of ϕ. Tables of the ψ function have been provided by J.E. Merrill (Merrill, 1950a) in terms of x (limb darkening coefficient), k (ratio of the radii), and α. It is more convenient, therefore, to choose values of ϕ at tabular values of α. Having calculated ψ for each of these phase angles, the tables are entered to determine k for some particular value of x. Table 17 shows the results of these calculations. Also given in Table 17 are

$$A^{OC} = \sin^2\phi(\alpha = 0.6)$$

$$B^{OC} = \sin^2\phi(\alpha = 0.6) - \sin^2\phi(\alpha = 0.9) \quad .$$

It is clear from the mean values of k and their standard errors that the coefficient of limb darkening is a difficult

Table 17

The ψ Solution

Visual

	A^{oc} = 0.06578			B^{oc} = 0.04187	
α^{oc}	ψ	^2k	^4k	^6k	^8k
0.05	3.42860	0.5941	0.6115	0.6319	0.6566
0.10	2.81238	.5768	.5991	.6235	.6527
0.20	1.93215	.5410	.5671	.5968	.6290
0.30	1.34707	.5524	.5818	.6146	.6511
0.40	0.85283	.5752	.6076	.6426	.6811
0.50	0.41043	.6115	.6458	.6825	.7221
0.60	0.0	--	--	--	--
0.70	-0.35397	.5321	.5684	.6071	.6490
0.80	-0.67122	.4442	.4832	.5240	.5686
0.90	-1.0	--	--	--	--
0.95	-1.17667	.4580	.5002	.5455	.5932
0.97	-1.26050	.4389	.4832	.5309	.5818
0.985	-1.32301	.4649	.5086	.5565	.6081
	Means	0.53 ± 6	0.56 ± 6	0.60 ± 5	0.64 ± 5

Table 17

(Continued)

Blue

	A^{oc} = 0.068609			B^{oc} = 0.043689	
α^{oc}	ψ	^2k	^4k	^6k	^8k
0.05	3.036005	0.4930	0.5077	0.5247	0.5455
0.10	2.493034	.4690	.4882	.5097	.5346
0.20	1.780613	.4568	.4812	.5089	.5386
0.30	1.286613	.5004	.5288	.5607	.5956
0.40	0.840886	.5577	.5896	.6242	.6655
0.50	0.405354	.5939	.6275	.6645	.7044
0.60	0.0	--	--	--	--
0.70	-0.364472	.6076	.6430	.6811	.7219
0.80	-0.686530	.5603	.5960	.6355	.6778
0.90	-1.0	--	--	--	--
0.95	-1.177947	.4489	.4913	.5370	.5851
0.97	-1.263844	.4473	.4688	.5173	.5688
0.985	-1.332027	.4356	.4809	.5308	.5843
	Means	0.51 ± 6	0.54 ± 6	0.57 ± 7	0.61 ± 7

Table 17

(Continued)

Ultraviolet

	A^{oc} = 0.070688			B^{oc} = 0.045591	
α^{oc}	ψ	^2k	^4k	^6k	^8k
0.05	3.268129	0.5551	0.5714	0.5909	0.6136
0.10	2.743888	.5558	.5768	.6016	.6290
0.20	2.015237	.5818	.6090	.6390	.6728
0.30	1.431369	.6171	.6482	.6816	.7191
0.40	0.893857	.6317	.6644	.7008	.7399
0.50	0.422534	.6519	.6853	.7223	.7630
0.60	0.0	--	--	--	--
0.70	-0.373223	.6632	.6983	.7357	.7760
0.80	-0.699236	.6422	.6761	.7137	.7556
0.90	-1.0	--	--	--	--
0.95	-1.162504	.5537	.5901	.6314	.6761
0.97	-1.235766	.5456	.5828	.6255	.6712
0.985	-1.311870	.5004	.5415	.5870	.6366
	Means	0.59 ± 5	0.62 ± 5	0.66 ± 6	0.70 ± 6

quantity to determine. Some idea of the limb darkening coefficient may be obtained by comparing the ψ solutions with another solution approach described below. Notice the trend of calculated k values in Table 17. A peak is reached in all colors midway through the eclipse branch and the smallest k values occur near the bottom of eclipse. This shows the same trend evidenced in many eclipsing systems, i.e., that the same value of the ratio of the radii cannot be applied throughout the eclipse. Superficially, this states that the observed light curve is not of the simple shape predicted by the Russell-Merrill model. It is tempting to make further conclusions, but this would not be fruitful until some of the perturbing effects are better understood. Upon calculating some sample light curves using the mean k values of Table 17, it was found that limb darkening coefficients near 0.6 fit slightly better in the visual and blue, but x values near 0.4 fit slightly better in ultraviolet. These values will act as a guide in selecting the preliminary solution in conjunction with the results of the next solution attempt.

The Intermediate ψ Solution

This approach was suggested by J.E. Merrill and is outlined in Princeton Observatory Contributions Number 26, page 59ff. The procedure is to take weighted means of $\sin^2\phi$ for three groups of light levels taken at the top, middle, and bottom of the eclipse curve. Group I includes $\sin^2\phi$ values corresponding to α values of 0.05, 0.10, 0.20, and 0.30 with

weights 2, 2, 2, and 1, respectively. Group II uses α values of 0.50, 0.60, and 0.70 with unit weights. Group III includes α values of 0.95, 0.97, and 0.985 with weights 1, 2, and 2, respectively. The weighted means of $\sin^2\phi$ for each group are designated M_1, M_2, and M_3, from which a value, R, can be calculated as follows,

$$R = \frac{M_1 - M_2}{M_2 - M_3} \quad .$$

Using equation (5-1) in the form,

$$\psi^{oc} = (\sin^2\phi - A^{0c})/B^{oc} \quad ,$$

it is clear that,

$$\begin{aligned} M_1[\sin^2\phi] &= A + BM_1[\psi] \quad , \\ M_2[\sin^2\phi] &= A + BM_2[\psi] \quad , \\ M_3[\sin^2\phi] &= A + BM_3[\psi] \quad , \end{aligned} \tag{5-2}$$

where $M_1[\psi]$, $M_2[\psi]$, and $M_3[\psi]$ are the weighted means in ψ corresponding to the previously calculated $M_1[\sin^2\phi]$, $M_2[\sin^2\phi]$, and $M_3[\sin^2\phi]$. From equations (5-2) it follows that,

$$R = \frac{M_1[\psi] - M_2[\psi]}{M_2[\psi] - M_3[\psi]} \quad .$$

Merrill has provided tables giving values of R, $M_1[\psi]$, $M_2[\psi]$, and $M_3[\psi]$ as a function of k and x for both occultation and transit eclipses. Given the value of R, inverse interpolation

yields k, $M_1[\psi]$, $M_2[\psi]$, and $M_3[\psi]$. Then equations (5-2) are used to obtain values of A^{oc} and B^{oc}. Table 18 shows the results of this procedure.

The usefulness of this technique is that it produces values of k which fit the entire run of the eclipse. In that sense it is probably preferable to taking means of the k values obtained in the ψ solution. Examining the results of the two methods shows that k is the same for x = 0.6 in the visual. The comparisons in the blue and ultraviolet are not as good, but the differences are smaller for small values of x.

The Adopted Solution

The real test of the solution is the fit to the observations. Many of the above solutions were plotted against the observations, including some past solutions by other authors. The intermediate ψ solution given by x = 0.6 seems to be the best fit in the visual. This solution was clearly preferred and an attempt was made to keep the value of k sensibly around the value for this solution (k = 0.6026) in the other two colors, without doing damage to the fit of the observations. This lead to the ψ solution given by x = 0.6 for the blue, which fitted the observations quite well. The preferred solution in the ultraviolet was the intermediate ψ solution for x = 0.2. This seemed clearly better than the others.

The solutions seemed close enough to assume that they should be identical for wavelength independent parameters. The average value of k for all the previously mentioned

Table 18

The Intermediate ψ Solution

	x			
	0.2	0.4	0.6	0.8
Visual				
k	0.5522	0.5757	0.6026	0.6335
$M_1[\psi]$	2.461235	2.468497	2.476399	2.485532
$M_2[\psi]$	0.012488	0.012228	0.011904	0.0116737
$M_3[\psi]$	-1.250531	-1.256798	-1.254265	-1.266061
B^{oc}	0.042679	0.042477	0.042573	0.0421879
A^{oc}	0.066033	0.066046	0.066059	0.066073
Blue				
k	0.4677	0.4901	0.5157	0.5455
$M_1[\psi]$	2.2494	2.25457	2.264007	2.27531
$M_2[\psi]$	0.00927	0.00905	0.00885	0.00869
$M_3[\psi]$	-1.26939	-1.27597	-1.28516	-1.28630
B^{oc}	0.04399	0.043775	0.043471	0.04344
A^{oc}	0.068797	0.068808	0.06882	0.068827
Ultraviolet				
k	0.5556	0.5792	0.6060	0.6371
$M_1[\psi]$	2.470583	2.477731	2.485738	2.494611
$M_2[\psi]$	0.012625	0.012368	0.012041	0.011799
$M_3[\psi]$	-1.243159	-1.247021	-1.251722	-1.256867
B^{oc}	0.046034	0.045903	0.045744	0.045567
A^{oc}	0.070856	0.070870	0.070887	0.070900

"best" solutions was taken and ψ values calculated for this value of k. The A^{oc} and B^{oc} parameters were then adjusted until the internal and external tangency points agreed for all colors. This insures the same value of inclination. These new "mean" solutions were then plotted against the observations. The fits in the visual and blue remain quite good, but this approach failed for the ultraviolet. The solutions listed in Table 19, then, are the "mean" solutions for the visual and blue, but the previously determined "best" solution for the ultraviolet. In Table 19, i_r is the "rectified" inclination, r the fractional radius, and L the fractional light, where subscripts g and s refer to the greater and smaller stars, respectively. Also listed are the geometrical parameters when the effects of rectification are removed. Figure 5 shows the normal point intensities during primary eclipse along with the eclipse curves given by these solutions.

The values of Table 19 represent a good preliminary solution to U Cephei. A procedure has been outlined (Russell and Merrill, 1952) to proceed to a refinement of the solution. Unfortunately, the procedure requires some good light values inside of secondary eclipse. As has already been noted, this cannot be done for the light curve of this epoch. The preliminary solution is, then, all that can be reliably obtained from these data. As a comparison to past solutions, Table 20 lists elements, authors, and epochs.

Table 19

The Russell-Merrill Solution

Parameters for the Rectified Light Curves

	k	i_r	r_g	r_s	L_g	L_s	x_s
Visual	0.5768	$83^{\circ}.36$	0.3278	0.1891	0.1847	0.8153	0.6
Blue	.5768	83.36	.3278	.1891	.1106	.8894	0.6
Ultraviolet	.5556	82.77	.3391	.1884	.0576	.9424	0.2

Parameters for the Observed Light Curves

	j	a_g	a_s	b_g	b_s	L_g	L_s
Visual	$83^{\circ}.43$	0.3278	0.1891	0.3243	0.1871	0.1137	0.8863
Blue	83.43	.3278	.1891	.3243	.1871	.0513	.9487
Ultraviolet	82.84	.3391	.1884	.3358	.1866	.0267	.9733

Figure 5. The primary eclipse is plotted in the three colors from the data in Table 13 as points. The solid curves represent the Russell-Merrill solutions given in Table 19.

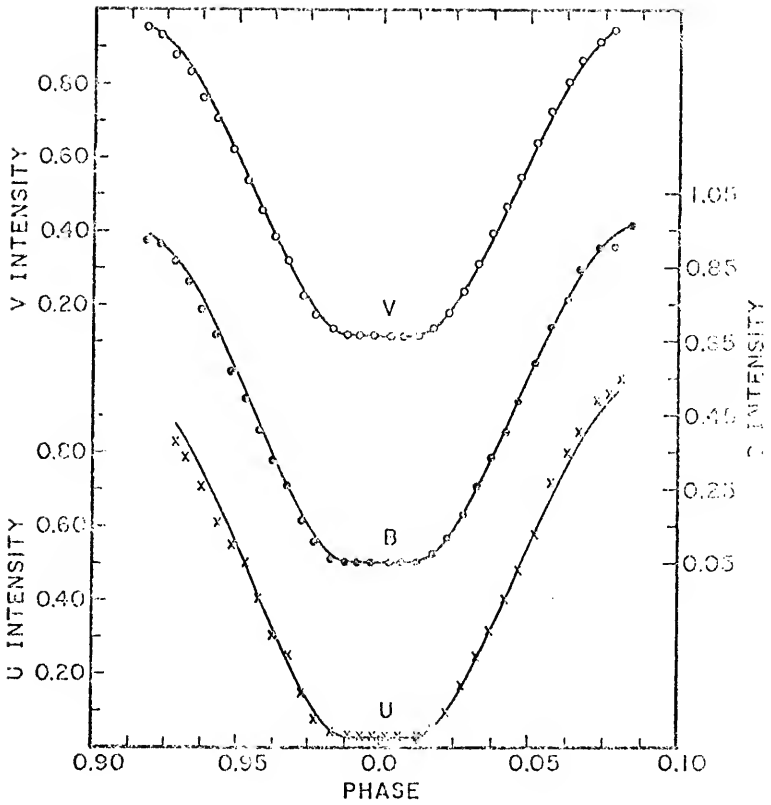
V INTENSITY
0.80
0.60
0.40
0.20
V
B
U
U INTENSITY
0.80
0.60
0.40
0.20
1.05
0.85
0.65
0.45
0.25
0.05
0.90
0.95
0.0
0.05
0.10
PHASE

Table 20

Comparison of Solutions

a_g	b_g	a_s	b_s	k	j	x_s	L_g	L_s	λ_{eff}	Reference
0.3225	0.3082	0.2000	0.1911	0.62	86°.4	0.6	0.1615	0.8385	5500 Å	Dugan, 1920
.325		.203		.63	87.8	0.6			5500	Broglia, 1959 (see Batten, 1974)
.337		.185		.55	84.6				8100	Khozov & Minaev, 1969
.3410	.3340	.1700	.1665	.50	83.14	0.6	.139	.861	4600	Tschudovitchev, 1950; solved by Hall & Walter, 1974
.3457	.3341	.1723	.1665	.50	83.15	0.2	.340	.660	8100	Khozov & Minaev, 1969; solved by Hall & Walter, 1974
.3418	.3339	.1704	.1665	.50	83.14	0.4	.184	.816	5500	Catalona & Rodona, 1974; solved by Hall & Walter, 1974

The Wilson-Devinney Solution

The computer solution technique of Wilson and Devinney (1971) was employed using the same normal points as the Russell-Merrill solution. The Wilson-Devinney program (hereafter called W-D) uses the Roche model described in detail by Kopal (1959). Since U Cephei is an example of an Algol type eclipsing binary and mass flow has been observed spectroscopically, the assumption was made that the secondary component fills its Roche lobe. This assumption corresponds to mode five of the W-D program, which also couples the luminosity (L_2) and temperature (T_2) of the secondary through the Planck function. Provision has very recently been made to allow the user to employ the model atmospheres of Carbon and Gingerich (1969) for either star. This provision, however, was not available at the time of this solution.

A new feature of the W-D program allows the user to specify an asynchronous rotation rate for either star. Since spectroscopic evidence indicates that the primary component of U Cephei is rotating five times synchronous, this value was used for that star while the secondary was allowed to rotate synchronously.

The free parameters were divided into two sets. Set one consisted of i, the inclination; T_2, the polar temperature of the secondary; Ω_1, the potential of the surface of the primary; q, the mass ratio; and L_1, the luminosity of the primary. Set two included G_1, the gravity exponent for the primary (this is 1.00 for the von Zeipel law); G_2, the same

as G_1 for the secondary; A_2, the bolometric albedo of the secondary; and x_1, the limb darkening coefficient for the primary. Each of these sets contain only one wavelength dependent parameter (L_1 for set one and x_1 for set two). The three colors were solved simultaneously in order to find the wavelength independent parameters which best represented all colors.

The polar temperature of the primary, T_1, was set at 13,600°K from the spectral classification of Batten (1974) and the temperature scale of Morton and Adams (1968). The B7V spectral type of the primary indicates that the atmosphere should be entirely radiative and A_1, the bolometric albedo of the primary, was, therefore, set equal to one. The limb darkening coefficient for the secondary, x_2, should be rather small since its atmosphere is extended out to the Roche limit. The distortions evident in secondary eclipse suggest that x_2 should be fixed to avoid spurious results and was, therefore, set equal to zero. The parameters A_2 and G_2 depend upon the shape of secondary eclipse as well and should, therefore, suffer from the same distortions. They were found, however, to converge rather quickly.

The following technique was used in the solution: An initial set of parameters was chosen from previous solutions and set one was allowed to vary. The indicated corrections were made and rerun using set two as free parameters. These corrections were then used with set one and so forth until the indicated corrections were smaller than their probable errors. Another indicator of the convergence of the solution

was that the sum of the squares of the residuals should continue to decline from run to run. As a check the reverse procedure was also followed, i.e., set two was used first, then set one, etc. The solutions were the same for both procedures, indicating that the global minimum had been found.

Set two converged very quickly, but the parameters of set one were rather highly correlated and converged rather slowly. After set two had converged, the parameters in that set were fixed at their solution values and set one was subdivided into two less highly correlated sets. Set 1a included i and L_1, while set 1b consisted of T_2, Ω_1, and q. The same alternating run method described above was used to achieve convergence in these parameters. Table 21 shows the results of the solution. In that table, $r_{(1,2)POINT}$ is the radius of the star in the direction facing the other component, $r_{(1,2)BACK}$ is the radius in the direction facing away from the other component, $r_{(1,2)SIDE}$ is the radius in the orbital plane perpendicular to the line of centers, and $r_{(1,2)POLE}$ is the radius perpendicular to the orbital plane. Figure 6 shows the solution curve plotted with the normal points for the entire light curve and Figure 7 shows the fit of the solution curve to the normal points in primary eclipse.

The D.B. Wood Solution

The computer solution technique of D.B. Wood (1972), called WINK, was used as a check on the previous solutions.

Table 21

The Wilson-Devinney Solution

Wavelength Independent Parameters

$i = 82^{\circ}.22 \pm 15$	$\Omega_1 = 6.911 \pm 34$
$G_1 = 0.46 \pm 5$	$\Omega_2 = 3.1429$ (computed)
$G_2 = 0.99 \pm 2$	$q = 0.644 \pm 8$
$T_1 = 13600°K$ (assumed)	$A_1 = 1.00$ (assumed)
$T_2 = 5454°K \pm 13$	$A_2 = 0.41 \pm 2$

Wavelength Dependent Parameters

λ (Å)	L_1	L_2	x_1	x_2
		(computed)		(assumed)
5500	0.8661 ± 3	0.1339	0.350 ± 34	0.0
4300	0.9348 ± 1	0.0652	0.621 ± 23	0.0
3500	0.9713 ± 1	0.0287	0.535 ± 41	0.0

Sizes of the Components

	r_{pole}	r_{point}	r_{side}	r_{back}
primary (1)	0.1594	0.1791	0.1776	0.1788
secondary (2)	.3198	.4425	.3345	.3665

Figure 6. The normal points of Table 13 are plotted as points and the Wilson-Devinney solution of Table 21 is represented as the solid lines.

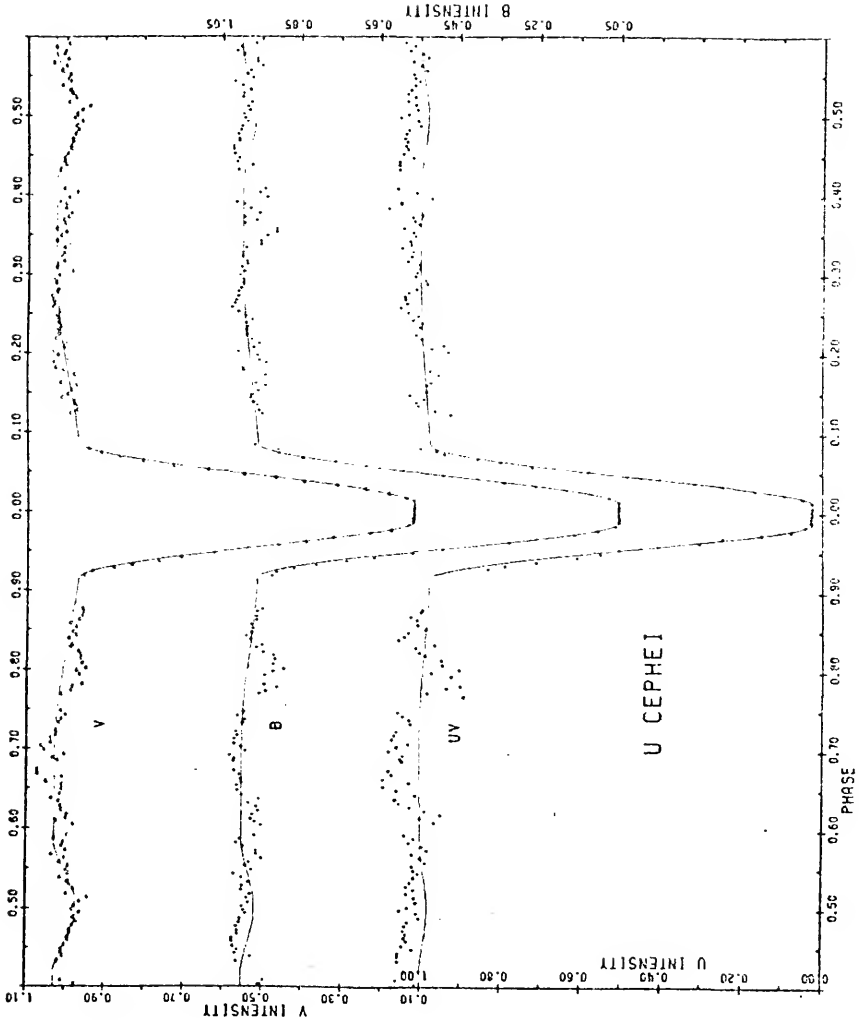
U CEPHEI
V
B
UV
PHASE
V INTENSITY
B INTENSITY
U INTENSITY

Figure 7. Same as Figure 6 for the primary eclipse only.

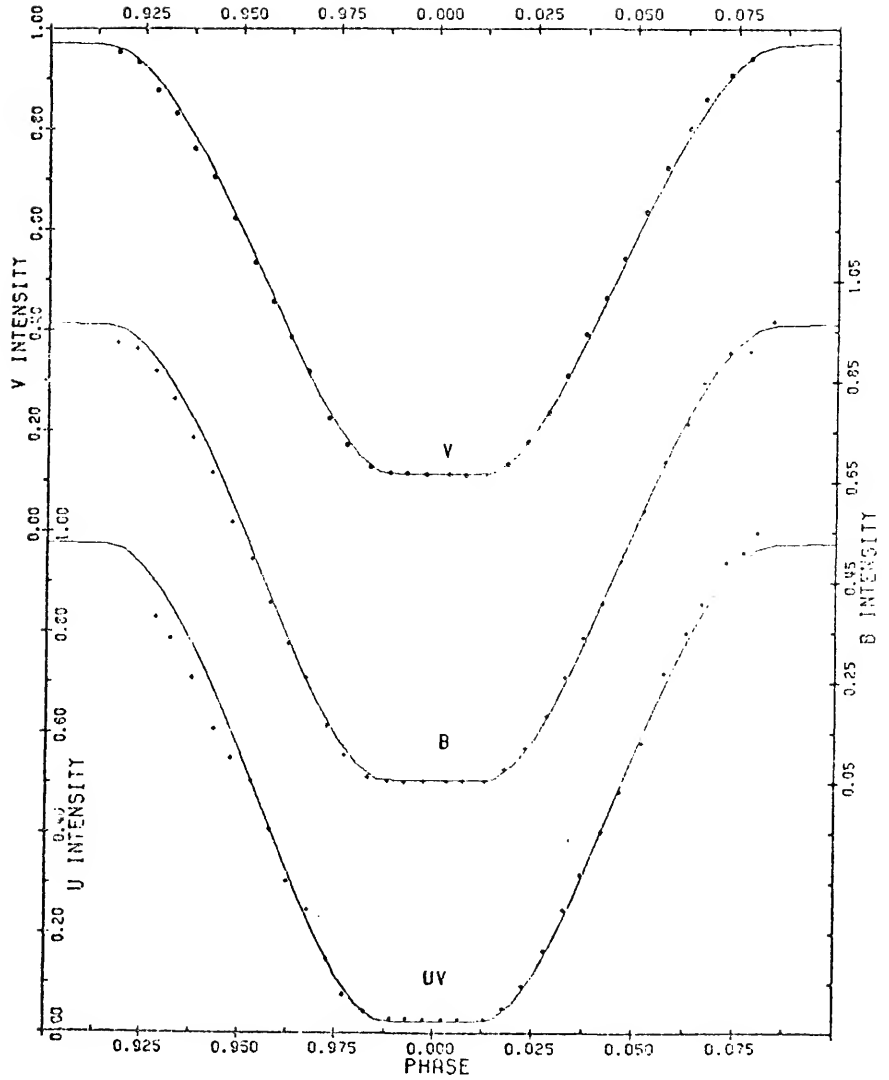
0.925
0.950
0.975
0.000
0.025
0.050
0.075
V INTENSITY
U INTENSITY
B INTENSITY
V
B
UV
PHASE

It models the components of binary systems as tri-axial ellipsoids. WINK allows for eccentricity of orbit, non-linear limb darkening and model atmospheres for the stars. Conversion of the solution parameters from W-D to the astrophysical space of WINK supplied the starting point for the differential corrections. The first set of free parameters used included i, T_2, r_1, the equatorial radius of the primary perpendicular to the line of centers, q, and QUAD MAG, the magnitude at 0.25P. This set failed to converge after six iterations, principally because the value of q was corrected from 0.6 to 1.83. The mass ratio enters the calculations through the shape of the stars rather than through the potentials as in the Roche model. As such, it is a rather poorly determined quantity for this model.

The next attempt at solution used i, T_2, r_1, and QUAD MAG as free parameters. This run converged in three iterations but produced a partial primary eclipse, contrary to observations. The value of r_1 came from the W-D solution, which incorporated a rather large asynchronism for the primary star. This causes an equatorial bulge on the primary star. The mass ratio from the W-D solution, however, requires this star to be nearly spherical, so that using the large value of r_1 from W-D made the star too large and prohibited a total eclipse. This demonstrates that U Cephei is just marginally total, which can also be seen from the loci of solution points on the nomographs of Merrill.

Reducing the initial value of r_1 to the polar radius of the W-D program again caused convergence in three iterations. The primary eclipse was total, but of much shorter duration than observed. The solution tended to enlarge the radius of primary. In all of these solutions the values of i, T_2, and QUAD MAG were only nominally corrected by the program.

Any progress in the solution beyond this stage would probably be illusory and the solution by WINK was abandoned. Some interesting conclusions can, however, be drawn. The source of distortion in shape for the tri-axial ellipsoid model is tidal forces. The primary star in U Cephei is abnormally distorted by rotation. WINK models this distortion as the influence of a massive companion. The mass ratio is, therefore, reversed in order to account for the shape of the primary. The WINK program is apparently not very useful for systems of asynchronously rotating components. More importantly for U Cephei, however, is that the effect of the asynchronous rotation is visible in the light curve.

CHAPTER VI

THE PERIOD STUDY

The Current Ephemeris

The times of primary minima were determined by bisection of the lower portions of primary eclipse. Inspection of the light curves in this portion of the eclipse reveals that any asymmetry is minimal. On those nights when the entire eclipse was not observed, the eclipse curve near the bottom was superposed with other minima close in time. The depth of the eclipse is sufficiently great that only small time errors are introduced in this way. The times of minima used for the determination of the ephemeris are shown in Table 22.

Table 22

Observed Times of Minima Used for Ephemeris Determination

Heliocentric Julian Date	O-C
244 2352.6933	-0^{d}.007
2362.6699	- .002
2367.6598	.002
2509.7623	- .001
2524.7225	.001
2646.8816	- .067
2873.7393	- .012
2903.6698	- .001

Several techniques were used to calculate the current ephemeris.

1) A plot of the residuals (O-C) for the times of minima listed in Table 22 from the light elements given by Tchudovitchev (1939) yields a sloped line from which a new period can be found.
2) A least squares fit of all photoelectric times of minima in the interval of my observations (Rafert, 1977) gives T_o, the initial epoch and P, the period.
3) A similar least squares fit to all times of minima (including visual determinations) in the same interval (Rafert, 1977) yields a third ephemeris.

The mean of T_o and P for these three techniques gives the current light elements as,

$$\text{Min J D} = \underset{\pm\ 3}{2442352.6999} + \underset{\pm\ 4}{2^d.493071} \cdot E \quad ,$$

where E is the cycle count from the initial epoch. This ephemeris was used to calculate the phases of Table 13 and the O-C's of Table 22.

The O-C Diagram

The data and computer programs used in the following sections are due to Rafert (1977). Figure 8a shows the residuals (O-C's) of the times of minima from the light elements $2407890.2957 + 2^d.4929005 \cdot E$ given by Tchudovitchev (1939). A parabolic regression of this data weighted to the

Figure 8. The observed minus the computed times of minima using the ephemeris 2407890.2957 + 2.4929005 are shown in part (a) vs. the cycle count. Part (b) shows the residuals from the solid line parabolic fit through the data of part (a).

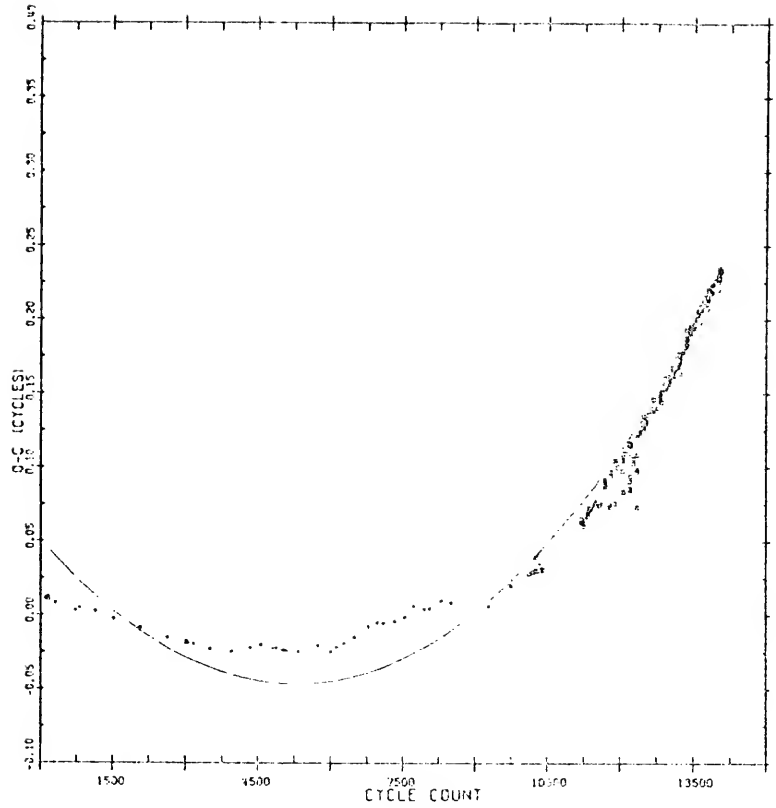
O-C (CYCLES)
0.20
0.15
0.10
0.05
0.00
-0.05
-0.10
1500
4500
7500
10500
13500
CYCLE COUNT

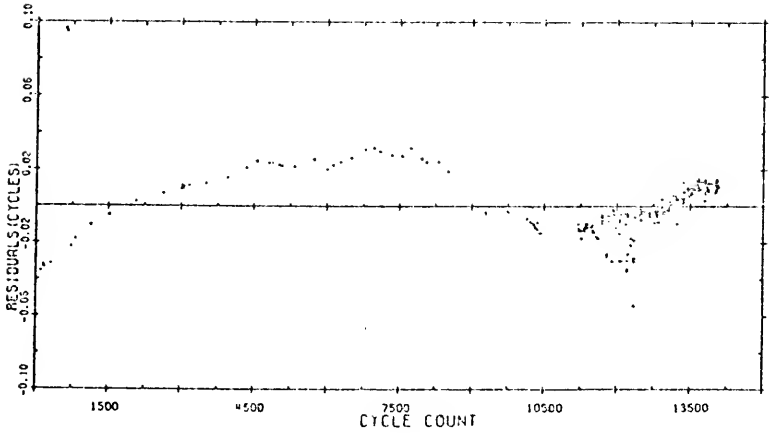
RESIDUALS (CYCLES)
0.10
0.06
0.02
-0.02
-0.06
-0.10
1500
4500
7500
10500
13500
CYCLE COUNT

precision of each determination yields,

$$\text{MIN J D} = \underset{\pm\ 11}{2407890.421} + \underset{\pm\ 28}{2^{d}.4928089} \cdot E + \underset{\pm\ 17}{(8.68 \times 10^{-9})E^{2}} \quad ,$$

which is shown as the solid line in Figure 8a. The residuals from this parabolic fit are shown in Figure 8b. Hall (1975) has suggested that many small amplitude parabolas superpose upon the major parabola, which may indicate enhanced mass transfer. Alternatively, the residual curve (Figure 8b) may indicate a sine term. Rafert (1977) has shown, however, that if a sine term is present, it does not remain phase coherent during the run of the data. While either of these alternatives has its physical cause, neither seems well enough established to be of use in predicting future behavior. The recent residuals from the parabolic ephemeris are quite small and it appears as if this ephemeris continues to predict the times of minima very well with only minor amplitude and time deviations.

One important astrophysical quantity can be derived from the parabolic ephemeris above. If conservation of mass and steady mass transfer are assumed (both of which are suspect in view of the history of U Cephei), then one can deduce the mass transfer rate. Let

$$\frac{d\,T}{d\,E} = P \qquad (6\text{-}1)$$

where T is the time of minimum. Integrating this expression yields the ephemeris,

$$T = \int P \cdot dE \quad . \tag{6-2}$$

The assumption of a steady mass transfer rate can be written as

$$P = P_o + \frac{dP}{dE} \cdot E \quad .$$

Substituting into equation (6-2) and integrating yields,

$$T = T_o + P_o \cdot E + \frac{1}{2} \frac{dP}{dE} E^2 \quad . \tag{6-3}$$

We may write dP/dE as,

$$\frac{dP}{dE} = \frac{dP}{dt} \cdot \frac{dt}{dE} \tag{6-4}$$

and substitute equations (6-1) and (6-4) into (6-3) to obtain

$$T = T_o + P_o \cdot E + (\frac{1}{2} P \frac{dP}{dt})E^2 \quad . \tag{6-5}$$

This is the form of the parabolic ephemeris given above. If we denote the quantity in parentheses in equation (6-5) by A, then for a unit time interval,

$$\frac{\Delta P}{P} = \frac{2A}{P^2} \quad . \tag{6-6}$$

If an amount of matter $\Delta m > 0$ is transferred from a less to a more massive star (which is the conclusion of the spectroscopic data for U Cephei), then the resultant change of period is

$$\frac{\Delta P}{P} = \frac{3(2\mu - 1)\Delta m}{\mu(1 - \mu)m} \quad ,$$

where m is the sum of the masses and $\mu = m_1/m$, m_1 being the mass of the primary star. Using equation (6-6) and the parameters of the parabolic ephemeris,

$$\Delta P/P = 2.79 \times 10^{-9} \quad .$$

Using the masses derived by Batten (1974) of $m_1 = 4.2 \pm 0.6\ M_\odot$ and $m_2 = 2.8 \pm 0.5\ M_\odot$, one obtains,

$$\Delta m = 7.81 \times 10^{-9}\ M_\odot/\text{cycle}$$
$$= 1.14 \times 10^{-6}\ M_\odot/\text{year} \quad .$$

The residuals shown in Figure 8b make it apparent that the times of minima do not strictly show the parabolic shape expected for this steady mass transfer rate. Large deviations from the mean mass transfer rate may be expected. These deviations may have several causes.

1) The hydrodynamical model of Prendergast and Taam (1974) shows that a small percentage of material is lost from the system. This loss not only deprives the system of that mass, but also removes the angular momentum of that mass. The loss of angular momentum changes the period.
2) The mass may be transferred rather sporadically to give the overall mean transfer rate. The spectroscopic work of Batten (1974) supports this conclusion. After an extensive search of many spectra of U Cephei, Batten was only rarely able to report emission in the Balmer lines of hydrogen. Such emission lines

show radial velocities indicative of a gaseous stream toward the primary star. The events reported in this dissertation, however, were accompanied by the appearance of a very strong emission in the Balmer lines as well as lines of other elements. This suggests that the mass transfer rate was especially great at these times. It is unlikely that these events are unique which suggests that mass transfer in U Cephei is rather sporadic.

3) The sustained high rate of rotation of the primary star is presumably a direct cause of the mass transfer. Particle trajectory calculations show that the transferred mass is quite effective in increasing the rotation of the primary star. Angular momentum from the transferred mass which goes into rotational angular momentum behaves, however, just as if it had been lost to the system in so far as period changes are concerned. Wilson and Stothers (1975) give an expression to estimate the ratio of the period change due to this so-called non-conservation of angular momentum (NCJ) to the period change due to mass transfer (MT) given above. If k is a factor between zero and unity which depends on the latitude at which the gas stream hits the surface of the primary and RM is the ratio of the masses in the sense m_1/m_2, then,

$$\frac{dP_{NCJ}}{dP_{MT}} = 0.69\ k \left[\frac{(1 + RM)^{1/3}\ RM^{0.77}}{(1 - RM)} \frac{(m_2)^{0.11}}{P^{1/3}} \right] .$$

If we adopt the parameters $m_2 = 2.8\ M_\odot$, $P = 2^d.4928089$, $k = 0.8$, and $RM = 1.55$, then,

$$(dP/dt)_{NCJ\ (max)} = -1.58\ (dP/dt)_{MT} \quad . \qquad (6\text{-}7)$$

In the real system the orbital angular momentum of the transferred mass is not completely converted into rotational angular momentum. Mechanisms may also be present (see Chapter VII) to cause the gas stream to strike the surface of the primary at higher latitudes, thereby reducing k. Equation (6-7) indicates, however, that these two causes of period changes are competing and may be comparable. The neglect of NCJ will yield a mass transfer rate which is a lower limit to the true rate.

The fit of the least squares parabola to the data in Figure 8a may lead one to question the choice of a parabola as the functional form. In fact, two straight line segments joining at about 9000 cycles (1940) may yield residuals at least as small as the parabolic residuals.

Evidence for Recent Period Changes

The more recent data of Figure 8a were reanalyzed in an attempt to find the best ephemeris for accurate predictions of future times of minima. Figure 9a shows the times of minima from November 1965, until June 1976, using the same light elements as Figure 8a. Small changes in slope appear

Figure 9. Part (a) shows the O-C diagram for the times of minima from November 1965, until June 1976, using the same ephemeris as Figure 8. The three straight line segments represent the least squares fit of these segments, the residuals of which are shown in part (b).

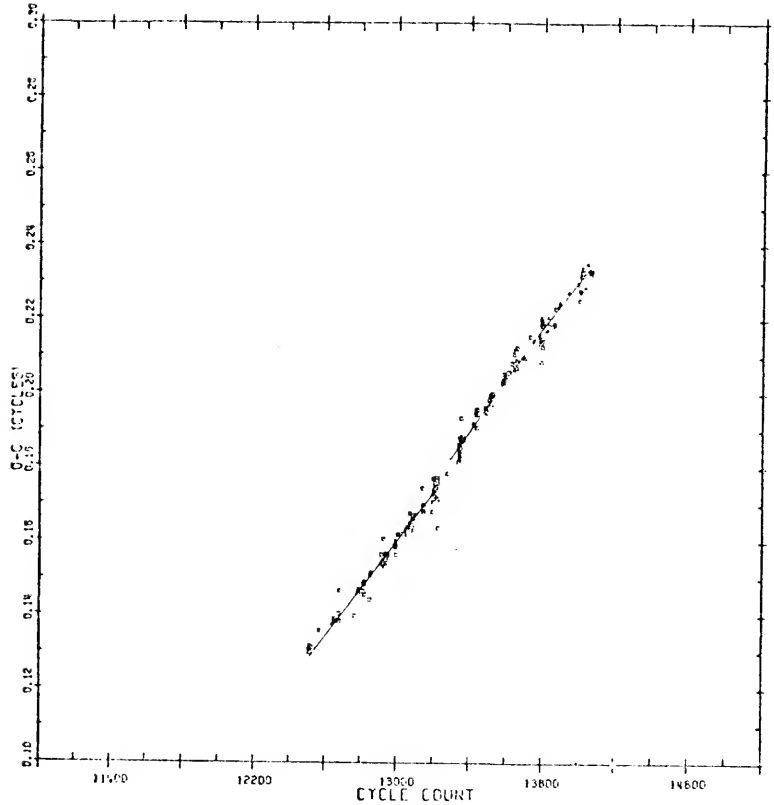
0.30
0.28
0.26
0.24
0.22
0.20
0.18
0.16
0.14
0.12
0.10
O-C (CYCLES)
11400
12200
13000
13800
14600
CYCLE COUNT

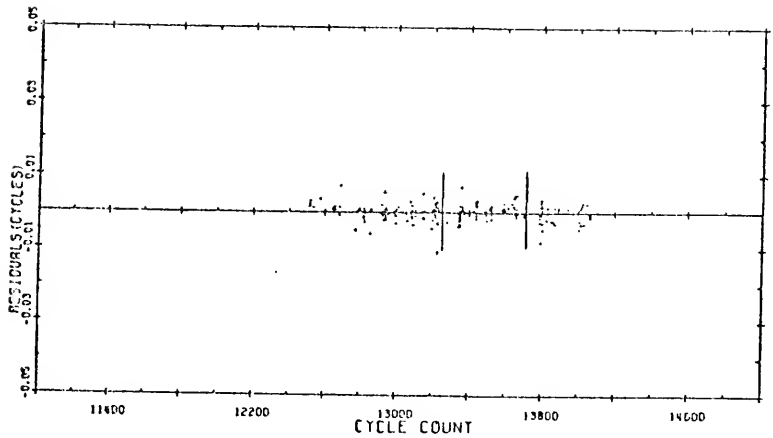
0.05
0.03
0.01
-0.01
-0.03
-0.05
RESIDUALS (CYCLES)
11400
12200
13000
13800
14600
CYCLE COUNT

near cycles 13278 (February 1971) and 13730 (March 1974). The data were divided into three sets at these points and separate linear regressions produced the solid lines drawn through the data. The resulting light elements are listed below.

$$\text{Set 1} \quad \text{Min JD} = \underset{\pm\ 10}{2439086.7724} + \underset{\pm\ 19}{2^{d}.4930634} \cdot E$$

$$\text{Set 2} \quad \text{Min JD} = \underset{\pm\ 5}{2440991.4802} + \underset{\pm\ 28}{2^{d}.4930765} \cdot E$$

$$\text{Set 3} \quad \text{Min JD} = \underset{\pm\ 19}{2442118.3508} + \underset{\pm\ 10}{2^{d}.493058} \cdot E \quad .$$

The errors quoted are standard errors. If one accepts these results as significant, the period changes amount to 1.3×10^{-5} day ($1^{s}.1$) between sets 1 and 2 and -1.85×10^{-5} day ($-1^{s}.6$) between sets 2 and 3.

Olson (1977) has used "11 essentially undisturbed eclipses" by Hall and Keel, R. Crawford, Scarfe, and Olson between November 1974, and November 1976, to calculate the light elements,

$$\text{Min JD} = 2442377.6242 + 2^{d}.4930709 \cdot E \quad .$$

This ephemeris has the advantage of being based on photoelectric observations, but includes far fewer observations than my set 3. The differences between the periods of my set 3 and Olson's or of my current ephemeris and Olson's are not significant in view of the errors of each determination. If Olson's values are used, then the period change between sets 2 and 3 becomes -9.1×10^{-6} day or $-0^{s}.79$.

If sets 2 and 3 are combined and a linear regression performed, the mean ephemeris is,

$$\text{Set 2 and 3} \quad \text{Min JD} = 2440991.4811 \pm 7 + 2^{d}.4930699 \pm 15 \cdot E \ .$$

This ephemeris compared to Olson's indicates that the period has not changed significantly since February 1971. In fact, if only the photoelectric observations are considered, the noted period change about March 1974, is difficult to see. This is not to say that the visually determined times of minima are to be ignored. The accuracy of photoelectric observations may, in fact, be a handicap in this case. The previously mentioned changes in shape of the primary eclipse can make an accurate determination of the time of minimum difficult. The rather limited sample of photoelectric times of minima may bias the sample by reflecting these types of errors. The great number of visual determinations, while individually not as accurate, may, en masse, provide a better determination of the ephemeris.

The sudden changes of period noted above may be an indication of sudden mass transfer. If such is the case, a major event may have occurred prior to March 1974. One must, however, question why no such sudden period change has occurred to signal the events of the summer of 1974, and the fall of 1975. One possible explanation is that the time base of the observations since these events is not sufficiently long for a change to be noticed. Alternatively, the changes of

period produced by mass transferred in these events may have been cancelled by changes of period produced by the orbital angular momentum of this mass being temporarily converted into rotational angular momentum of the primary star.

CHAPTER VII

THE MODEL

Introduction

The purpose of this model will be to test the effect of abnormal surface brightness distributions on the residual light in eclipse. It would be convenient if an analytical solution could be found. Analytic forms for the light changes during eclipse on stars with normal surface brightness distributions (i.e., fractional linear limb darkening accounts for the brightness distribution) have been given by Tsesevich (1973). Unfortunately, these integrals cannot be solved in closed form since they involve elliptic functions. Solution of the eclipse integrals for abnormal brightness distributions is still more difficult. A numerical procedure was, therefore, employed to solve for the eclipse curves.

Before beginning a discussion of how the surface brightness distribution was constructed, it would be instructive to examine the residuals from the solution in primary eclipse given in Figures 13 to 25. The successful model must deal with the following observed facts.

1) For most of the observed eclipses, the residual light was in excess of the solution.
2) The variation of the residuals throughout the eclipse seemed to be smooth.

3) On nights of high photometric activity (during major outbursts) the variation of the excess seemed to display the same dual-peaked type of profile. Nights of rather low activity seemed to vary in a less regular manner.

4) During major activity the excess disappeared at or near second contact. The excess drops to zero before first and fourth contacts.

5) The peaks of the excess before and after totality on 10 November and 15 November 1974 (see Figures 15-18) show a slow rise, rapid decline before totality and a rapid rise, slow decline after totality.

The following conclusions and assumptions can be made incorporating these facts.

1) The observations were normalized using the same intensity as unity, regardless of whether the observations were used in the formation of normal points for the solution. This suggests that positive residuals represent a surplus of light and negative residuals a deficiency of light from the predictions of the Russell model. This apparently simple conclusion determines the normalization of the theoretical model if it is to represent the observations.

2) The apparent smoothness of the variation of the excess light indicates that one extended source is responsible.

3) This source of the excess must originate on the primary star since it tends to disappear during totality. The geometry of the solutions indicate that the contact points fall in the polar regions of the primary (the latitude on the primary of second and third contacts is $54^{\circ}.78$). Since the excess light falls to near zero at second contact and begins anew near third contact, one suspects that the source of the excess is in the polar regions of primary. This assumption does not exclude other possibilities and other positions of the source will be tested. The decline of the excess to zero before first and fourth contacts indicates that the source is not visible at these times.

Constructing the Test Grid

The loss of light during eclipse can be modeled by summing the contributions from a grid of test points representing areas on the eclipsed star. The eclipsing star plays no role other than adding its luminosity (L_2) to the total light and acting as an occulting disk. The eclipsing star should present a nearly circular cross-section during primary eclipse and no detectable ellipsoidal type light variations should result. Additionally, in the case of U Cephei, the secondary star contributes relatively little to the total light and small variations in its light will be unimportant. The eclipsed star is modeled as circular and is eclipsed by a

circular disk moving in a circular orbit. The inclination of the system is taken into account as is any desired degree of limb darkening on the eclipsed star. All computations are projected onto the plane of the sky.

The coordinate system used for the computations is on the plane of the sky. The x-axis is in the line of sight, the y-axis connects the line of centers of the two stars at quadratures, and the z-axis is perpendicular to the y-axis in the plane of the sky. Figure 10 diagrams the coordinate system and shows the primary star for perspective. Notice that the north pole of the primary star is tilted toward the observer by the compliment of the inclination angle and that this pole will remain fixed on the primary star as it is projected on the sky throughout the orbit.

A test grid was established on the primary star using test points to represent equal areas on the surface of the star. These test points are then projected onto the y-z plane. The grid is built up in concentric rings about the projection onto the sky of the sub-earth point (the origin of coordinates). Let there be NP test points representing NP equal areas on the visible hemisphere of the star. Since we see only one hemisphere, then each equal area must be,

$$A = 2\pi r_1^2/NP \quad ,$$

where r_1 is the fractional radius of the primary star. The first of these areas will cover the origin. This is the surface area of a spherical cap on the x-axis. This spherical

Figure 10. The geometry of the model and the source regions. Part (a) shows the coordinate system used to construct the test grid. The test points lie on the sphere and are given by angles β, measured radially from the sub-earth point, and α, measured counterclockwise from the +z axis. Part (b) shows a typical source region as constructed in the model. This diagram is for 0.0P so that the physical interpretation of l_1 and l_2 can be shown. The projected equator of the star is drawn as a dotted curve and ω represents the direction of rotation.

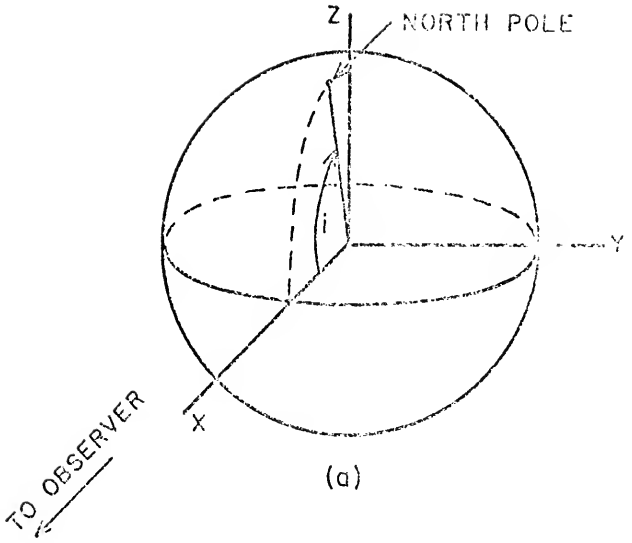
Z
NORTH POLE
i
Y
TO OBSERVER
(a)

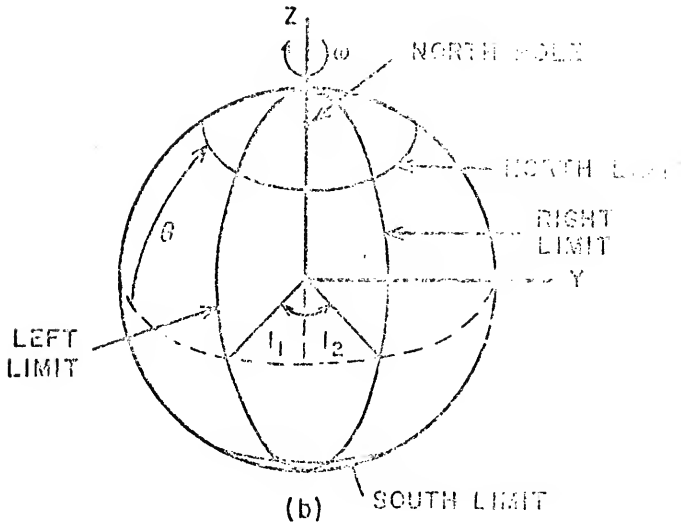
Z
ω
NORTH POLE
SOUTH LIMIT
RIGHT
LIMIT
Y
θ
LEFT
LIMIT
l_1
l_2
SOUTH LIMIT
(b)

cap has surface area,

$$A_p = 2\pi r_1 h \quad ,$$

where h is the extent of this cap on the x-axis and is given by,

$$h = r_1(1 - \cos\beta_p) \quad .$$

β is the radial angular measure from the sub-earth point to any point on the star and β_p is the extent in β of this spherical cap. Thus,

$$A_p = 2\pi r_1^2(1 - \cos\beta_p) \quad ,$$

and we would like $A_p = A$. This constraint gives β_p as

$$1 - \frac{1}{NP} = \cos\beta_p \quad . \tag{7-1}$$

The remaining range of β is $\pi/2 - \beta_p$ and we now divide this remaining range into n concentric rings of equal angular extent, $\Delta\beta$. The test points will fall in the middle of each ring and the last ring of test points will be on the limb. This requires

$$\Delta\beta = \frac{\frac{\pi}{2} - \beta_p - \frac{\Delta\beta}{2}}{n} \quad ,$$

or

$$\Delta\beta = \frac{\pi - 2\beta_p}{2n + 1} \quad . \tag{7-2}$$

The angles, β, at which the test points will fall are given by,

$$\beta = \beta_p + (2m - 1)\frac{\Delta\beta}{2} \quad (m = 1, 2, 3, \ldots, n + 1) \quad . \tag{7-3}$$

If the grid areas, A, are small enough, they may be expressed as elemental surface areas of the sphere or,

$$A = r_1^2 \sin\beta\Delta\alpha\Delta\beta \quad ,$$

where α is measured clockwise around a ring of test points beginning at the +z-axis. Setting the two expressions for A equal gives $\Delta\alpha$ as

$$\Delta\alpha = \frac{2\pi}{(NP)\Delta\beta \sin\beta} \quad .$$

$\Delta\beta$ and β are given by equations (7-2) and (7-3), respectively. The symmetry of the test grid requires the calculation of positions for test points in one quadrant of the visible hemisphere only. The complete grid is then obtained by mirroring this quadrant throughout the entire hemisphere. The longitudinal angle, α, need only run until $\pi/2$ for the calculation of positions in this quadrant. It would be coincidental if an integer number of segments, $\Delta\alpha$, occupied a ring in the quadrant of interest. Test points representing differential areas, $\Delta\alpha$ by $\Delta\beta$, are given unit weight, whereas the fractional area remaining in the quadrant is given weight p, where

$$p = \frac{\pi}{2\Delta\alpha} - \text{INT}\left(\frac{\pi}{2\Delta\alpha}\right)$$

and INT represents the integer part of the quantity in parentheses. Thus the angle, α, for each test point is given by

$$\alpha = (m - 1)\Delta\alpha \quad \left(m = 1, 2, 3, \ldots, \text{INT}\left(\frac{\pi}{2\Delta\alpha}\right)\right) \qquad (7\text{-}4a)$$

and for the final test point on each ring in the quadrant by,

$$\alpha_f = \frac{1}{2}(\pi - p\Delta\alpha) \quad . \tag{7-4b}$$

The test points given by equations (7-3) and (7-4) must now be projected onto the y-z plane. The y and z coordinates of each test point are,

$$y = r_1 \sin\beta \sin\alpha$$

$$z = r_1 \sin\beta \cos\alpha \quad .$$

The unit normal intensity of each test point must be modified by the foreshortening angle, γ, given by,

$$\cos\gamma = \cos\beta \quad .$$

The Progression of the Eclipse

The programmer is free to test the level of light throughout eclipse at any specified interval of phase angle given in degrees. The first such level corresponds to the first phase angle outside of external tangency, ϕ_e, where,

$$\sin^2\phi_e = \frac{(r_1 + r_2)^2 - \cos^2 i}{\sin^2 i} \quad ,$$

and r_2 is the fractional radius of the secondary star, and i is the inclination of the orbit. This level represents the full light of the eclipsed star. The contributions of all the test points for a normal surface brightness distribution are used as a normalizing factor for all other light levels.

Test points are considered to be eclipsed if the distance from the point to the center of the eclipsing star is less than r_2. The center of the eclipsing star describes an ellipse on the sky as the orbit progresses. At any phase angle, ϕ, the y-z coordinates of this center are,

$$y_c = -\sin\phi$$

$$z_c = -\cos\phi \cos i \quad .$$

At present the major source of error in the procedure occurs by neglecting partially eclipsed test areas. If a test point is uneclipsed, it is entered into the summation of intensities given by,

$$I'(\phi) = \sum_i (1 - x + x \cos\gamma_i) \cos \gamma_i w_i \quad . \qquad (7\text{-}5)$$

In equation (7-5) x is the limb darkening coefficient and w_i the weighting factor for each test area (either one or p). The summation extends over all uneclipsed test points. The $\cos\gamma$ factor outside the parentheses accounts for the diminishing size of the test areas as the limb of the star is approached. For a test grid of 4000 points, this procedure reproduces the light levels of the Russell-Merrill method to $\pm$ 0.0005, standard error. If L_{norm} is the result of equation (7-5) for the first point outside of eclipse, then the other light levels are normalized by,

$$I(\phi) = \frac{I'(\phi)\ L_1}{L_{norm}} + L_2 \quad ,$$

where L_1 and L_2 stand for the lights of the primary and secondary stars, respectively.

The Geometry of the Source Region

In view of the above considerations, a geometry of the source of the excess light can be proposed. To retain sufficient choice in the location of the source, it can be modeled as either a band centered on the equator or as polar sections (hereafter called the polar source regions). Since inclination is considered in the model, the latitudinal limits of the source (hereafter called the north or south limit) are small circles on the star which become ellipses projected onto the sky. The equatorial band will lie between these limits, whereas the polar source regions lie northward and southward of these limits. If θ is the angle above or below the equator of these limits, the centers of the projected ellipses lie at,

$$y_{1c} = 0$$

$$z_{1c} = \pm r_B \sin\theta \quad .$$

These will be similar ellipses of semi-major axes along the y-axis of $r_1 \cos\theta$ and semi-minor axes along the z-axis of $r_1 \cos\theta \cos i$. The functional form of these ellipses can then be written as,

$$\frac{y^2}{r_1^2 \cos^2\theta} + \frac{(z \pm r_1 \sin\theta)^2}{r_1^2 \cos^2\theta \cos^2 i} = 1 \quad .$$

The lower half of each ellipse is on the visible hemisphere, so that,

$$z_{north} = -\cos i\sqrt{r_1^2 \cos^2\theta - y^2} + r_1 \sin\theta$$

$$z_{south} = -\cos i\sqrt{r_1^2 \cos^2\theta - y^2} - r_1 \sin\theta \quad , \quad (7\text{-}6)$$

where z_{north} and z_{south} are the corresponding z values on the north and south limits for a given value of y. The argument of the square roots will be negative for y-values whose absolute values exceed the semi-major axis. The y-coordinate of each test point on the star is inserted into equations (7-6) to determine the latitudinal limits. The z-coordinate of each test point is then compared to the computed z_{north} and z_{south} for possible inclusion in the desired source region.

Those test points meeting the latitudinal condition are then tested in longitude for membership in the source region. The longitudinal limits (hereafter called right and left limits) represent great circles on the star. In order to simplify the calculations, these circles intersect on the z-axis at the projected limb of the star. These intersections would be the poles of the star for an inclination of 90°. In general, one would like to use great circles intersecting at the true poles of the star. The projection of these circles onto the sky, however, yield functional forms of degree four. The simplified forms that were used confine the use of the model to inclinations close to 90°. The great circles used in the calculations become ellipses when projected onto the

sky. These ellipses will be centered on the origin with a semi-major axis of r_1 along the z-axis. The semi-minor axis may be determined knowing the coordinates of a point on the ellipse and solving for b in,

$$\frac{z^2}{r_1^2} + \frac{y^2}{b^2} = 1 \quad . \tag{7-7}$$

We would like the source to rotate with the star (either synchronously with the orbital rate or at any specified value). The left and right limits can then be given as angular deviations (l_1 and l_2) from the z-axis at 0.0P. The coordinates of the intersection of the line of centers with the equator of the star can be used to solve equation (7-7) for b. These are,

$$y_{0c} = -r_1 \sin\phi$$

$$z_{0c} = -r_1 \cos\phi \cos i \quad ,$$

where ϕ is the phase angle. This point will be on the z-axis at 0.0P. The intersections of the desired ellipses with the equator are then,

$$y_{2c} = -r_1 \sin (\phi + l_j)$$

$$z_{2c} = -r_1 \cos (\phi + l_j) \cos i \quad (j = 1, 2) \quad .$$

Solving (7-7) for b yields,

$$b^2 = \frac{r_1^2 \sin^2 (\phi + l_j)}{1 - \cos^2 (\phi + l_j) \cos^2 i} \quad (j = 1, 2) \quad .$$

Now (7-7) can be used as a condition on y for test points that meet the condition in equations (7-6). The y condition is,

$$y_{L,R} = \pm \sqrt{\frac{(r_1^2 - z^2) \sin^2 (\phi + l_j)}{1 - \cos^2 (\phi + l_j) \cos^2 i}} \qquad (j = 1,2). \quad (7\text{-}8)$$

Care must be taken to resolve the sign of $y_{L,R}$ for each phase angle. Should one of the ellipse segments fall on the back of the star for a particular phase angle the appropriate limb of the star is used for that limit. The greater of l_1 and l_2 corresponds to the left limit.

Those test grid points lying within the limits given by (7-8) and meeting the desired latitudinal limits of (7-6) are within the source region of interest. These points are entered into the summation of intensity (7-5) with the coefficient of limb darkening equal to one (in lieu of some better assumption) and a multiplying factor I_s, i.e.,

$$I_s' (\phi) = \sum_k I_s \, w_k \cos^2 \gamma_k \quad . \qquad (7\text{-}9)$$

The weights, w_k, have the same meaning as in (7-5) and the summation extends over all test points in the visible source region. The constant I_s is the ratio of the point intensity normal to the star's surface in the source region to that elsewhere on the star. It enters the summation in a natural way and can easily be converted to a temperature excess (or deficiency) in the source region by,

$$\Delta T = T_1 (I_s)^{\frac{1}{4}} - T_1 \quad , \qquad (7\text{-}10)$$

where T_1 is the temperature of the primary star and Planck's law is assumed. Equation (7-5), for test points outside the source region, and equation (7-9), for test points in the source region, together give the intensity of the star with an abnormal surface brightness distribution. This intensity is normalized in the same way as the normally bright model.

The user may, in addition, place a shell of attenuating material about the equatorial regions when the source region is a polar segment. This is accomplished by supplying a positive, non-zero value for τ, the optical depth. The effective optical depth for any test point is given by,

$$\tau_e \approx \tau/\cos\gamma \quad ,$$

and equation (7-5) is then modified by the multiplying factor $e^{-\tau_e}$.

The list of input parameters reads as follows:

i, the inclination of the orbit. The rotational axis of the primary is assumed perpendicular to the orbital plane;

r_1, the fractional radius of the primary star;

r_2, the fractional radius of the secondary star;

L_1, the fractional light of the primary;

L_2, the fractional light of the secondary ($L_1 + L_2 = 1$);

I_s, the intensity ratio of the source to the normal star;

θ, the latitudinal extent of the source above and below the equator of primary;

NP, the number of test grid points on the visible hemisphere of primary;

n, the number of concentric rings of test points on primary;

INTφ, the phase angle interval (in degrees) at which the light levels are computed;

x_1, the limb darkening coefficient of the primary;

τ, the optical depth of the attenuating cloud;

l_1, the longitudinal deviation (in degrees) of the left hand limit of the source from the y-axis at mid-eclipse;

l_2, same as l_1 for the right hand limit;

MODE, 1 for a polar segment source, 2 for an equatorial band.

The flexibility of the model allows one to test a great many theoretical situations, such as:

1) any type of primary eclipse. Notice that by exchanging the role of primary and secondary, the same model can also be used to test abnormal brightness distributions on the secondary star during secondary eclipse;
2) hot or cold ($I_s < 1$) source regions in the polar regions of the primary;
3) hot or cold source regions on the equator of primary;
4) an attenuating cloud about the equator either in combination with a polar source region or by itself (set $I_s = 1$);
5) a polar source region rotating synchronously with the primary star rather than synchronously with the orbit. This was felt to be non-physical for a source region on the equator, presumably caused by infalling material from the secondary star. At present this is a

change in a source statement in the program, but it may become an input parameter if sufficient usefulness is demonstrated. Notice that the rate of asynchronism of the primary must be its synodic period with the line of centers rather than its spectroscopically determined sidereal period.

Residuals from the model with a normal surface brightness distribution are formed which should correspond to the residuals of the observations from the Russell-Merrill solution. Figures 11 and 12 show some residual curves computed for the situations given above.

One piece of astrophysical information is also given by the model. Assuming that a hot source region is formed by infalling material heating the surface, a mean velocity of this material can be calculated by,

$$\bar{v} = \sqrt{\frac{3\ k\Delta T}{m}} \quad ,$$

where k is Boltzmann's constant and m is the mass of a particle. Most of this material will be hydrogen and thus m is the mass of a proton. The mean velocity does not account for the efficiency of the supposed shock heating and assumes a Maxwellian velocity distribution for the infalling material. As such, this mean velocity probably represents a lower limit.

Fitting the Model to the Observations

The first set of models tried to fit the observations using previous suggestions for the location of the source

Figure 11. Sample residual profiles produced by the model. The dashed line segments indicate second and third contacts. First and fourth contacts fall at phases 0.9154 and 0.0846, respectively, and have not been drawn. Part (a) represents the Main Stream Hot Spot (synchronous hot equatorial source). Part (b) is Olson's model (synchronous cold equatorial source). Parts (c) and (d) represent the synchronous hot and cold polar sources, respectively. The ordinates are arbitrary, but the proper sign and zero point have been given.

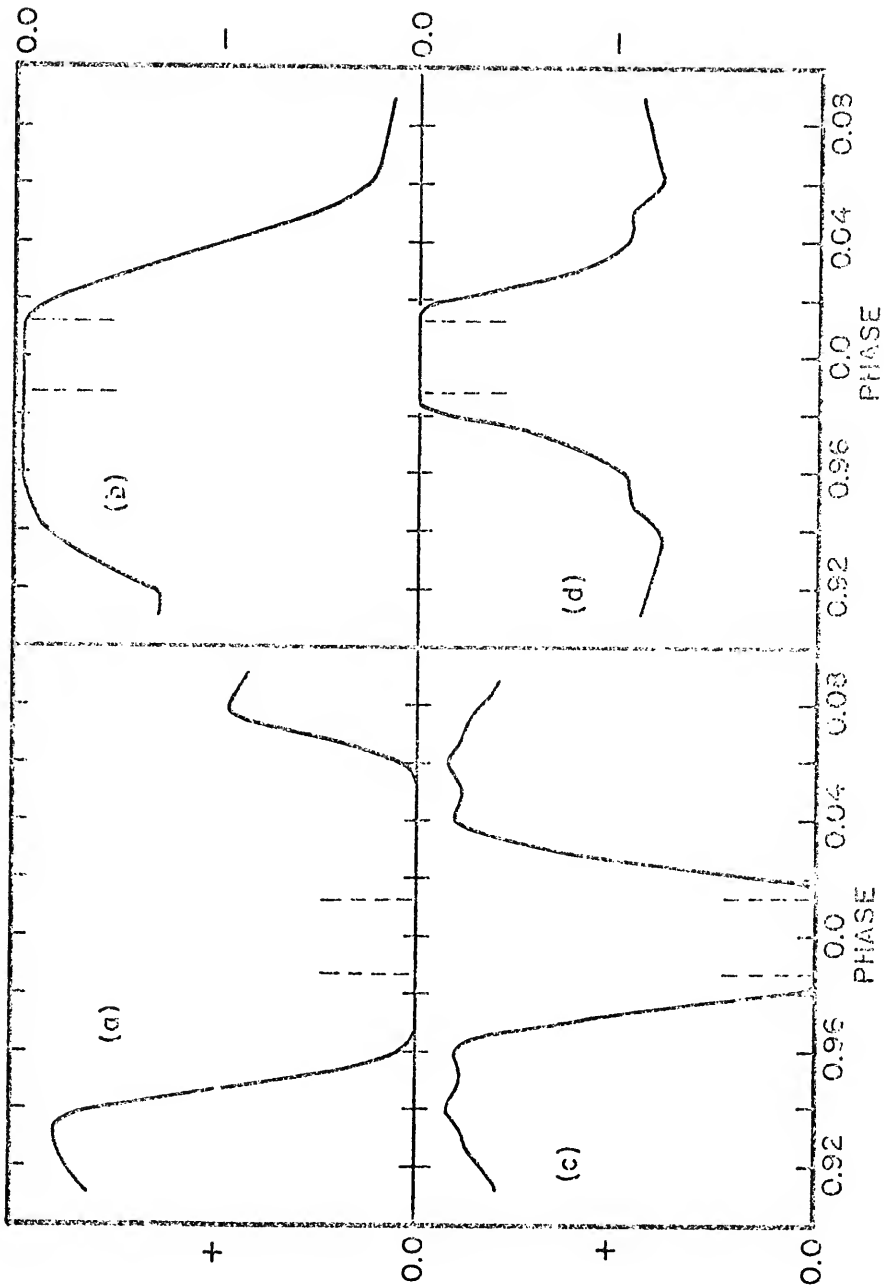
(a)
(b)
(c)
(d)
+
-
0.0
0.92
0.96
0.0
0.04
0.08
PHASE

region. Figure 11a corresponds to an equatorial band at the impact location of the main gas stream of particle trajectory models. The location of this source cannot be varied greatly and must rotate synchronously with the orbit. Such a model has severe difficulties accounting for the sudden disappearance and reappearance of the excess light at second and third contacts. The source region remains eclipsed for a large range of the primary eclipse. The excess light is also approaching maximum at first and fourth contacts, contrary to observation.

A recent model by Olson (1977) found that dark regions of rather large extent must exist on the equator of the primary to account for substantial dips in the light curve around phases 0.2P and 0.6P. My observations clearly show part of the dip at 0.6P on 12 October 1975, and may also show the dip at 0.2P (see Chapter IV). Figure 11b shows the result of my model for the dark region causing the dip at 0.2P. The other dark region suggested by Olson is not visible during primary eclipse. This model shows the same difficulty as the main gas stream hot spot model. Additionally, the residuals are negative. It may be that such dark regions were not evident during my observations of primary eclipse.

At this point attention was turned toward polar source regions to explain the observations. The previously mentioned behavior of the excess light near the contact points put severe constraints on the possible longitudinal extent of the source region. The return of the residuals to zero before first and fourth contacts suggests that the source cannot be

visible at these times. The source region cannot, therefore, rotate synchronously with the orbit, since the phase range of eclipse is not sufficient to turn the source through the visible hemisphere.

The spectroscopically observed rotation rate of the primary star is five times the synchronous orbital rate. The synodic period of rotation relative to the line of centers of four times synchronous is then observed for any fixed point on the primary star. The polar source need not rotate synchronously with the orbit as the equatorial source should. The assumption of the source showing the rotation rate of the star is not only a physically reasonable assumption, but probably the best way to model such a polar source. Examples of the residuals derived from an asynchronously rotating polar source are shown in Figures 12a and 12b.

The procedure for fitting the observed residuals was one of trial-and-error. The number of free parameters in the model (I_s, θ, τ, l_1, l_2, as well as MODE, and the rotation rate) would seem prohibitively large to expect unique solutions. Certain of the free parameters, however, are uniquely correlated to observed features of the excess light. From the previous discussion it would seem that the most productive assumption for residuals like those observed on 10 November 1974 (see Figure 15) would be a polar hot source rotating with the primary star. This fixed MODE as one and also the rotation rate. For this source it was discovered that the peak in the observed residuals fixed θ to within three degrees.

Figure 12. Same as Figure 11. Part (a) and (b) represent the asynchronous polar hot and cold source, respectively. Part (c) is the profile for an attenuating equatorial cloud with an asynchronous polar hot source. Part (d) represents the attenuating cloud alone.

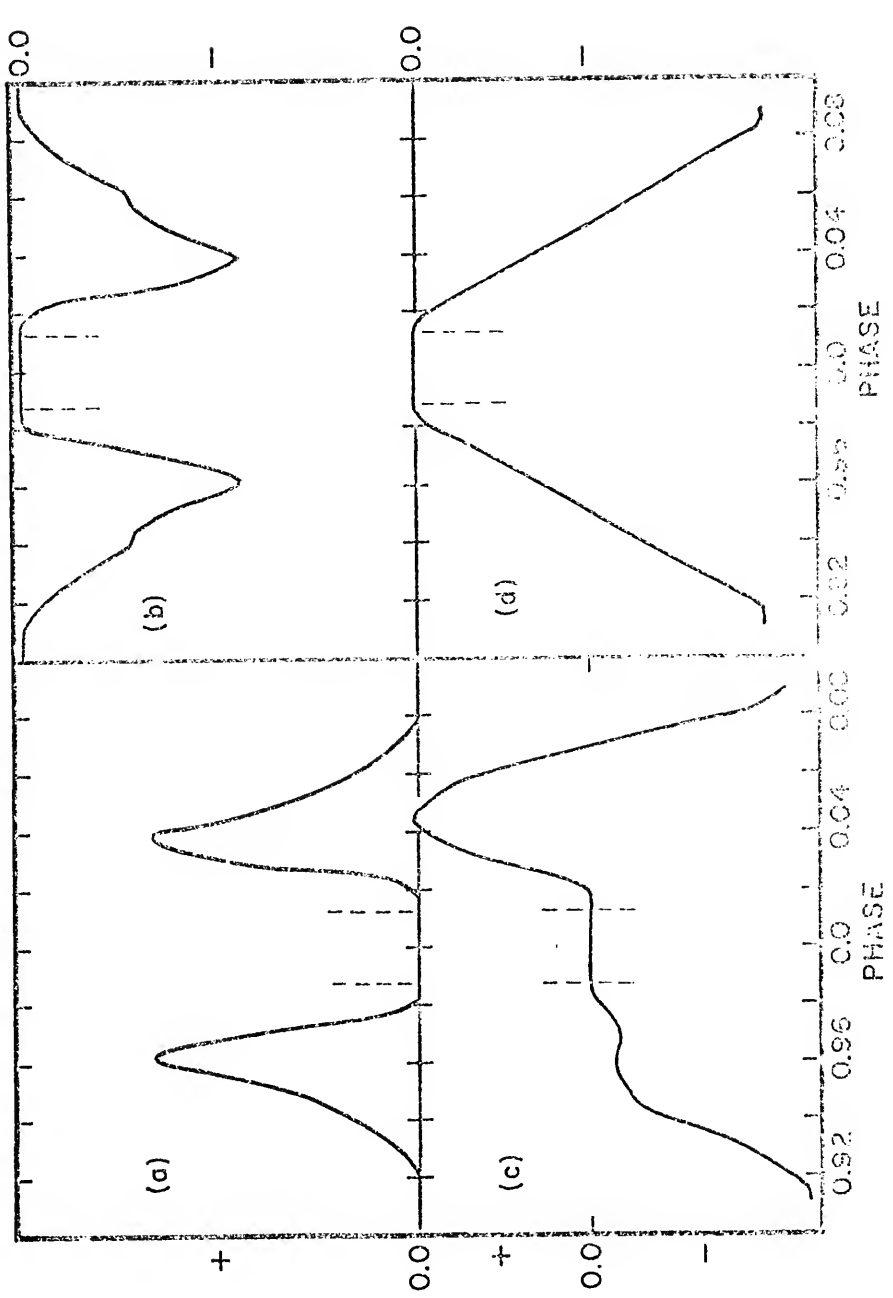
(a)
(b)
(c)
(d)
PHASE
PHASE
0.92
0.96
0.0
0.04
0.08
0.92
0.96
1.0
0.04
0.08
+
0.0
+
0.0
-
0.0
-
0.0

The ratio of the heights of the peaks during ingress and egress determine the difference $l_2 - l_1$. The rise of the ingress peak determines l_1 and the decline of the egress peak fixes l_2. Once these parameters have been estimated, the height of the peaks determines I_s. The use of the optical depth, τ, is more poorly correlated to the observations, If, however, one assumes that only one source is responsible for the residual light, the residual profiles similar to 4 April 1976 (see Figure 22) may be modeled by the use of τ. Any positive non-zero value of τ will result in negative residuals. Nights which show positive residuals were then modeled using zero for τ. It appears then that rather unique solutions can be found for any particular night and it is hoped that the night to night variations can be modeled by small changes in the parameters.

Table 23 shows the "best" fits for the observed eclipses. Plots of these models with the corresponding observations are given in Figures 13-25. No attempt was made to model ultraviolet observations for two reasons. The scatter in the ultraviolet observations is greater than in the other two colors. Inspection of Table 23 shows that eclipses that were observed in all three colors also occurred during periods of relatively low activity, with the exception of 15 October 1975. The effects that the model attempts to explain are very small at these times. As is the case with all models that attempt to account for natural phenomena, this model also has limits of applicability, beyond which the prudent

Table 23

The Model Parameters for the Observed Eclipses

Date	Color	I_s	θ	l_1	l_2	τ	$\Delta T(°K)$	$\bar{v}$ (km/s)
10/31/74	V	9.0	65°	45°	-45°	0.00	9956	15.7
	B	No attempt to model -- large scatter						
11/10/74	V	27.0	70°	45°	-55°	0.00	17401	20.8
	B	16.0	67	40	-55	0.01	13600	18.4
11/15/74	V	10.0	65	55	-40	0.00	10585	16.2
	B	6.0	63	55	-50	0.00	7685	13.8
04/06/75	V	9.0	65	45	-45	0.00	9956	15.7
	B	No attempt to model -- large scatter						
*04/21/75	V	1.0	30°	--	--	0.10	--	--
	B	Assumed the same as visual						
*08/21/75	V	1.0	30°	--	--	0.10	--	--
	B	Assumed the same as visual						
09/25/75	V	No attempt to model -- insufficient data						
	B	No attempt to model -- insufficient data						
*10/15/75	V	No attempt to model -- insufficient data						
	B	No attempt to model -- insufficient data						
*04/04/76	V	15.0	62°	15°	-75°	0.09	13165	18.1
	B	11.0	60	15	-75	0.09	11168	16.6
*05/04/76	V	(5.5)	(21)	(50)	(-45)	(0.07)	(7227)	(13.4)
	B	(5.0)	(21)	(55)	(-50)	(0.15)	(6737)	(12.9)
*05/19/76	V	(5.5)	(21)	(50)	(-45)	(0.07)	(7227)	(13.4)
	B	(5.0)	(21)	(55)	(-50)	(0.15)	(6737)	(12.9)

(Asterisks denote nights where ultraviolet data are available.)

investigator dare not go. Observations of finite accuracy must not be modeled below the ability of the instrument to detect the variation. It is for these reasons that a complete set of graphs is provided for the visual and blue observations of primary eclipse so that the reader may decide whether the results of Table 23 to indeed match the trends of the observations.

One further note of explanation seems required. Those eclipses that have been modeled with non-zero values of τ probably represent an underestimate of the optical depth. The obscuring cloud responsible for the optical depth was assumed to cover the entire equatorial region from $-\theta$ to θ. It is likely that such a simplifying assumption is not the case, but rather that such a cloud is of less latitudinal extent and that τ may vary across the star's surface. Eclipses which required non-zero values of τ, however, do indicate that some obscuring cloud is necessary to fit the observations.

The nights of 31 October 1974, and 6 April 1975, seem to display the same type of behavior in the visual and, therefore are plotted together on Figure 13. The parameters are, however, not definitive for these nights, since only the ingress branch was observed. Particularly affected will be the values of I_s, l_1, and l_2.

The night of 10 November 1974, showed the highest level of activity (see Figures 15 and 16). The success of the model in fitting the rising branch of the ingress peak and the declining branch of the egress peak is particularly encouraging.

Figure 13. Plot of the residuals from the Russell-Merrill solution versus the phase in primary eclipse for the nights of 31 October 1974, and 6 April 1975, in the visual band. Only ingress is shown here. The solid line represents the results of the model for the parameters of Table 23. Since the residuals for the model must fall to zero at second and third contacts, these contact points will be obvious in Figures 13 through 25 and have not been indicated. First and fourth contacts occur at phases 0.9154 and 0.0846.

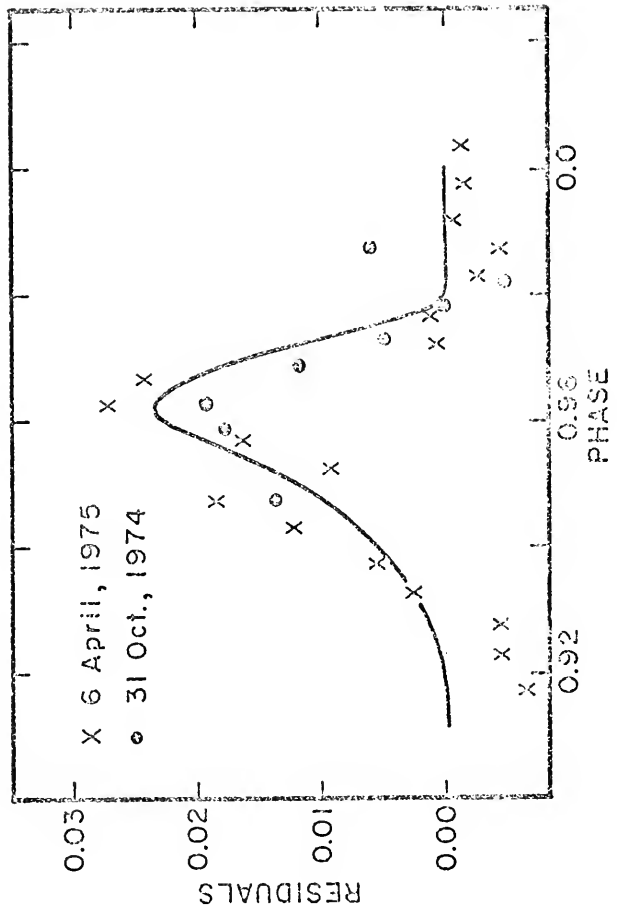
X 6 April, 1975
• 31 Oct., 1974
RESIDUALS
0.03
0.02
0.01
0.00
0.92
0.96
0.0
PHASE

Figure 14. Same as Figure 13 for the night of 31 October 1974, in the blue band. No model was attempted.

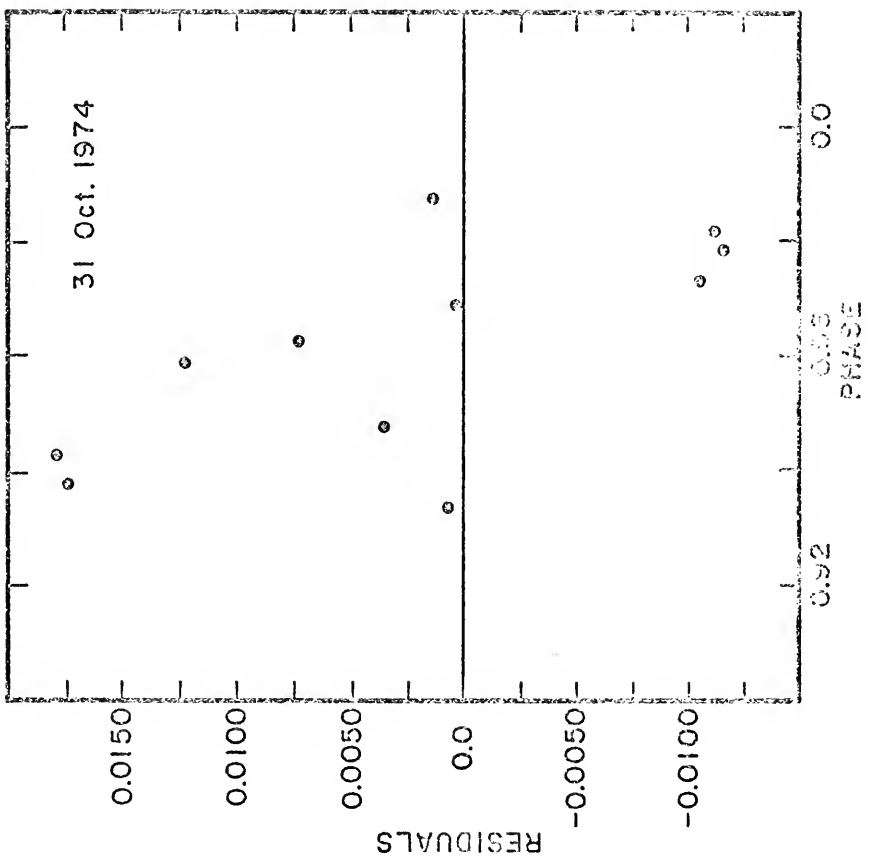
31 Oct. 1974
RESIDUALS
0.0150
0.0100
0.0050
0.0
-0.0050
-0.0100
0.92
0.0
PHASE

Figure 15. Same as Figure 13 for the night of 10 November 1974, in the visual band.

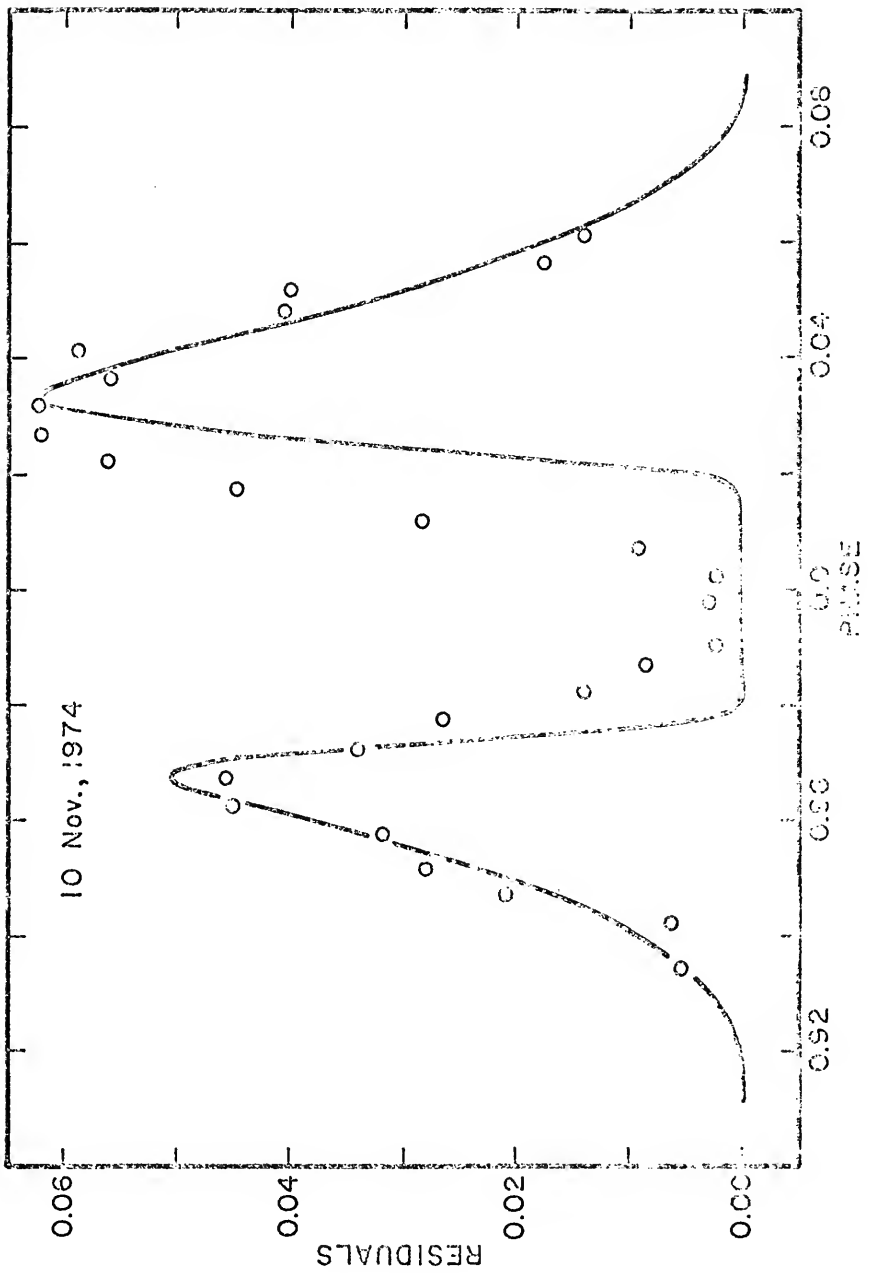
10 Nov., 1974
RESIDUALS
0.06
0.04
0.02
0.00
0.92
0.96
0.0
0.04
0.08
PHASE

Figure 16. Same as Figure 13 for the night of 10 November 1974, in the blue band.

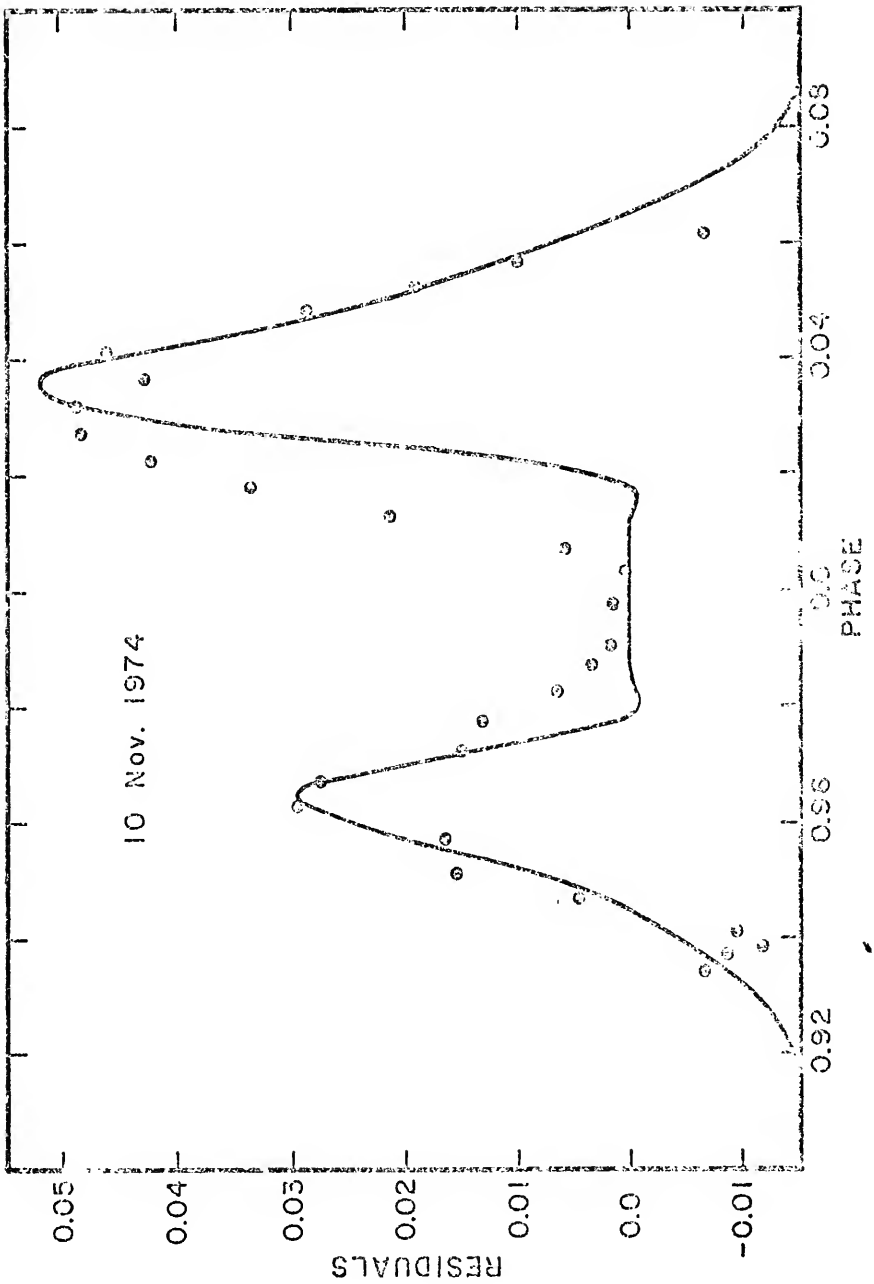
10 Nov. 1974
RESIDUALS
0.05
0.04
0.03
0.02
0.01
0.0
-0.01
0.92
0.96
0.0
0.04
0.08
PHASE

Figure 17. Same as Figure 13 for the night of 15 November 1974, in the visual band.

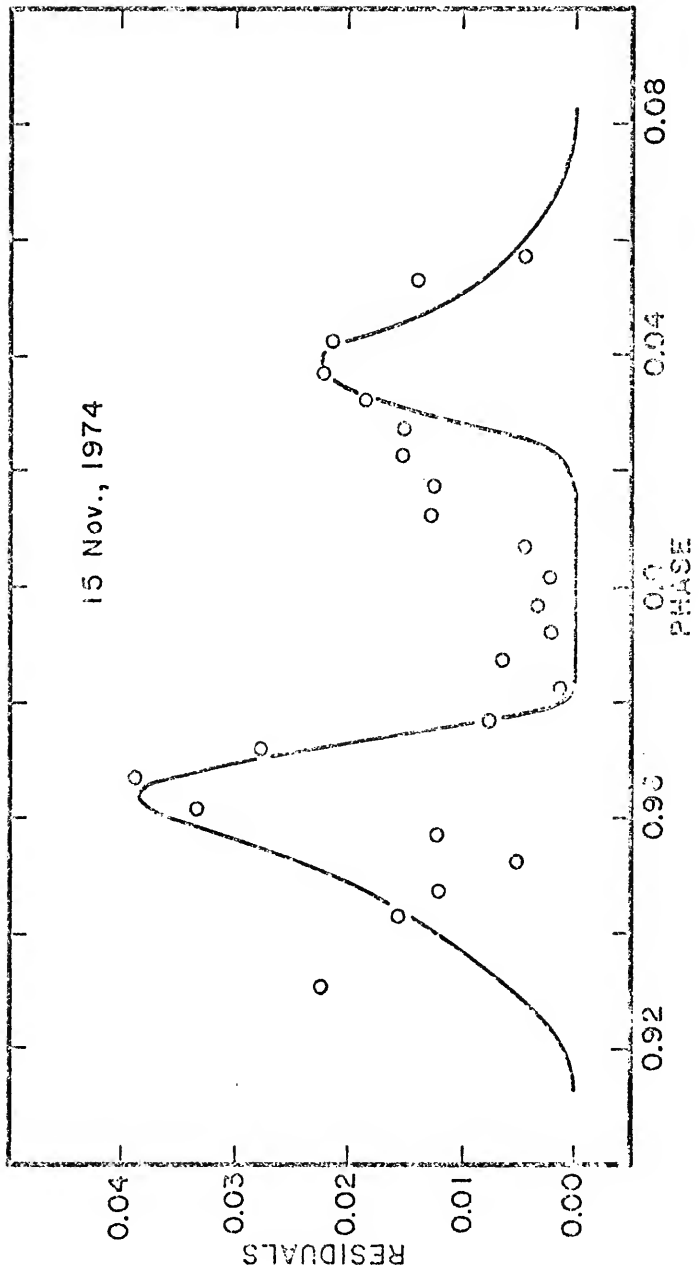
15 Nov., 1974
RESIDUALS
0.04
0.03
0.02
0.01
0.00
0.92
0.96
0.0
0.04
0.08
PHASE

Figure 18. Same as Figure 13 for the night of 15 November 1974, in the blue band.

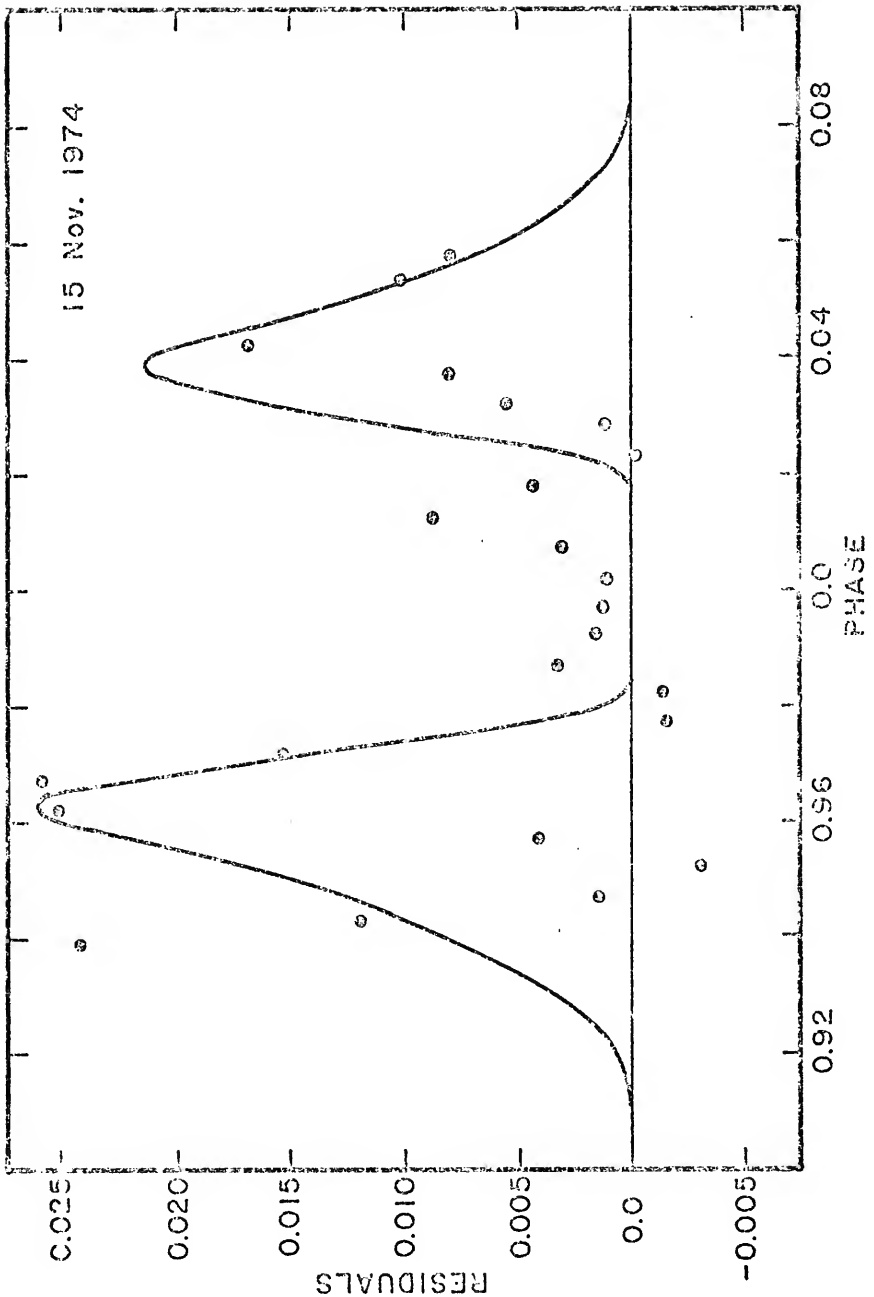
15 Nov. 1974
RESIDUALS
0.025
0.020
0.015
0.010
0.005
0.0
-0.005
0.92
0.96
0.0
0.04
0.08
PHASE

Figure 19. Same as Figure 13 for the night of 6 April 1975, in the blue band. No model was attempted.

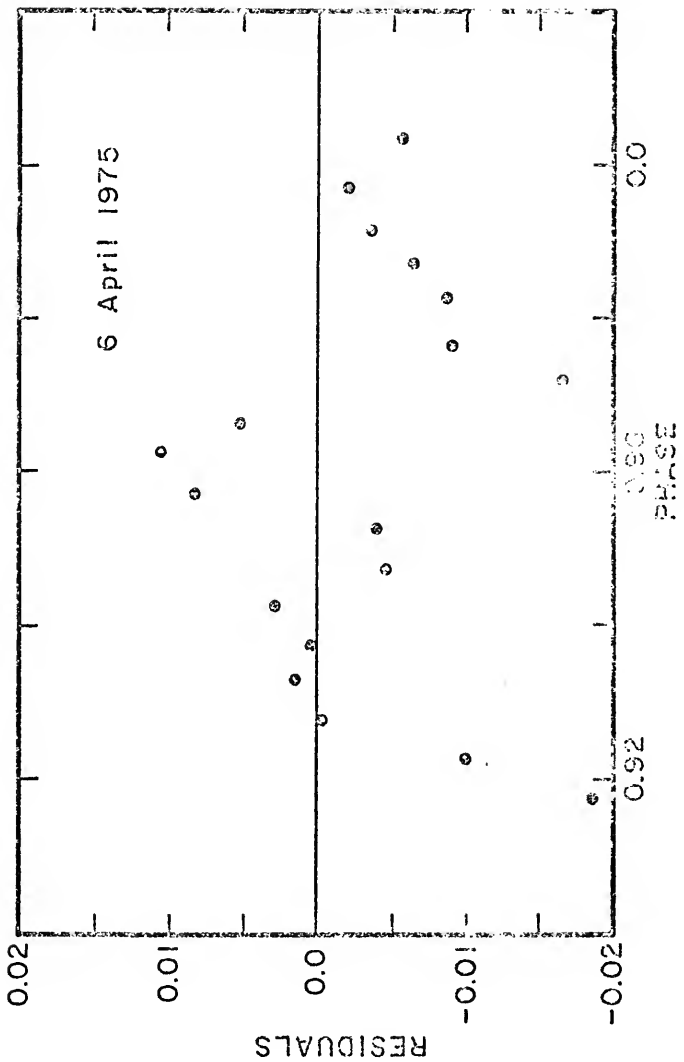
6 April 1975
RESIDUALS
0.02
0.01
0.0
-0.01
-0.02
0.92
0.96
0.0
PHASE

Figure 20. Same as Figure 13 for the nights of 21 April 1975, and 21 August 1975, in the visual band.

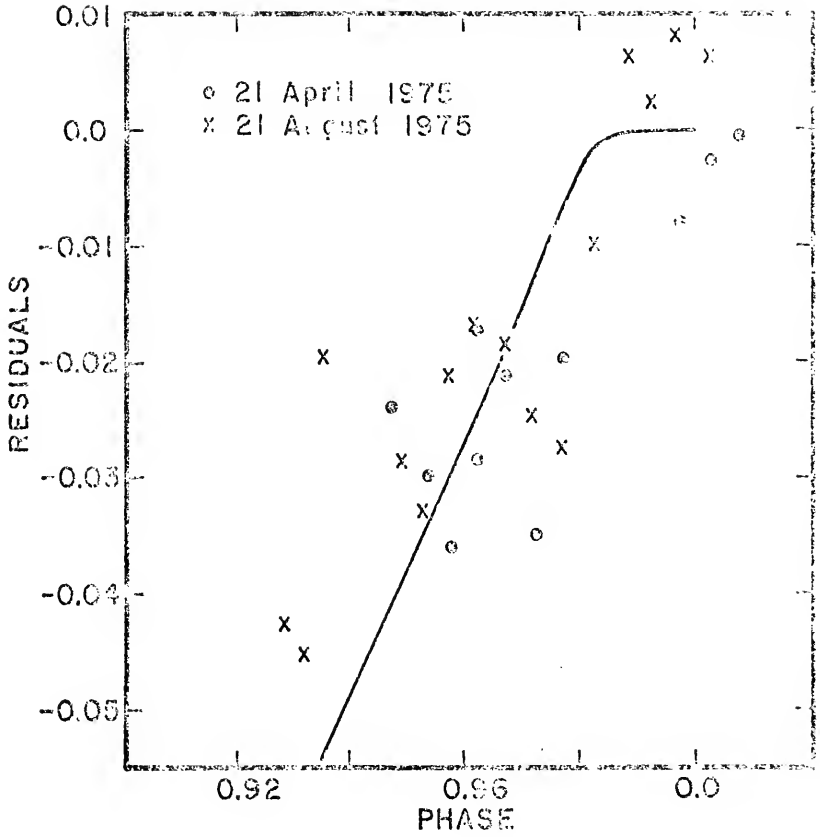
0.01
0.0
-0.01
-0.02
-0.03
-0.04
-0.05
RESIDUALS
o 21 April 1975
x 21 August 1975
0.92
0.96
0.0
PHASE

Figure 21. Same as Figure 13 for the nights of 25 September 1975, and 15 October 1975, in the visual band. No model was attempted.

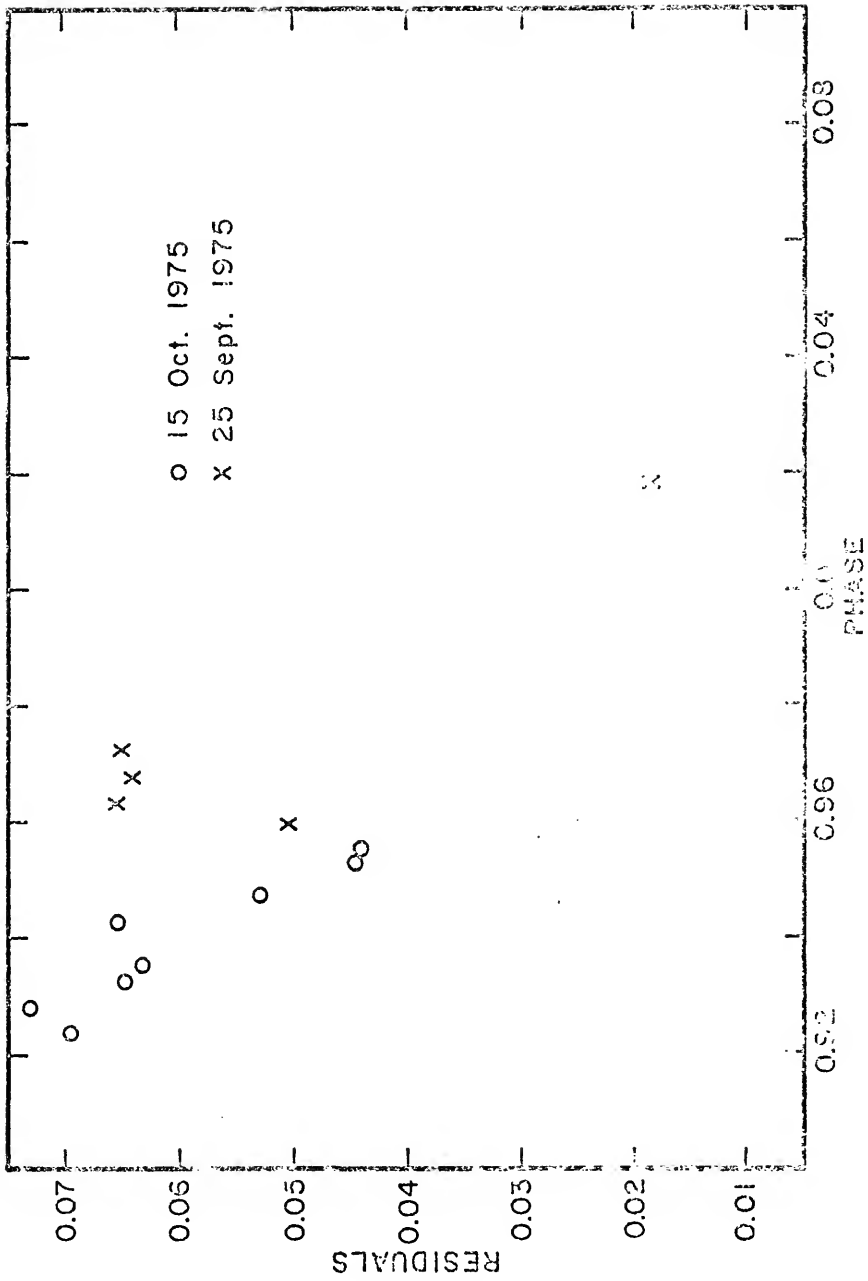
o 15 Oct. 1975
x 25 Sept. 1975
RESIDUALS
0.07
0.06
0.05
0.04
0.03
0.02
0.01
0.92
0.96
0.03
0.04
PHASE

Figure 22. Same as Figure 13 for the night of 4 April 1976, in the visual band.

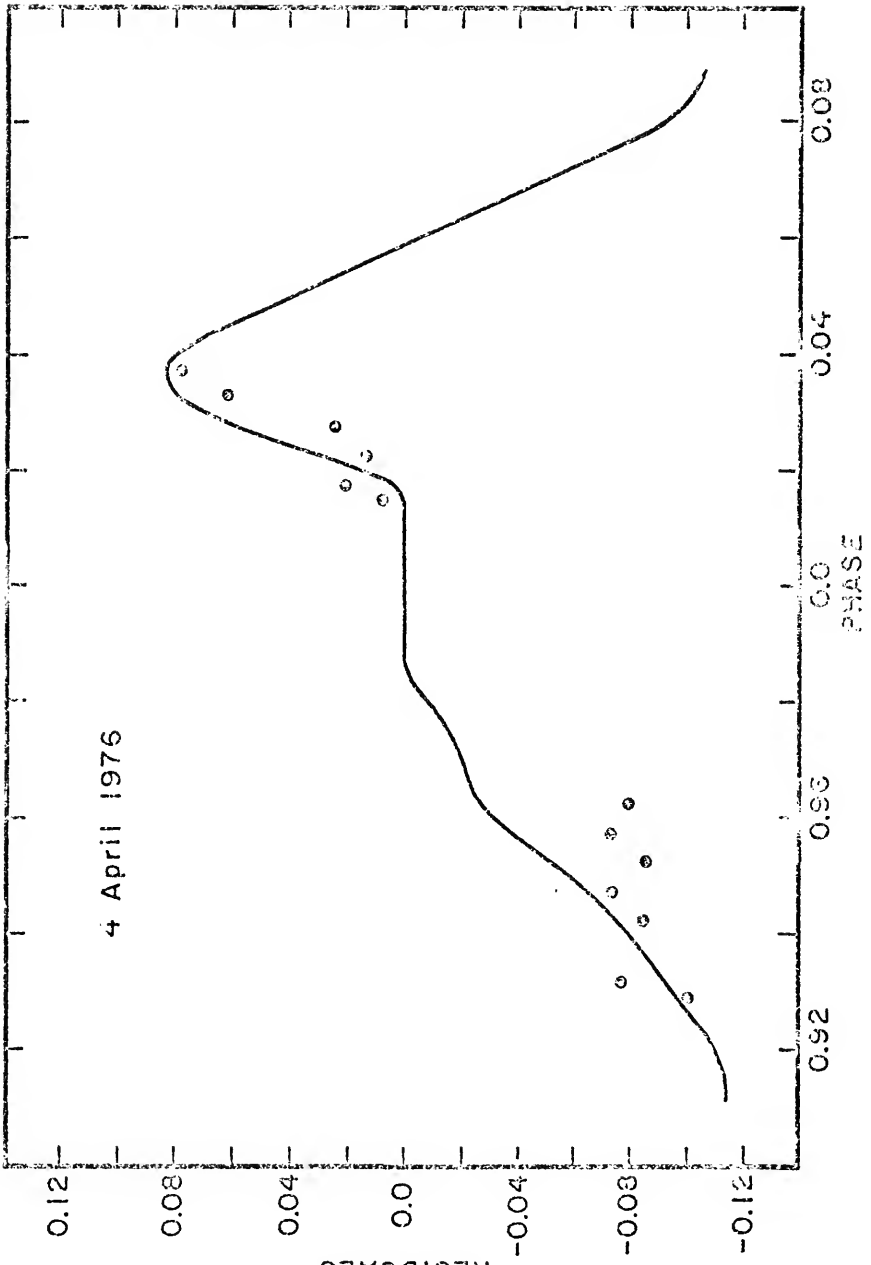
4 April 1976
RESIDUALS
0.12
0.08
0.04
0.0
-0.04
-0.08
-0.12
0.92
0.96
0.0
0.04
0.08
PHASE

Figure 23. Same as Figure 13 for the night of 4 April 1976, in the blue band.

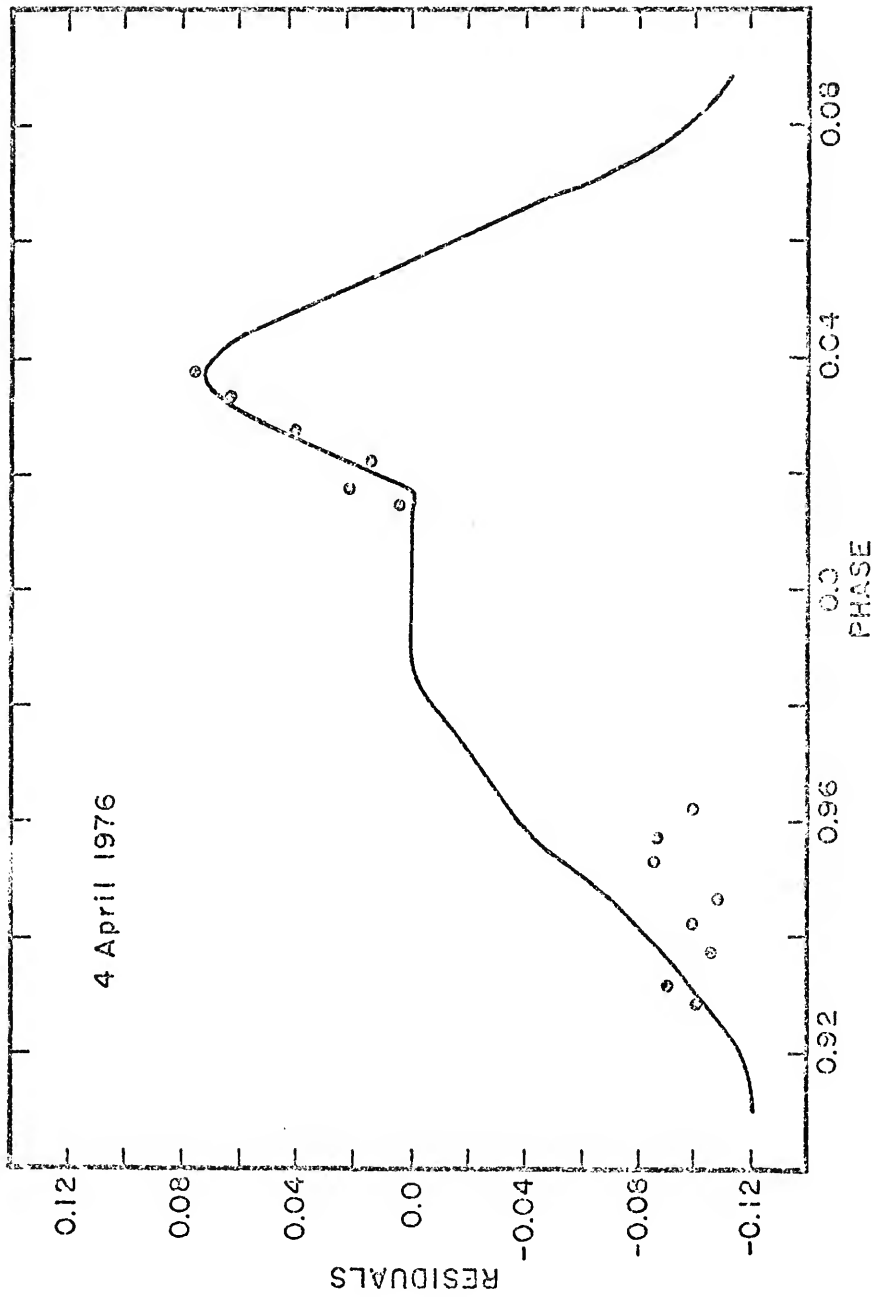
4 April 1976
RESIDUALS
0.12
0.08
0.04
0.0
-0.04
-0.06
-0.12
0.92
0.96
0.0
0.04
0.08
PHASE

Figure 24. Same as Figure 13 for the nights of 4 May 1976, and 19 May 1976, in the visual band.

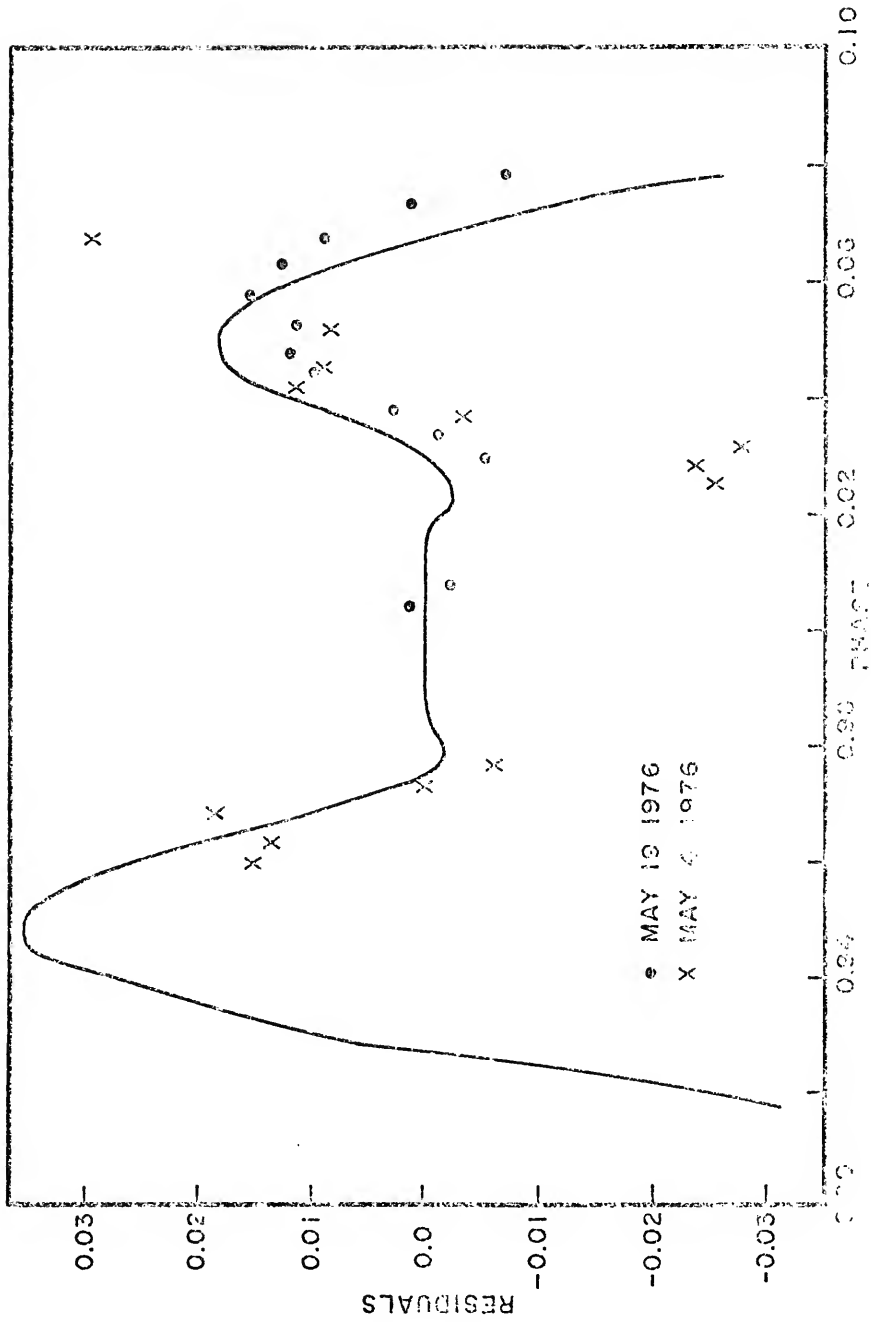
RESIDUALS
0.03
0.02
0.01
0.0
-0.01
-0.02
-0.03
0.10
0.03
0.02
• MAY 13 1976
× MAY 4 1976

Figure 25. Same as Figure 13 for the nights of 4 May 1976, and 19 May 1976, in the blue band.

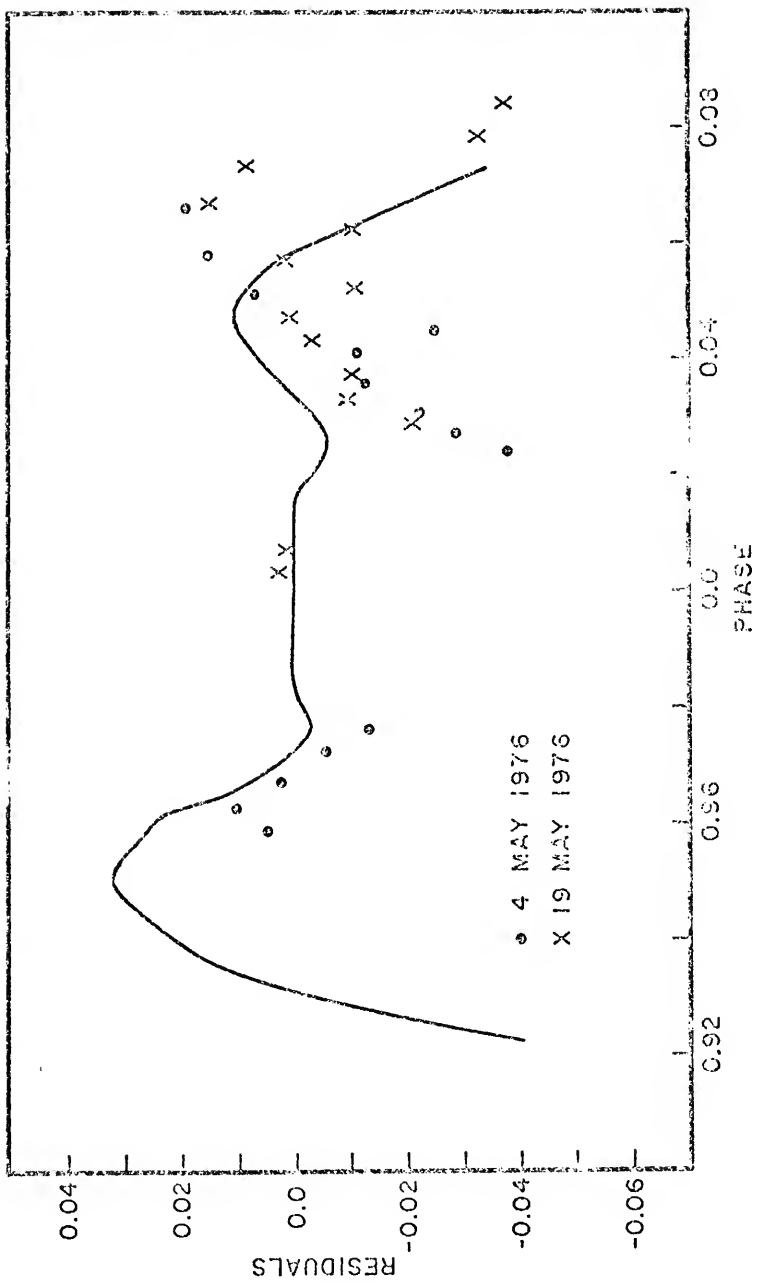
0.04
0.02
0.0
-0.02
-0.04
-0.06
RESIDUALS
0.92
0.96
0.0
0.04
0.08
PHASE
• 4 MAY 1976
X 19 MAY 1976

The straight line segment about 0.0P indicates the total portion of the eclipse, during which no contribution from the primary star is present, and therefore, no abnormal brightness distribution effects can be modeled. The observations clearly show that some excess light is present at second contact and that the excess appears well before third contact. The probable cause of this excess light is material falling onto the source region seen projected onto the sky above the limb of the primary. As the primary star again becomes visible, the source region on the star quickly becomes responsible for the excess light. This same type of behavior is evident in the egress branch on 15 November 1974 (see Figures 17 and 18).

The behavior of the excess light during ingress on 15 November 1974, is more complicated than the model can presently fit. Striations in the source region may be responsible for this behavior.

The nights of 21 April 1975, and 21 August 1975, were particularly interesting (see Figure 20). There appears to be no indication of any source region during these eclipses. Both eclipses were observed during periods of low activity and seem to indicate that an attenuating cloud had been formed. A synchronous cold polar source such as in Figure 11d may also fit the observations, although the physical reasons for such a source are obscure. Since only ingress was observed for both eclipses, no attempt was made to find the best fit. These nights, however, will be important in determining the chronological behavior of U Cephei.

The eclipses of 25 September 1975, and 15 October 1975 (see Figure 21), occurred during the fall 1975, outburst. Unfortunately, the weather conspired to limit the data for these eclipses. The level of activity is very high and 25 September 1975, gives the only evidence that the main stream hot sopt (Figure 11a) may be responsible for the excess light.

The data for 4 April 1976, were also limited, but the model curves drawn in Figures 22 and 23 give some indication that the model can represent these observations. The model chosen here was an attenuating cloud about the equator in combination with a polar hot source which is behind the star until well into the eclipse. The rather flat distribution of points in ingress indicate that other explanations are possible, but the data are insufficient to distinguish between the possibilities. One alternate explanation is that an equatorial cold source similar to those postulated by Olson (1977) precedes the polar hot source.

The two eclipses observed in May 1976 (see Figures 24 and 25) were quite difficult to model. The egress peak occurred quite late and is broader than the previous eclipses. The large drop in light just after third contact is difficult to model as is the rather gradual decline just prior to fourth contact. The model parameters quoted in Table 23 are in parentheses because of the uncertainty of the fit. The model indicates a polar hot source of mild intensity but great extent (to account for the late egress peak), but no great

confidence can be placed in these results. The level of activity is rather low and other effects may be as large as those this model was designed to describe.

CHAPTER VIII

THE U CEPHEI SYSTEM

The Geometrical Parameters

An inspection of the two solution attempts given in Chapter V reveals that they fit the observations equally well. The only noticeable differences in primary eclipse (see Figures 5 and 7) occur in the total portion of the ultraviolet eclipse. Recall, however, that the Russell-Merrill solution for the ultraviolet is not the same as the solutions for the visual and blue, whereas the Wilson-Devinney solution solved the three colors simultaneously.

The depression of the ingress branch of primary eclipse is a well-known phenomenon in U Cephei and these observations show it clearly. The depression becomes somewhat more severe in shorter wavelengths, in agreement with the widely accepted notion that a gaseous stream flowing toward the primary star is responsible. This gaseous stream is projected onto the surface of the primary star during ingress, producing the depression. At other times in the orbit, however, it can add its light to the system without covering one of the components. As the stream hits the surface of the primary star, shock heating will create additional light. Taken together, these effects are probably responsible for the small amount of

light that seems to be necessary in the blue and to a greater extent in the ultraviolet for the W-D solution. Although no third light was added in the solution, its addition would account for the discrepancy noted in the total portion of the ultraviolet eclipse. If third light is indeed necessary, its source is rather hot gas with the impact heating caused by the gaseous stream as the primary candidate.

The W-D solution was successful in fitting the secondary eclipse in the visual. Neither solution attempt was able to fit the secondary eclipse in the blue or the ultraviolet. The blue light curve in secondary eclipse gives the impression of extra light near the beginning of the eclipse, effectively retarding the normal ingress branch. Since these effects were not visible in the visual band on the same nights, the disturbing influence must once again be rather hot gas. I shall return to this point again in the discussion of the primary star.

The light levels in primary eclipse for the two solutions are very close, leaving the residuals unchanged. The solution parameters needed by the model are also very close in the two solutions, resulting in little change in the model curves. The largest change from the Russell-Merrill parameters to the W-D parameters is in the coefficient of limb darkening. This is inherently a second order effect, however, and should affect the model curves very little.

The Primary Star

Several questions arise from the model presented in Chapter VII. If a polar hot source is present, how does material get to the poles? Obviously, the polar brightening due to rotation would be a constant effect, not changing from cycle to cycle as do these observations. Why is the angle θ (the polar extent of the source) relatively constant?

The most reasonable explanation for the polar source region involves a magnetic field for the primary star. Ionized material from the gaseous stream can then be pulled up out of the equatorial plane and impact the poles. The heating causing the polar source regions would be very similar to auroral activity on the earth. If such activity exists, it must be a rather constant feature of the U Cephei system, so long as mass transfer is in progress. During quiescent stages of the system, insufficient material is pulled up to the poles to create noticeable amounts of added light. During outbursts, however, the mass transfer rate may be one or two orders of magnitude greater than normal, and the extra light due to the shock heating at the poles becomes evident. Batten (1974) has estimated that as little as ten charged particles per cubic centimeter would be required to produce the emission features he observed prior to the 1974 event.

The energy requirements for the infalling material are reflected in the mean velocities of Table 23. If these exceed the mean impact velocities of particles in the gaseous stream, then serious problems arise with the model. Particle

trajectory models (Rafert, 1977) for stars with parameters close to the U Cephei system indicate that for thermal boil-off of material from the inner Lagrangian point, impact velocities of 40-50% of the synchronous velocity are expected. For U Cephei this amounts to 24-30 km/s, substantially greater than all but the most photometrically active night (10 November 1974).

The model was able to account for cycle to cycle variations by simply moving the source region a small amount in longitude. The shift in longitude may be explained as an effect of the rotation of the primary star. For example, the shift between 10 and 15 November 1974 was about ten degrees. During these two cycles the model primary star rotated eight times. If the true rotation rate were, however, 8 1/36 per two cycles or 4 1/72 times the synchronous rate, then the true rotation rate explains the apparent shift in longitude of the source region. The difference between this rotation rate and the rate assumed for the model (i.e., four times the synchronous rate), is less than one kilometer per second. Much more data would be required before a quantitative analysis of this shift could be done.

The shape of the source regions in the model is certainly a simplifying assumption. One source of error is undoubtably the sharp boundary of the source region. The models consistently gave a value to θ of approximately 65°. If the source regions are caused by infalling material along the magnetic field lines, then one expects the impact region to be

symmetric about the magnetic poles. The results of the model may be telling us that the magnetic poles of U Cephei are tilted with respect to the perpendicular to the orbital plane by about 12°.

One good observational check can be made on the polar hot source hypothesis. If the source rotates with the star as was assumed, then periodic extra light should appear in the light curve. Since the rotation rate of the primary star is not exactly an harmonic of the orbital period, we would expect this extra light to migrate in the light curve. Observations over 1½ years may show the peaks of extra light somewhat broadened from their true shape. The excess light may also disappear periodically as the mass transfer rate diminishes. With a synodic rotation rate of approximately four times the synchronous rate, extra light should appear during both eclipses and at quadratures. Some evidence for this trend is apparent in Figure 26, which shows the residuals of the normal points from the Russell-Merrill solution. The polar hot source may be responsible for the non-conformity of the secondary eclipse. The expected shape of the excess light in secondary eclipse would be one broad peak of the same extent in phase as both peaks in primary eclipse combined.

The Chronology of the Outburst

Table 23 gives some information about the progress of an outburst. The early outburst may show an equatorial spot of

Figure 26. The residuals of the normal points from the Russell-Merrill solution for the entire light curve. The absissa is phase. Notice the quasi-periodical variation of the residuals, possibly supporting the polar hot source model.

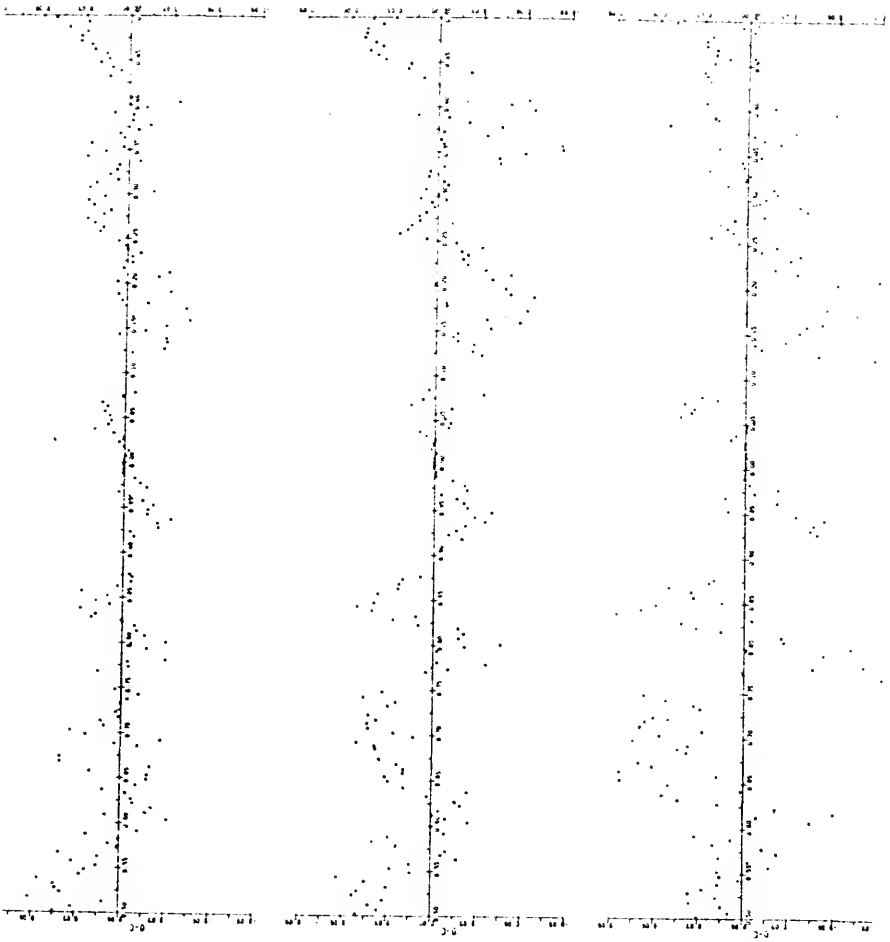

equal brightness to the polar spot as evidenced by 25 September 1975. As the outburst continues, the polar source becomes dominant. Occasionally, the polar source may be accompanied by attenuating material about the primary star. On a time scale of 2-4 months, the polar source disappears and an attenuating cloud may be established. The attentuating cloud may not be permanent but may survive for some months past the disappearance of the polar source.

Future Research

The model presented in this dissertation, while simple in design, is very flexible for modeling abnormal surface brightness distributions on components of close binary systems. The success of the model is evident in the vast range of residual profiles for which the model is applicable. The future success of the model will depend on its continued ability to account for the observations. If the conclusions in this chapter have any validity, then this model can be applied to future outbursts. In obtaining data to confirm these conclusions, it will be important to observe the entire primary eclipse. Observations of secondary eclipse will serve as an important check. Definitive conclusions may be drawn about the validity of this or other models for U Cephei if the entire light curve could be obtained in a short time during an outburst.

BIBLIOGRAPHY

Batten, A.H. 1974, Pub. D.A.O. 14 (10).

Batten, A.H., Scarfe, C.D., and Baldwin, B.W. 1974, I.A.U. Circ. No. 2701.

Carbon, D.F. and Gingerich, O. 1969, Theory and Observation of Normal Stellar Atmospheres, ed. O. Gingerich (MIT Press, Cambridge, MA), p. 401.

Carpenter, E.F. 1930, Ap. J. 72, 205.

Catalano, S. and Rodono, M. 1974, unpublished.

Ceraski, W. 1880, Astr. Nachr. 97, 319.

Chen, K-Y. and Rekenthaler, D.A. 1966, Quart. J. Fl. Ac. Sc. 29 (1).

Cowling, T.G. 1941, M.N.R.A.S. 98, 734.

Dugan, R.S. 1920, Contr. Prin. U. Obs., No. 5.

Hall, D.S. 1975, Acta Ast. 25, 1.

Hall, D.S. and Walter, K. 1974, Astron. and Astrophys. 37, 263.

Hardie, R.H. 1962, Stars and Stellar Systems, vol. II, ed. W.A. Hiltner (U. of Chicago Press), ch. 8.

Jeffers, H.M., van de Bos, W.H., and Greeby, F.M. 1963, Catalogue of Visual Double Stars (U. of Cal. Press).

Johnson, H.L. and Knuckles, C.F. 1955, Ap. J. 122, 209.

Joy, A.H. 1947, P.A.S.P. 59, 171.

Khozov, G.V. and Minaev, N.A. 1969, Trudy Astr. Obs. Leningrad State U. 26, 55.

Kopal, Z. 1959, Close Binary Systems (Wiley, New York).

Merrill, J.E. 1950a, Contr. Prin. U. Obs., No. 23.

1950b, Ibid., No. 24.

1970, Vis. in Ast. 12.

Morton, D.C. and Adams, T.F. 1968, Ap. J. 151, 611.

Oliver, J.P. 1976, Rev. Sci. Instrum. 47 (5).

Olson, E.C. 1977, in press.

Plavec, M. 1973, Extended Atmospheres and Circumstellar Matter in Spectroscopic Binary Systems (I.A.U. Symp. No. 51), ed. A.H. Batten (Dordrecht, D. Reidel), p. 216.

Prendergast, K.H. and Taam, R.E. 1974, Ap. J. 189, 125.

Rafert, J.B. 1977, dissertation, U. of Fl.

Russell, H.N. and Merrill, J.E. 1952, Contr. Prin. U. Obs., No. 26.

Struve, O. 1944, Ap. J. 99, 222.

Tchudovitchev, N.I. 1939, Bull. Engelhardt Obs., No. 17.

1950, Astron. Circ. Kazan, No. 100, p. 14.

Tsesevich, V.P. 1973, Eclipsing Variable Stars, ed. V.P. Tsesevich (Wiley, New York), ch. 2.

Walter, K. 1975, Astron. and Astrophys. 42, 135.

Wilson, R.E. and Devinney, E.J. 1971, Ap. J. 166, 605.

Wilson, R.E. and Stothers, Richard 1975, M.N.R.A.S. 170, 497.

Wood, D.B. 1972, A Computer Program for Modeling Non-Sperical Eclipsing Binary Star Systems, Goddard Space Flight Center, X-110-72-473.

BIOGRAPHICAL SKETCH

Norman Lee Markworth was born on 9 June 1950, in Palatine, Illinois. He was raised in Des Plaines, Illinois, where his parents still reside. He graduated from Maine Township High School West in June, 1968. He attended the University of Illinois from September, 1968, to June, 1972, and graduated with a Bachelor of Science in Physics. While at the University of Illinois, he completed the requirements for a degree in Astronomy.

His graduate work began at the University of Florida in September, 1972. Under the tutorial guidance of Dr. F.B. Wood, he soon became interested in eclipsing binary systems. He worked as a research associate in the variable star search program at the Remeis-Sternwarte, Bamberg, West Germany, during the summer of 1974.

On 5 July 1975, he married Mary Hudak.

The Doctor of Philosophy is expected to be conferred in August, 1977.

I certify that I have read this study and that in my opinion it conforms to acceptable standards of scholarly presentation and is fully adequate, in scope and quality, as a dissertation for the degree of Doctor of Philosophy.

Frank Bradshaw Wood

Frank Bradshaw Wood, Chairman
Professor of Astronomy

I certify that I have read this study and that in my opinion it conforms to acceptable standards of scholarly presentation and is fully adequate, in scope and quality, as a dissertation for the degree of Doctor of Philosophy.

Kwan-Yu Chen

Kwan-Yu Chen, Cochairman
Associate Professor of
Astronomy

I certify that I have read this study and that in my opinion it conforms to acceptable standards of scholarly presentation and is fully adequate, in scope and quality, as a dissertation for the degree of Doctor of Philosophy.

Edward J. Devinney

Edward J. Devinney
Associate Professor of
Astronomy

I certify that I have read this study and that in my opinion it conforms to acceptable standards of scholarly presentation and is fully adequate, in scope and quality, as a dissertation for the degree of Doctor of Philosophy.

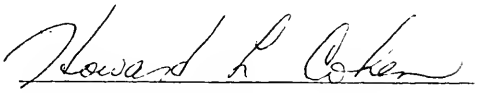

Howard L. Cohen
Associate Professor of Physical Sciences and Astronomy

I certify that I have read this study and that in my opinion it conforms to acceptable standards of scholarly presentation and is fully adequate, in scope and quality, as a dissertation for the degree of Doctor of Philosophy.

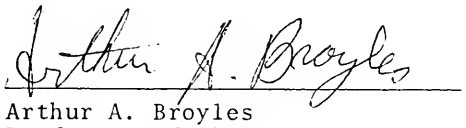

Arthur A. Broyles
Professor of Physics

This dissertation was submitted to the Graduate Faculty of the Department of Physics and Astronomy in the College of Arts and Sciences and to the Graduate Council, and was accepted as partial fulfillment of the requirements for the degree of Doctor of Philosophy.

August 1977

Dean, Graduate School